Structural Studies of Anodic Films on Pure Aluminium

By

Musbah Almajdub

A thesis submitted to the University of Warwick for admission to the degree of Doctor of Philosophy

Department of Physics

February 1998

Dedicated to the memory of my late father, parents, children, and wife.

TABLE OF CONTENTS

1. CHAPTER ONE INTRODUCTION 1

1.1 INTRODUCTION 1
1.2 USES OF ALUMINIUM 2
1.3 CORROSION OF METALS 4
1.3.1 POLARISATION CURVES 6
1.4 CORROSION PREVENTION 7
1.5 THE ELECTROCHEMISTRY OF CORROSION 8
1.5.1 POURBAIX DIAGRAMS 8
1.6 ANODIC ALUMINA FILMS ON ALUMINIUM 10
1.6.1 THE MORPHOLOGY OF ALUMINA FILMS 11
1.6.1.1 Barrier alumina films 12
1.6.1.2 Porous alumina films 12
1.6.2 ELECTROLYTE SPECIES INCORPORATION IN ALUMINA FILMS 13
1.7 PASSIVATING ALUMINA FILMS 13
1.8 LITERATURE REVIEW 15
1.9 OBJECTIVE AND PLAN OF THESIS 19

2. CHAPTER TWO THEORETICAL ASPECTS OF THE EXPERIMENTAL TECHNIQUES 22

2.1 INTRODUCTION 22
2.2 ELECTROCHEMICAL TECHNIQUES 22
2.3 X-RAY ABSORPTION SPECTROSCOPY (XAS) 24
2.3.1 INTRODUCTION 24
2.3.2 EXAFS THEORY 27
2.3.3 EXAFS DATA ANALYSIS 29
2.3.3.1 Pre-edge background subtraction and normalisation 29
2.3.3.2 EXAFS in wave vector form 30
2.3.3.3 k-weighting 30
2.3.3.4 Fourier transform 31
2.3.3.5 Fitting for the phase 31
2.3.3.6 Fitting for amplitude 32
2.3.4 X-RAY ABSORPTION NEAR-EDGE SPECTROSCOPY (XANES) 32
2.3.5 EXAFS DETECTION METHODS 33
2.3.5.1 Transmission EXAFS 34
2.3.5.2 Fluorescence EXAFS 35
2.3.5.3 Electron yield EXAFS 36
2.3.6 REFLECTION EXAFS (REFLEXAFS) 37
2.4 X-RAY PHOTOELECTRON SPECTROSCOPY (XPS) 38
2.4.1 INTRODUCTION 38
2.4.2 THEORY OF XPS PROCESS 39

2.4.3 ELECTRON ENERGY ANALYSERS 41

3. CHAPTER THREE EXPERIMENTAL DETAILS 45

3.1 INTRODUCTION 45
3.2 SAMPLE PREPARATION 46
3.2.1 ALUMINIUM METAL BULK SAMPLE PREPARATION 46
3.2.2 ALUMINIUM FILM SAMPLE PREPARATION 47
3.3 ELECTROCHEMICAL TECHNIQUES 47
3.4 SYNCHROTRON BASED EXPERIMENTAL TECHNIQUES 50
3.4.1.1 EXAFS station 9.2 of the SRS 52
3.4.2 SOFT X-RAY STATION ON BEAMLINE 3.4 OF THE SRS 54
3.4.2.1 Data collection and analysis 56
3.4.3 REFLEXAFS APPARATUS ON BEAMLINE 3.4 AT DARESBURY 57
3.4.3.1 Introduction 57
3.4.3.2 Apparatus description 57
3.4.3.3 ReflEXAFS data collection and analysis 59
3.5 X-RAY PHOTOELECTRON SPECTROSCOPY (XPS) 59
3.5.1 INTRODUCTION 59
3.5.2 SAMPLE TREATMENT 59
3.5.3 XPS APPARATUS 60

4. CHAPTER FOUR FLUORESCENCE EXAFS OF TUNGSTEN IN ALUMINA FILMS64

4.1 INTRODUCTION 64
4.2 ELECTROLYTE SPECIES INCLUSION INTO ANODIC FILM 64
4.3 EXAFS STUDY OF TUNGSTEN INCORPORATED INTO ALUMINA FILMS 66
4.4 TUNGSTEN AND OXYGEN PHASE SHIFTS DETERMINATION 66
4.5 TRANSMISSION EXAFS OF W-FOIL 67
4.6 TRANSMISSION EXAFS OF W-L_3 IN POTASSIUM TUNGSTATE 68
4.7 FLUORESCENCE EXAFS OF W-L_3 INCORPORATED IN ANODIC ALUMINA FILMS 70
4.8 DISCUSSION OF RESULTS AND CONCLUSIONS 71

5. CHAPTER FIVE ELECTROCHEMISTRY AND XPS RESULTS AND DISCUSSION74

5.1 INTRODUCTION 74
5.2 POLARISATION OF ALUMINIUM 74
5.2.1 POLARISATION CURVES OF ALUMINIUM BULK 74
5.2.2 POLARISATION CURVES OF EVAPORATED ALUMINIUM FILMS 75
5.3 XPS RESULTS OF THIN FILMS ON ALUMINIUM 76
5.3.1 INTRODUCTION 76
5.3.2 DATA COLLECTION AND ANALYSIS 76
5.3.3 XPS OF AIR-FORMED FILMS 78

5.3.4 XPS OF ALUMINA OXIDE FILM ON ALUMINIUM IN BOILING WATER 79
5.3.5 XPS OF ANODIC OXIDES ON ALUMINIUM IN WATER AT DIFFERENT PH'S 80
5.3.5.1 pH 7 81
5.3.5.2 pH 10 82
5.3.5.3 pH 2 83
5.3.6 XPS OF OXIDE FILMS ON ALUMINIUM POLARISED IN AQUEOUS SOLUTION AT PH 283
5.3.6.1 +2.5 V/SCE 84
5.3.7 XPS OF FILMS ON ALUMINIUM POLARISED IN AQUEOUS SOLUTION AT PH 7 85
5.3.7.1 -2.2 V vs SCE 86
5.3.8 XPS RESULTS OF FILMS ON ALUMINIUM POLARISED IN PH 10 87
5.3.8.1 +0.9 V/SCE 87
5.4 SUMMARY AND DISCUSSION
5.4.1 ELECTROCHEMISTRY RESULTS 88
5.4.2 XPS RESULTS 88

6. CHAPTER SIX EXAFS, XANES, AND REFLEXAFS OF THIN PASSIVATING FILMS ON ALUMINIUM 93

6.1 INTRODUCTION 93
6.2 MODEL COMPOUNDS 93
6.3 EXAFS RESULTS FOR PASSIVATING THIN OXIDE FILMS ON ALUMINIUM 97
6.3.1 EXAFS RESULTS OF OXIDE FILMS ON ALUMINIUM IN AQUEOUS SOLUTION AT PH 79
6.3.2 EXAFS OF FILMS ON ALUMINIUM IN AQUEOUS MEDIA AT PH 2 99
6.3.3 EXAFS OF FILMS ON ALUMINIUM IN AQUEOUS SOLUTION AT PH 10 101
6.4 XANES RESULTS 105
6.4.1 XANES OF MODEL COMPOUNDS 105
6.4.2 XANES OF ALUMINIUM AT DIFFERENT PREPARATION STAGES 106
6.4.3 XANES OF OXIDE FILMS ON AL. POLARISED AT VARIOUS POTENTIALS AND DIFFERENT PH'S 107
6.5 REFLEXAFS RESULTS 109
6.5.1 REFLECTIVITY CURVES 109
6.5.2 REFLEXAFS OF OXIDE FILM ON ALUMINIUM AT PH 10 FOR 27 HOURS 109
6.6 DISCUSSION OF RESULTS 110
6.6.1 EXAFS 111
6.6.2 XANES 112
6.6.3 REFLEXAFS 112

7. CHAPTER SEVEN CONCLUSIONS AND FURTHER WORK 114

7.1 SUGGESTED FURTHER WORK 119

Table of Figures

Figure 1.1 A schematic representation of the corrosion of iron in water 4

Figure 1.2 Polarisation curve (i-v) for a metal exhibiting an active-passive transition 6

Figure 1.3a Pourbaix diagram where the stable oxide film on aluminium in water is boehmite 9

Figure 1.3b Pourbaix diagram where the stable oxide film on aluminium in water is hydrargillite 9

Figure 1.4 *a and b* The morphology of alumina films 12

Figure 1.5 Model of Passive film growth 14

Figure 1.6 *a, b, and c* Structural model of alumina films on aluminium 17

Figure 2.1 Potentiodynamic curves for steel in H2SO4 a, b, and c are 304 L, 800 L, and 316 L steels respectively (2) 25

Figure 2.2 *An EXAFS spectrum of a monatomic Krypton gas* 25

Figure 2.3 *A* Schematic diagram of different regions on the EXAFS and XANES spectrum of a solid 26

Figure 2.4 Absorbing process of an atom surrounded by neighbours 26

Figure 2.5a Pre- and post-edge background subtraction 29

Figure 2.5b k^3 weighted EXAFS and its Fourier transform 30

Figure 2.5c *Fourier transform of the EXAFS* 31

Figure 2.6 A transmission EXAFS arrangement 35

Figure 2.7 Atomic relaxation processes, a) fluorescence b) Auger 36

Figure 2.8 Physical process of the XPS 41

Figure 2.9 Plane mirror analyser (PMA) layout 43

Figure 3.1 Electrochemical cell used in polarisation experiments 49

Figure 3.2 Layout of the SRS at Daresbury 51

Figure 3.3 Distribution of the Emitted radiation of the SRS 52

Figure 3.4 Layout of station 9.2 of the SRS at Daresbury 53

Figure 3.5 SOXAF station layout 55

Figure 3.6 Schematic diagram of the ReflEXAFS apparatus 59

Figure 3.7 Layout of the VG-XPS spectrometer 62

Figure 4.1 a Transmission EXAFS at the L_3 edge of tugnsten foil 67

Figure 4.1 b k weighted EXAFS of W-L_3 and the Fourier transform of tugnsten foil..... **68**

Figure 4.2 a Transmission EXAFS spectrum of W in potassium tungstate..... **69**

Figure 4.2 b *Pre- and post-edge subtraction and EXAFS function transformation into K-space*..... **69**

Figure 4.2 c k^3 weighted EXAFS of W-L_3 in K_2WO_4, the Fourier transform, showing the oxygen shell distance..... **69**

Figure 4.3 a Fluorescencs EXAFS spectra of W-L_3 incorporated in anodic alumina film formed on aluminium at 100 V in tungstate electrolyte..... **70**

Figure 4.3 b Fluorescencs EXAFS spectra of W-L_3 in alumina after removal of background ... **70**

Figure 5.1 a, b, and c Polarisation curves of aluminium in 0.05 M Na2 SO4 at pH 2, 7, and 10..... **74**

Figure 5.2 Polarisation curves of aluminium evaporated films in aqueous solutionspH 10..... **75**

Figure 5.3 *a, b, and c* show a raw Al 2p spectrum of aluminium and its oxide, a theoretical..... **77**

Figure 5.4 XPS Al 2p transition of air- formed film on Aluminium..... **79**

Figure 5.5 *XPS Al 2p transition of oxide film formed on aluminium in boiling water, ion gun 4KV*..... **79**

Figure 5.6 XPS Al 2p transition of anodic oxide film formed on aluminium in aq. sol. at pH 7..... **81**

Figure 5.7 XPS Al 2p transition of oxide formed on aluminium in aq. sol. at pH 10, ion gun at 2 keV..... **82**

Figure 5.8 XPS Al 2p transition of oxide film formed on aluminium in pH 2, ion gun at 2 KeV..... **83**

Figure 5.9 *Al 2p XPS of oxide film on Al in water at pH 2 to + 2.5 V, ion gun at 4 keV*..... **84**

Figure 5.10 *XPS of oxide film formed on Al polarised to + 2.5 V/SCE in aq. sol. at pH 7, ion gun at 4 KeV*..... **85**

Figure 5.11 *Al 2p transition intensities of Al polarised to -2.2 V/SCE in pH 7 aqueous solution*..... **86**

Figure 5.12 *XPS Al 2p transition of oxide film formed on aluminium in pH 10 polarised to +0.9V, ion gun at 4 KeV*..... **87**

Figure 6. 1 EXAFS spectrum of aluminium foil measured in transmission mode above the aluminium K-edge..... **94**

Figure 6. 2 *EXAFS spectrum of alpha alumina model compound measured in total electron yield above the aluminium K-edge* **94**

Figure 6. 3 *Theoretical fit for aluminium experimentall k^3 weighted EXAFS function above the Al K-edge. Also the Fourier transform is shown which indicates the first three shells distance in Å.* **95**

Figure 6. 4 *The experimental and theoretical fit of the EXAFS function weighted by k^3 as well as the Fourier transform of alpha alumina.* **95**

Figure 6. 5 *Experimental and theoretically fitted EXAFS function, $k^3\chi(k)$, for the oxide film formed by polarising aluminium to + 2.5 V in pH 7, also the Fourier transform is shown which indicate the shell distance in Å.* **98**

Figure 6. 6 *Experimental and theoretically fitted $k^3\chi(k)$ are presented for the EXAFS of the oxide film formed by polarization at +2.5 V, pH 7 and left connected for 4 hours; Fourier transform is given as well where the shell distance is indicated.* **99**

Figure 6. 7 *Experimental and theoretically fitted $k^3\chi(k)$ are presented for the EXAFS of the oxide film formed by polarisation to -2.17 V in pH 2, Fourier transform is given as well where the shell distance is indicated* **100**

Figure 6. 8 *Experimental and theoretically fitted EXAFS function, $^{k3}\chi(k)$, for the oxide film formed by polarising aluminium to + 2.5 V in aqueous solution at pH 2, also the Fourier transform is shown which indicate the shell distance in Å.* **101**

Figure 6. 9 *Experimental and theoretically fitted EXAFS function, $k^3\chi(k)$, for the oxide film formed by polarising aluminium to + 0.9 V in aqueous solution at pH 10, also the Fourier transform of the Experimental and fitted EXAFS function is shown as function of distance in Å.* **104**

Figure 6. 10 a) *Normalised XANES spectra of model compounds, alpha alumina, gibbisite, andalusite, boehmite, gamma alumina, and yttrium aluminium garnet. All have their energy adjusted to the edge energy of the alpha alumina taken as zero and* **b)** *its derivative* **105**

Figure 6. 11 a) *Normalised XANES spectra of aluminium metal at various stages of its surface preparation, and* **b)** *its derivative* **106**

Figure 6. 12 a) *Normalised XANES spectra of aluminium metal in aqueous solution at pH 7 at open circuit, polarised to -2.2 V and + 2.5 V, and* **b)** *its derivative* **107**

Figure 6. 13 a) *Normalised XANES spectra of aluminium metal in aqueous solution at pH 2 at open circuit for an hour, polarised to -2.17 V and + 2.5 V, and* **b)** *its derivative* **107**

Figure 6. 14 a) *Normalised XANES spectra of aluminium metal in aqueous solution at pH 10 at open circuit for one hour, polarised to -2.2 V and + 0.9 V, and* **b)** *its derivative*..... **108**

Figure 6. 15 *Reflectivity profile of aluminium film immersed in aqueous solution at pH 10 for 27 hours, ReflEXAFS*..... **109**

Figure 6. 16 *Experimentally and theoretically fitted EXAFS function* k^3 *weighted of aluminium at open circuit for 27 hours in pH 10*..... **110**

List of Tables

Table 5.1 *XPS depth profile of an air- formed film on aluminium* **78**

Table 5.2 *XPS depth profile of thick oxide film formed on aluminium in boiling water, ion gun at 4 keV* **79**

Table 5.3 *XPS depth profile of oxide film formed on Al in aq. sol. pH 7, ion gun at 2 keV* **81**

Table 5.4 *XPS depth profile of oxide film formed on Al in aqueous solutions at pH 10.* **82**

Table 5.5 *XPS of sputtered oxide film formed on aluminium in pH 2 aq. sol., ion gun at 2 keV* **83**

Table 5.6 *Depth profile of XPS of Al polarised to +2.5 V/SCE in pH 2, ion gun at 4 keV* **84**

Table 5.7 *XPS of Al polarised to +2.5 V in water at pH 7, ion gun at 4 keV* **85**

Table 5.8 *XPS Al 2p transition of oxide film formed on Al polarised in pH 7 to -2.2 V/SCE, ion gun at 4 keV* **86**

Table 5.9 *XPS Al 2p of oxide film formed on Al in pH 10 polarised to +0.9V, ion gun at 4 KeV* **87**

Table 6.1 *Structural parameters of the first three shells of aluminium atoms surrounding the absorbing aluminium atom.* **95**

Table 6.2 *Structural parameters obtained from the best fit of four summed* α *-alumina EXAFS spectra. The bond length and the co-ordination number values are compared with the crystallographic (4) values.* **96**

Table 6.3 *Structural parameters of the oxide film formed by polarisation of aluminium in aqueous solution at pH 7 to + 2.5 V* **97**

Table 6.4 *Parameters of the local structure around aluminium absorbing atom in the oxide film formed by polarisation to + 2.5 V and then the sample was left connected to the voltage source for four hours.* **98**

Table 6.5 *Bond length, co-ordination number for the two backscattering shells, where the first is due to the oxygen in the oxide film and the second shell is metallic aluminium.* **100**

Table 6.6 *Parameters of the local structure around aluminium absorbing atom in the oxide film formed by polarisation to + 2.5 V in aqueous solution at pH 2.* **101**

Table 6.7 *Parameters of the local structure around aluminium absorbing atom in the* **102**

Table 6.8 *Parameters of the local structure around aluminium absorbing atom in the oxide film formed by polarisation to - 1.8 V in aqueous solution at pH 10.* **103**

Table 6.9 *Structural parameters of the oxide formed by polarisation of aluminium in aqueous solution at pH 10 to + 0.9 V.* **103**

Table 6.10 *Structural parameters for the oxide film that forms on aluminium by anodic polarisation to +0.9V and then left for four hours connected to the potential source in alkaline (pH 10) aqueous media.* **104**

Table 6.11 *Type of atoms in the backscattering shell, bond length and co-ordination number of each shell, and the Debye-Waller term for the respective shells of the oxide film formed on aluminium film immersed in aqueous solution at pH 10 for 27 hours. ReflEXAFS was measured at 750 mdeg.* **110**

Acknowledgement

I would like to express my appreciation and gratitude to Dr. J. Robinson, who has supervised my work and helped me through out the writing of this thesis. I am indebted to him for his guidance and supervision.

My thanks are due to the technicians, Mr. R. Johnston and Mr. P. Thompson of the Surface Physics Group who have been helpful through out my work. Much appreciation is to Mr. D. Lee, of the Materials Preparation Laboratory for his help in aluminium metal polishing and preparations.

I am indebted to Mr. Salem Al-Harthi, Mr. M. S. Kariapper, and Mr. A. Gargoum for their help and support. Also, my thanks are to my friends in the surface physics group, Mr J. Khang, Mr N. Kaijak, Mr Y. Le-goaziou, and Mr. T. Wilson.

I am very grateful to the Head of the Libyan Interests section, Saudi Embassy and the Head of the Student Affairs Department in the Libyan Interests section and their staff for their help, assistance, and financial support during my stay.

Also I would like to thank the Director of Daresbury SRS and his staff for the provision of synchrotron radiation.

Declaration

This thesis is submitted to the University of Warwick in support of my application to the degree of Doctor of Philosophy. The thesis contains an account of my independent work performed at the Physics Department of the University of Warwick under the supervision of Dr. J. Robinson, from October 1989 to February 1998. No part of this thesis has been submitted to this or any other University or used previously for another degree. The work reported in this thesis is the result of my own research except where specifically mentioned in the thesis.

M. Almajdub

Abstract

The morphology and composition of anodically formed alumina films on pure aluminium are well characterised, but their structure is not well known due to the long range order.

Two systems have been looked at in this study; the nature of the structure of tungsten incorporated from tungstate electrolyte during polarisation of aluminium at 100 V, and the other system is the thin passivating layers formed anodically on aluminium surface by polarisation within the range -2.2 - +2.5 V in aqueous solutions at various pH's.

Even though other techniques, such as, electron microscopy and XPS have been used to confirm the presence of anion species in alumina films only EXAFS can yield direct information about the structure of incorporated species. In this study, EXAFS has been used for the first time to resolve the structure of tungsten incorporated into anodic alumina. Accurate determination of structural parameters require the establishment of reliable phase shift. By fitting the EXAFS of tungsten foil and potassium tungstate, the reliability of the calculated phase shifts for oxygen and tungsten was established.

Based on phase shift transferability, the phase shifts calculated for O and W were used in the fitting of fluorescence EXAFS of tungsten in alumina oxide films formed on aluminium in tungstate solution at 100V. The experimental EXAFS function was fitted to a single oxygen shell with four atoms at a distance of 1.79 ± 0.01 Å. From the structural parameters for incorporated tungsten it is clear that it is in a WO_4^{2-} even though this can not be the entity which is outwardly mobile. It is suggested that the tungstate may be linked in some way to the alumina and that because aluminium cations are outwardly mobile so tungstate is dragged along.

The other kind of anodic films on aluminium are those produced by polarising aluminium in aqueous solutions at various pH's to various voltages within the range -2.2 - + 2.5 V. In some instances, passivating films grow on aluminium causing aluminium protection against corrosion. The structure of these films is not defined and because of their existence on aluminium, and their small thickness, so their structure is not easy to be studied. Electron microscope and XPS techniques have been used to determine their morphology and composition. Some work on indirectly extracting the structure of these films from XPS data was reported and it was claimed that these films have a pseudoboehmite like structure.

XPS results of these films reported in this study have confirmed that under open circuit conditions an oxide film forms, but to provide good corrosion protection aluminium is polarised at different potentials. The oxide film which forms in these conditions has been found to have both 4 and 6 coordiation. The Al K-edge EXAFS of these oxide films was fitted in the same way as those for the incorporated tungsten. In this case, the

EXAFS of aluminium foil and alpha alumina was fitted by the use of phase shifts calculated in EXCURV92 for aluminium and oxygen. The oxygen and aluminium phase shifts calculated in EXCURV92 were reliable, so they were used to fit the EXAFS of the passivating films on aluminium of unknown structure. The EXAFS results in this study have confirmed that these oxides do not have a single phase crystalline structure like boehmite or any others. Their structure is of a short range order and it is characterised in terms of co-ordination number and shell distances. All of the results reported in the EXAFS section of this work indicate that these oxide films are relatively thin and that is indicated by a metallic aluminium signal present most of the time. The sampling depth of the x-ray photons is much greater than the thickness of the oxide film and for this reason a metallic signal was recorded. By comparing the bond length value to the relation between the bond length and co-ordination number, it is obvious that these oxides films have a mixture of 4 and 6 co-ordination. In some cases, like aluminium polarised to + 0.9 V in pH 10, most of the co-ordination of the oxide is 6 except a little of it in the 4 co-ordination.

XANES spectra for the model compounds and those for oxide films on aluminium and their derivative have agreed with the EXAFS results about the structure of thin films formed on aluminium. Also these findings were complemented by the XPS data where the Al 2p of pseudoboehmite has a binding energy of 80.0 eV whilst that of the oxide films in general were ~ 74 eV. So, it is clear that the oxide films structure is not a psuedoboehmite, but it is a local one with different values for the bond length and as a consequence a mixture of different (4 and 6) co-ordination.

1. Chapter One Introduction

1.1 Introduction

Corrosion of metals, (aluminium in this study) is defined as the surface wastage as a result of different reactions, so it has a devastating effect on the economy. Aluminium is a very reactive metal because of its large free energy. Interestingly enough, this reaction may lead to the formation of oxide layers on the surface of aluminium which may protect the metallic substrate through the passivation process. Anodic reaction of aluminium with aqueous environments, results in the formation of oxide films on aluminium which is fundamentaly interesting as well as commercially rewarding. The passivating oxide films on aluminium provide protection against corrosion, and from a fundamental point of view, they have completely different electronic, vibrational, and structural properties from those of the aluminium substrate. For this reason, a general idea of the corrosion process, as well as its prevention, and passive oxide film formation is of interest.

Aluminium finds application in industry and technology as will be explained in detail in the following sections, due to the presence of a protective film on its surface. Depending on the growth conditions, the oxide film on aluminium can have various morphologies. The type of morphology of the oxide film determines the uses of the film or the aluminium substrate. An account of these uses is given in the next section. In all of the applications of aluminium and aluminium alloys, the oxide film's durability and reliability, which is a direct result of its stability in aqueous environments, depends on its structure and the chemical reactivity on the surface, beside other factors.

Whilst the morphology and composition of alumina films on aluminium are well understood, their structure is far from being resolved. Determination of the structure of these passivating layers and their relation to the anodisation conditions may aid in deciding the range of uses of aluminium and the reasons behind any failure.

Anodic aluminium oxide films are grown on the surface of aluminium, so their characterisation requires the use of techniques sensitive to, and selective of, these surface layers. Traditionally, much information was gained by the use of electron microscopy, especially of the film's morphology. X-ray photoelectron spectroscopy (XPS) has also been employed to characterise the composition of films, their thickness, and, indirectly, to infer structural information. Diffraction techniques which require long range order, are widely used for studies of bulk materials, but are of no use for investigating these oxides, since even though there is still a debate about the structural nature of these passive films, they are generally thought to posess only short range order. On the other hand, x-ray absorption spectroscopy (XAS), specifically extended x-ray absorption fine structure (EXAFS) and x-ray absorption near edge structure (XANES) can provide structural information for materials where only short range order exists. With the increasing availability of intense x-ray sources, in the form of synchrotron radiation sources, XAS which will be discussed in details in chapters 2 and 3, is a natural choice for the study of passive films on metal surfaces.

1.2 Uses of Aluminium

It is well known that, due to its large negative free energy, aluminium is a reactive metal, however despite this, it finds many applications and is the second most widely used metal

after iron. Aluminium owes its applicability in industry and technology to its natural resistance to corrosion, which arises from the existence of an adherent oxide film on its surface. The range of applications of aluminium is determined by the ability of the oxide layer on its surface to protect it from corrosion and degradation. Rather than rely on the air formed film, alumina films are sometimes deliberately grown on its surface by anodisation to enhance the corrosion resistance, e.g. in cooking utensils.

Aluminium is frequently used as a construction material for chemical and water treatment plants and for vessels to store highly corrosive materials, where because of its high corrosion resistance, it is favoured to steel which is more traditionally used. Aluminium also finds usage in the electronics industry, for example as ohmic contacts for semiconductors and in the fabrication of electrolytic capacitors. Because of its light weight and its resistance to corrosion aluminium is also very widely used in the aerospace industry. Foe example, Allgeyer and Pratz (1) have reported on the chemical treatment (passivation) of high strength Al-Cu alloy which was used for the construction of the external fuel tank of the space shuttle.

1.3 Corrosion of metals

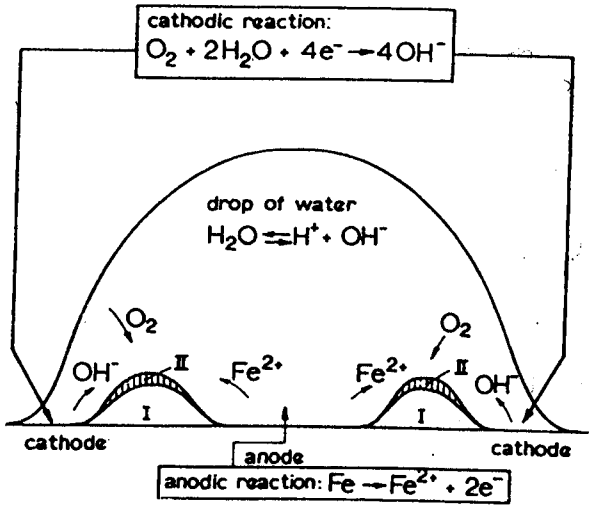

Figure 1.1 *A schematic representation of the corrosion of iron in water*

Corrosion is defined as loss of material through reaction with environment, especially oxygen. Corrosion is an oxidation process where the metallic species combines with oxygen to form an oxide film on the metal's surface which is a more stable phase of matter. In order for corrosion to take place, anodic and cathodic sites are required to complete an electrochemical cell. Frequently, such sites arise as a result of differential aeration (oxygenation). Fig 1.1, shows schematically the corrosion reactions occuring on an iron sample immersed in a neutral aqueous solution where oxidation occurs at an anodic site with simultaneous reduction at a cathodic one. This results in the formation of rust. Rust is the name used in this case to describe a number of oxides and hydroxides of iron. Iron dissolves into the solution as Fe^{2+} ions and simultaneously hydroxyl (OH^-) ions are formed at the cathodic sites as indicated on fig. 1.1. As the solubility product of the hydroxide is

exceeded, an oxide starts to precipitate (rust) which is oxidised by oxygen in the water to a brownish oxy-hydroxide form.

Corrosion affects most materials, especially metals when they are exposed to reactive environments and it causes surface damage which can lead ultimately to mechanical weakness and failure. Corrosion can be considered to take two forms; uniform, and non-uniform. Uniform corrosion is the simplest kind which results in the progressive, and uniform, thinning of the metal. Non-uniform, or localised corrosion, arises due to discontinuities in the geometry of the metal or a protective passive layer, e.g. pitting and crevice corrosion. Pitting is the most destructive type of corrosion and it is usually the result of surface film breakdown or a discontinuity. Another type of non-uniform corrosion occurs when cathodic and anodic sites develop on a metal surface in aqueous solution, galvanic corrosion then occurs as result of the potential difference. The most common form of non-uniform corrosion is crevice corrosion which is a result of oxygen differentiation because the metal surface is at or close to an area which is shielded from the corrosive environment.

1.3.1 Polarisation curves

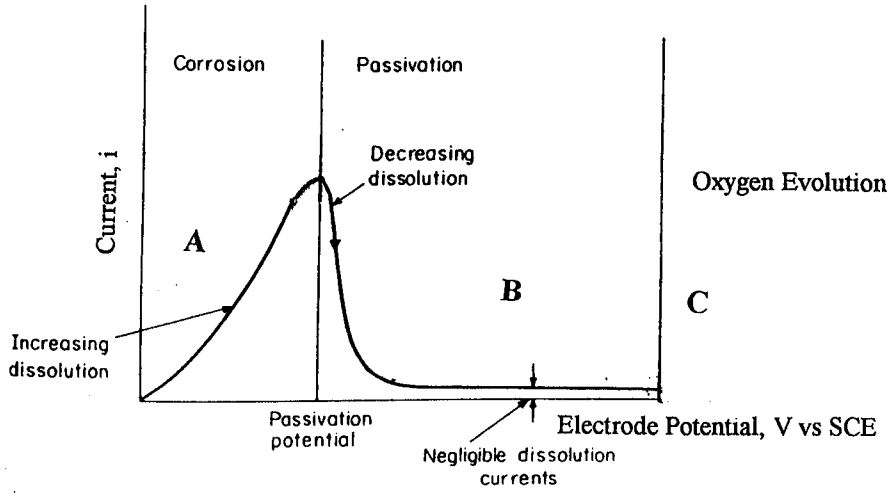

Figure 1.2 *Polarisation curve i-v for a metal exhibiting an active-passive transition*

Metal passivation in electrolyte solutions, as well as other reactions occuring on an electrode surface, e.g. anodic metal dissolution, breakdown of the passive film, or hydrogen/oxygen evolution can be monitored clearly by the use of polarisation curves. These curves are determined by measuring the current (i) as a function of electrode potential (E).

As seen in fig 1.2, starting from region A, as the electrode potential is made more positive, the current rises rapidly indicating that corrosion is taking place. In B region, the current starts to fall because of the formation of a passive oxide film. This film reduces the current to a minimum. As the potential is increased further, some metals exhibit oxygen evolution as seen in region C. This is not the case for aluminium which is a refractory metal. Reversing the sweep may, or may not, lead to the removal of the passivating film,

depending on whether the electrochemical process causing their formation is chemically reversible or not.

1.4 Corrosion prevention

The damaging effects of corrosion can be stopped, or at least reduced, in a number of ways. Some corrosion control techniques are based on separating the reactants from one another, for example, by the application of paints, coatings, or passive film formation. Other methods of combating corrosion include, the use of inhibitors, anodisation, and cathodic protection. Inhibitors, which are generally organic materials that are adsorbed on the surface, cause a reduction in corrosion rate. Chromium has also been used in the form of chromate coatings to reduce corrosion rates. However, this practice is now discouraged because of the toxicity of chromium. Cathodic protection is based on the lowering of the metal potential below its corrosion potential, in effect making it immune to corrosion. This can be achieved by connecting the metal to be protected to another metal which is more reactive. The reactive metal is consumed in the process, hence it is known as a sacrificial anode. Cathodic protection may also be achieved by attaching the metal to be protected to a power supply and holding the system at negative potential. This is the method employed to protect pipelines, as in the petroleum industry, whilst sacrificial anodes are used in protecting ships and household hot water systems. Anodisation is a corrosion prevention technique based on separating the reactants, where the metal to be protected is made the anode in an electrochemical cell. Oxide films of varying thickness, composition, and structure are grown on the metal surface. Oxide films formed in this way are in general called anodic films.

Chapter four of this thesis is devoted to resolving the local structure of tungsten incorporated species in a thick anodic alumina film formed on aluminium by polarising to 100 V in aqueous tungstate solution. The main theme of this thesis is to determine the structure of thin passivating films anodically formed on aluminium at low voltages in aqueous environment at various pH's.

1.5 The Electrochemistry of corrosion

All corrosion processes are electrochemical in nature. In the case of a metal immersed in aqueous solution, atoms may at first dissolve as ions, and then a solid product (e.g. an oxide film) may or may not form by subsequent chemical reactions. The rate of this form of corrosion is determined not only by the conducting properties of the surface film, but also by kinetic factors like, bulk diffusion, and electron transfer reactions.

1.5.1 Pourbaix diagrams

It is very important to determine the state of a metal/water reaction and this can often be achieved with the aid of a Pourbaix diagram. Pourbaix diagrams are potential-pH equilibrium diagrams which provide a graphical representation of the reactions possible between a metal and water for a wide range of pH and voltages. From these diagrams the thermodynamically stable phases under any set of conditions are identified.

These diagrams are produced by the collection of thermodynamic data about a reaction between a metal and water and combining it with information about the solubility of the oxide/hydroxide. It should be noted that Pourbaix diagrams are based solely on equilibrium thermodynamical data and that no kinetic data are included. Regions where a

metal is passive under a set of conditions can be readily identified from the Pourbaix diagrams.

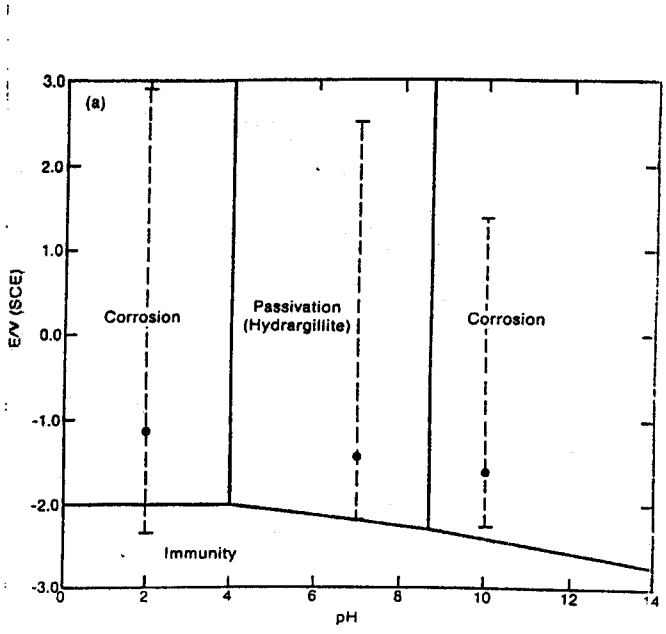

Figure 1.3a Pourbaix diagram where the stable oxide film on aluminium in water is boehmite

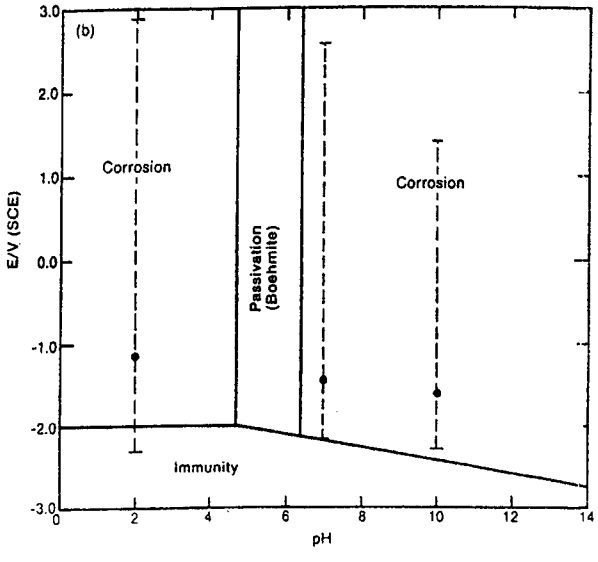

Figure 1.3b Pourbaix diagram where the stable oxide film on aluminium in water is hydrargillite

Figure 1.3 a and b show Pourbaix diagrams for aluminium in aqueous solutions with two different stable oxide films (hydrargillite and boehmite) (2) on its surface. Fig. 1.3 a, shows the regions (at a given pH and potential) where aluminium experiences corrosion, passivity, or immunity with boehmite as the stable form of the film on aluminium in the passive region. Also given in this figure is the corrosion potential for pH 2, 7, and 10 as points. The range of potential at which polarisation was carried out as will be discussed in detail in chapter three is denoted as a dashed line. The same parameters are presented in figure 1.3 b with gibbsite [hydrargillite] being the stable form of the passivating film on the aluminium surface. Immunity is the state of the metal resisting corrosion and anodic dissolution because it is thermodynamically stable on its own. Two of these regions are shown on fig. 1.3 a and b where aluminium is not expected to suffer corrosion. In the passive regions, the metal is resistant to corrosion because of the formation of an adherent oxide/hydroxide film on its surface and it is the stability of this film which determines the range of the metal's usability.

1.6 Anodic alumina films on aluminium

Aluminium and aluminium alloys are generally covered with a thin, compact oxide film which is the result of aluminium oxidation in environments containing oxygen. This film forms spontaneously and has a thickness of ~30 Å. However it has only a limited ability to protect aluminium from corrosion. The native alumina film can be thickened either thermally or electrochemically and it is the latter approach which is of relevance here.

Aluminium is one of the refractory metals, where no oxygen evolution occurs, and the films can be grown up to a thickness of in excess of 100 nm [as will be shown in section

(1.6.1.1)] by increasing the applied potential, until at a critical potential the film may break down. The film grows by a field assisted growth mechanism (3) with the egress of Al^{3+} and ingress of O^{2-} or OH^-. The oxide is therefore formed at both the aluminium /oxide and oxide/solution interfaces as shown by Pringle (4), and Shimizu et al. (5). Solution pH, temperature, time of anodisation, metal purity, and anodising voltage are amongst the factors determining the thickness, composition, morphology, and the structure of anodically formed alumina films.

Alumina films of different morphology can be grown on the aluminium by anodisation in aqueous solutions which is the method used in this study.

1.6.1 The morphology of alumina films

Based on the use of electron microscopy, the morphology of alumina films on aluminium is well understood. Thompson et al. (6-8) have made extensive morphological studies, employing electron microscopy with ultramicrotomy and ion beam thinning to reveal that alumina films on aluminium can have either a barrier-, or porous-type morphology depending upon the growth conditions. Figure 1.4a and b shows these morphologies schematically.

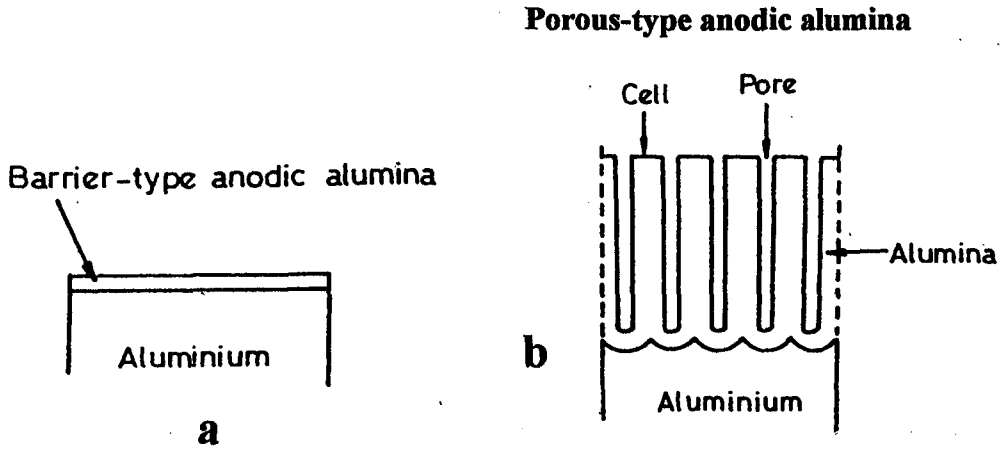

Figure 1.4 a *and* **b** *The morphology of alumina films*

1.6.1.1 Barrier alumina films

As shown in fig.1.4 a, barrier films are thin, compact, and uniform. They also have good dielectric and protective properties. They are formed when near-neutral solutions of borate, citrate, tartrate, phosphate, sulphate, etc. are used as an electrolyte. The buffering action of these electrolytes stops oxide dissolution at the oxide/electrolyte interface, so no pore initiation takes place. The typical voltage/thickness ratio is ~ 1nm/volt i.e. a film of alumina grown on aluminium to 100 V is ~100 nm thick (9).

1.6.1.2 Porous alumina films

As indicated in fig. 1.4 b, porous alumina films are thicker than the barrier-type. They are formed in aqueous phosphoric, sulphuric, oxalic, or chromic acid solutions (10) and the pore initiation is thought to be the result of the acidic electrolytes promoting oxide dissolution (11). Thompson et al. (12) have shown that these porous films always overlie a

thin layer of barrier-type film i.e. the porous films always start as barrier films, then pores start to develop. Even on the thickest of porous oxides, a barrier oxide layer is always maintained, next to the metal. This class of oxide film is used as an ultra filter and for keying in adhesive bonding of aluminium sheets employed in the aerospace industry. The morphology as well as the stability of the oxide film in the presence of water are important factors to ensure the strength and durability of the bond (13).

1.6.2 Electrolyte species incorporation in alumina films

During growth, especially at high voltages, electrolyte species are incorporated into the alumina films. The incorporation of these species can have a desirable effect, such as making the metal more resistant to corrosion. This topic is the subject of chapter four of this thesis where it is explored in more detail in relation to fluorescence EXAFS results of tungsten incorporated into alumina films anodised to 100 V in tungstate electrolytes

1.7 Passivating alumina films

Theories proposed to explain the passivation process involve the formation of a new phase, an oxide, with adsorption as an intermediate step, Griffin (14) illustrated the passivation kinetics of metal and semiconductor surfaces in aqueous solutions by a two-dimensional phase transition model, as shown in fig. 1.5, in which a dilute phase of isolated metal hydroxide ad-ions forms initially (step 1) and is then transformed into a condensed phase of a continuous oxide layer on the metal surface (step 3).

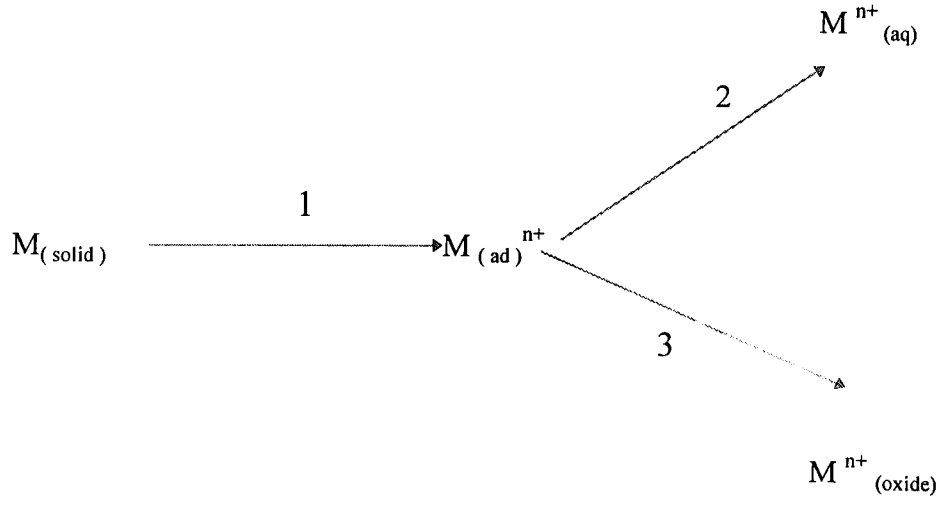

Figure 1.5 *Model of Passive film growth*

Step 2 is a dissolution step (desorption of hydrated metal ad-ions into the aqueous electrolyte). Steps 2 and 3 are in competition until at some critical value of potential, step 3 becomes the dominant process.

The alumina films formed on aluminium immersed aqueous solutions at neutral pH are the result of electrochemical reactions between aluminium and water (15,16). The overall process is shown in Equation 1

$$Al + 3H_2O \rightarrow Al(OH)_3 + 3H^+ + 3e^- \qquad (1)$$

In more acidic solutions (pH=2), the oxide layer dissolves and hence then corrosion rate increases leading to aluminium dissolution

$$Al \rightarrow Al^{3+} + 3e^- \qquad (2)$$

Whilst in alkaline solution, the reaction proceeds into two steps. Initially an anodic film is formed.

$$Al + 3OH^- \rightarrow Al(OH)_3 + 3e^- \qquad (3.a)$$

but then the film dissolves

$$Al(OH)_3 + OH^- \rightarrow Al(OH)_4^- \qquad (3.b)$$

Cathodic polarisation of aluminium in aqueous solutions results in the evolution of hydrogen either by the reduction of protons (at pH=2) or the reduction of water molecules at high pH. These two reactions lead to an increase in the local pH of the solution water near the aluminium surface.

The oxide film formed by polarising aluminium in water can have different compositions, e.g. it can be an oxide, a hydroxide, or an oxyhydroxide. A knowledge of the composition of the surface films leads to a better understanding of how it controls the corrosion behaviour of aluminium in aqueous environments. Augustynski (17) supports the argument that the passive alumina film is a trihydroxide with a chemical formula of $Al(OH)_3$, and it is the most favourable and thermodynamically stable phase. Alwitt (18) reported that a pseudoboehmite, which has the same chemical composition, but slightly different structure, as boehmite (AlOOH), is the oxide that forms on aluminium before evolving to the trihydroxide phase.

1.8 Literature review

Reported work has dealt with different aspects of anodically formed oxide films on aluminium. Using an electron microscope, Hass and Kehlr (19) have examined the structure of a thin alumina film formed in an aqueous solution of an organic acid at room temperature. They found that the images were structureless which suggests that the films were amorphous. Anodic oxides formed on an aluminium surface at 20 V were examined

by Brandenberger and Hafel (20), using x-ray diffraction. Their results suggested that the films had a boehmite like structure. Using electron microscopy, the structure of alumina films on aluminium anodised at constant voltage between 10-15 V in tartaric acid electrolyte at pH 5.5 was studied by Hass (21), who found them to be amorphous.

Oka et al (22) have characterised the amorphous structure of anodic alumina films formed on aluminium in sulphuric acid using a.c. and d.c. growth conditions. X-ray radial distribution function analysis suggested that aluminium ions are co-ordinated with 4, 5, and 6 oxygen ions. Transmission electron diffraction was used by Wilsdorf (23) to study alumina films formed by annealing aluminium in air at 400 °C for 75 hours. The diffraction pattern of these films consisted of two diffuse haloes and a model to explain the amorphous structure was proposed. The model is based on the idea of starting with a crystalline analogue for the alumina film which can be made up of Al_4O_6 units. By arranging these units in different ways, it is possible to obtain a range of average co-ordinations. When atomic defects and bond distortions are present, this leads to disorder resulting in the transformation of the structure to an amorphous state as seen in the following figure

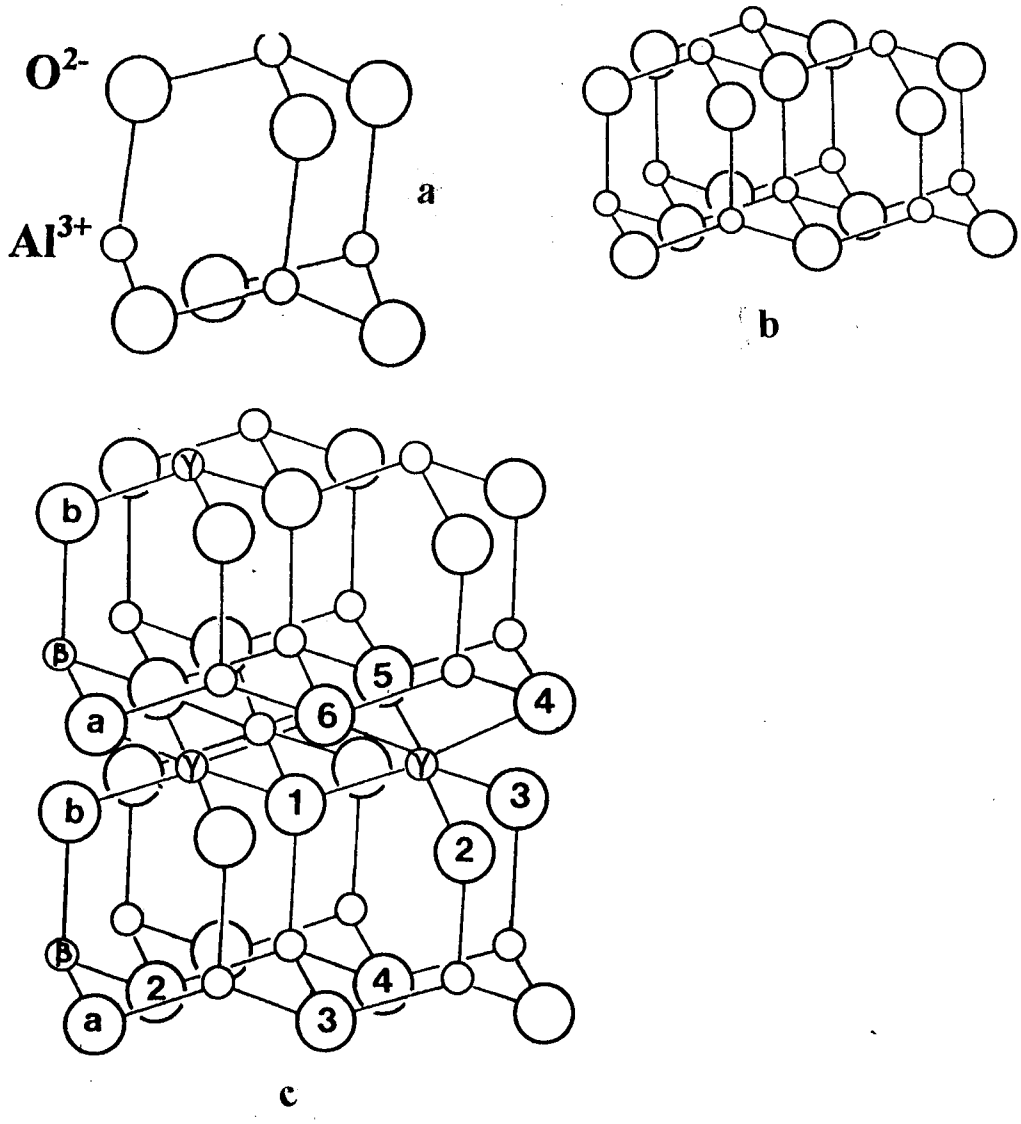

Figure 1.6 a, b, and **c** *Structural model of alumina films on aluminium*

Figure 1.6 represents the model suggested by Wilsdorf for alumina film structures. The model is based on a short-range crystalline order of tetrahedrally and octahedrally co-ordinated aluminium ions in alumina films which is seen in fig 1.6.a. A close packed array

of Al_4O_6 molecular units is shown in fig.1.6.b, whilst fig1.6.c represents three dimensional stacked sheets of the Al_4O_6. β represents an Al^{3+} ion bonded by four O^{2-} ions and γ indicates a six fold co-ordinated aluminium ion. El-Mashri et al.(24) have used EXAFS to establish Al-O bond length for alumina films anodically formed on aluminium in tartarate and phosphoric acid electrolytes. The bond length for a tartarate grown film was reported to be 0.19 nm and for a phosphoric acid grown film 0.18 nm. From the bond length measured in this study, the co-ordination of oxygen atoms surrounding the aluminium was determined to be a mixture of 4, 5, and 6 co-ordination.

When exposed to water, aluminium oxide films are hydrated. This transformation is believed to contribute to materials failure. The hydration process is governed by the type of electrolyte used and the film's morphology. Hunter et al. (25) studied the hydration of alumina layers formed in different electrolytes. They concluded that for the barrier type alumina film, it took 3 minutes in boiling water for the film to start converting into boehmite and complete conversion was achieved after 15 minutes. For porous films formed in acidic electrolytes, the hydration started after 15 minutes and it took a long time for full oxy-hydroxide conversion. Burgers et al. (26) studied alumina films formed on aluminium metal in a boiling solution of borate and boric acid at voltages in the range of 400-500 V and at low current density. In this study a sharp x-ray diffraction pattern was observed corresponding to a crystalline gamma alumina structure.

Even though the composition and the morphology of anodic alumina films on aluminium have been extensively investigated, their structure and especially that of the passivating alumina layers has not been characterised. Most of the earlier structural studies were made by the use of indirect techniques such as x-ray photoelectron spectroscopy

(XPS) which is primarily a technique for probing composition. There is clearly a need for a direct structural investigation of the passive films on aluminium. XAS appears to have the potential for such a study. This is the basis of the work reported in this thesis.

1.9 Objective and plan of thesis

In this thesis, the structure of passivating alumina films on aluminium anodically formed by polarisation in aqueous solutions, as well as for those spontaneously formed, is determined. This work is stimulated by an earlier investigation by Moshier et al.(27), where x-ray photoelectron spectroscopy was used to monitor the evolution of the alumina film structure.

The thesis is divided into seven chapters. Chapter two deals with the theoretical concepts behind the experimental techniques used. Chapter three includes schematic diagrams for the experimental apparatus and describes the procedures followed in preparing the samples and performing the experiments. In chapter four, results are presented for fluorescence EXAFS measured above the L_3 edge of tungsten which is incorporated into a thick anodic alumina during the polarisation of aluminium to 100 V in an aqueous tungstate electrolyte. In chapter five, the electrochemistry (polarisation curves) of aluminium in aqueous solutions, and x-ray photoelectron spectroscopy (XPS) results of oxide films on aluminium are presented along with a depth profiling study. Chapter six contains the extended x-ray absorption fine structure (EXAFS), x-ray near edge structure (XANES), and the reflection EXAFS (ReflEXAFS) spectra measured above the K-absorption edge of aluminium for passivating alumina films formed by simple immersion or polarisation in aqueous solutions at various pH values. These spectra were collected at

Daresbury Laboratory. Chapter seven outlines the conclusion of this work and makes suggestions for further work.

References

(1) Allgeyer, D. H., and Pratz, E. H., Surface and Interface Analysis, **18**(1992)465
(2) Deltombe E., Vanleugenhaghi C., and Pourbaix M., "Atlas of Electrochemical Equilibria in Aqueous Solutions". Pergamon Press, Oxford(1966)168
(3) Young, L., "Anodic Oxide Films", London Academic Press (1970)
(4) Pringle, J. P. S., I. Electrochem. Soc., **119**(1972)482
(5) Shimizu, K., Thompson, G. E., Wood, G. C., and Xu, Y., Thin Solid Films, **88**(1982)255
(6) Thompson G. E., and Wood G. C., in "Treatise on Material Science and Technology", Ed. by Scully J. C., Academic press, New York, **23**(1983)205
(7) Thompson G. E., Furneaux R. C., and Wood G. C., Corros. Sci., **18**(1978)481
(8) Thompson G. E., Xu Y., Skeldon P., Shimizu K., Gan S. H., and Wood G. C., Phil. Mag. B, **6**(1987)651
(9) Scully, J. C., "The Fundamentals of Corrosion", 2nd edition, Pergamon International Library, (1975)13
(10) Davis, G. D., Sun, T. S., Ahearn, J. S., and Venables, J. D., J. Matter. Sci, **17**(1982)1807.
(11) Fukushima, T., Fukuda, Y., Ito, G., and Shimizu, A., J. Met. Finish. Soc. Jap., **25**(1974)542
(12) Thompson, G. E., and Wood, G. C., Nature, **290**(1982)230
(13) Venables, J. D., McNamara, D. K., Chen, J. M., Sun, T. S., and Hopping, R. L., Appl. Surf. Sci., **3**(1979)88
(14) Griffin, G. L., J. Electrochem. Soc., **18**(1984)131
(15) Kaesche, H., "Localized Corrosion" (Staehle, Brown, Kruger and Agrawal, eds.), NACE, Williamsbare, N. A., (1974)516
(16) Craig, H. L., and Scott, J. R, J. Matter., **4**(1969)540
(17) Augustynski, J., "Passivity in Metals", (Frankenthal, R. P., and Kruger, J. eds.), Electrochem. Soc., Pennington, NJ(1978)973
(18) Alwitt, R. S., "Oxides and Oxide Films", Marcel Dekker, New York, **4**(1976)169
(19) Hass, G. and Kehler, H., Koll. Z., **26**(1941)95
(20) Brandenberger, E. and Halef, R., Helv. Chim. Act., **31**(1948)1168
(21) Hass, G., J. Opt. Soc. Amer., **29**(1949)532
(22) Oka, Y., Takahashi, T., Okada, K., and Iwai, S., J. Non-Cryst. Solids, **30**(1979)349
(23) Wilsdorf, H. G. F., Nature, **168**(1951)600
(24) El-Mashri, S. M., Jones, R. G., and Forty, A. J., Phil. Mag. A., **48**(1983)665
(25) Hunter, M. S., Towner, P. F., and Robinson, D. L., Amer. Electro-plat. Soc., Tech. Proc., (1959)220
(26) Burgers, W. G., Claassen, A., and Zernicke, J., Z. Phys., **74**(1932)592
(27) Moshier, W. C., Davis, G. D., and Ahearn, J. S., Corros. Sci., No-8, **27**(1987)785

2. Chapter Two Theoretical Aspects of the Experimental Techniques

2.1 Introduction

The electrochemistry of the growth of passivating alumina films in aqueous solutions is monitored by the use of linear sweep voltammetry (LSV) which is discussed in the next section.

Theoretical aspects of x-ray absorption spectroscopy (XAS) used to characterise the structure of thin films on aluminium, including EXAFS, XANES, and ReflEXAFS as well as the relevant methods used for their detection are outlined. Fluorescence yield, employed to measure EXAFS above the tungsten L_3 edge; total electron yield, used to measure EXAFS, XANES, and ReflEXAFS at the aluminium K-edge; and transmission, used to collect EXAFS spectra for a very thin aluminium foil, are discussed. The extraction of structural information (bond length and co-ordination number) from the experimental data, including background subtraction and curve fitting is described.

The basic principles of x-ray photoelectron spectroscopy (XPS), used in this study to provide information about the composition and relative thickness of thin films on aluminium in aqueous environments, are also presented.

2.2 Electrochemical Techniques

The potential sweep techniques; linear sweep voltammetry (LSV) and cyclic voltammetry (CV) find wide application in monitoring electrode/electrolyte reactions.

They are employed to provide an "electrochemical spectrum" (1) indicating potentials at which different electrochemical processes occur.

Linear sweep voltammetry is the simplest of this class of techniques. It involves sweeping the potential applied to the electrode with a wave-form generator, from a value E_1 to E_2. In the case of the CV technique, the sweep is reversed when E_2 is reached and the cycle may be repeated a number of times, whilst in the LSV technique the sweep is performed from E_1 to E_2 just once. In both techniques, the resultant current density is plotted as a function of the potential applied. A wide range of sweep rates can be used, but for polarisation curves in passivation studies a small rate is preferred so that the data are obtained under pseudo-steady conditions.

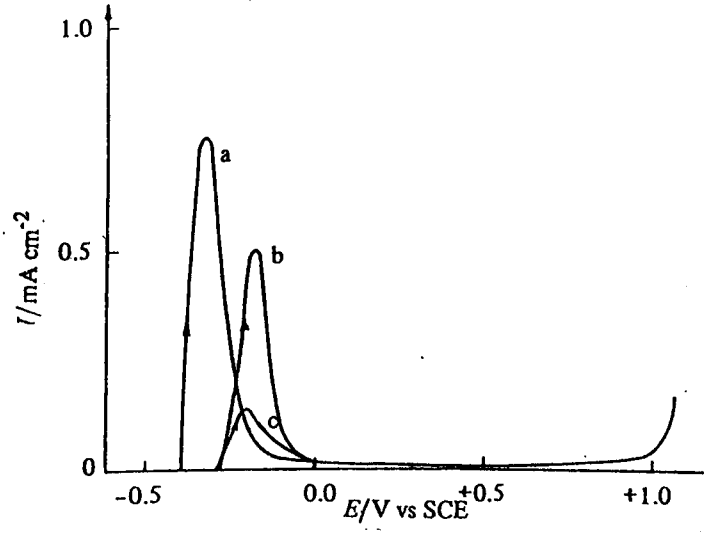

Figure 2.1 Potentiodynamic curves for steel in H2SO4 a, b, and c are 304 L, 800 L, and 316 L steels respectively (2)

Fig. 2.1 shows an example of potentiodynamic curves for the passivation process on different types of steel (2) in H_2SO_4. These are presented to demonstrate the ability of the LSV technique to record the electrochemical behaviour of different materials. As the

film grows on the metal surface with increasing applied potential, the current density increases, until an oxide forms and becomes thick enough to separate the reactants, thus forming a passivating layer. The presence of this passivating layer greatly reduces the current density. Reversing the potential sweep from E_2 to E_1, may or may not, depending on the reaction involved, remove the passivating layers. Interpretation of the polarisation curves can yield information about the processes taking place, e.g. dissolution, oxide film formation, film breakdown, oxygen or hydrogen evolution.

In this study, potential sweep voltammetry is used in the LSV mode, for quantitative recording of the electrochemical behaviour of pure aluminium metal in aqueous 0.05 M sodium sulphate electrolyte solutions.

2.3 X-ray Absorption Spectroscopy (XAS)

2.3.1 Introduction

Through their interaction with matter, either by diffraction or absorption, x-rays have played a significant and important role in revealing the structure of different materials with both long and short range order parameters.

The x-ray absorption spectroscopy technique generally requires an intense and continuous source of x-rays. Synchrotron radiation fulfils these requirements, and in recent years, as more synchrotron radiation sources have become available, more beam lines have been dedicated to x-ray absorption spectroscopy. Since the 1970's, the EXAFS technique has developed from a mere scientific curiosity to one with an exact theoretical explanation and understanding. One of the fields in which EXAFS has been increasingly employed is the characterisation of electrochemical systems, e.g.,

passivating oxide films on electrode surfaces (3), monolayer deposition (4), fuel cells and batteries (5), and the adsorption of different species on electrode surfaces (6).

Figure 2.2 shows a schematic diagram of the x-ray absorption spectrum of Krypton gas.

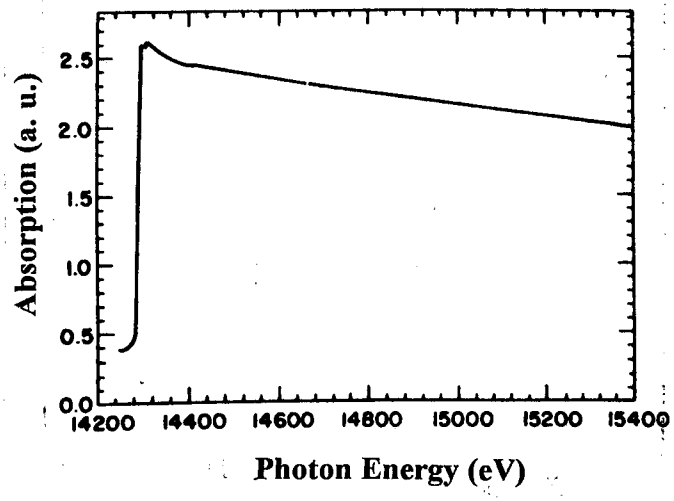

Figure 2.2 An EXAFS spectrum of a monatomic Krypton gas

The x-ray absorption coefficient, (μ) of the sample is measured as a function of photon energy ($h\upsilon$). As the incident photon energy is swept through the threshold of a core electron excitation, photons are absorbed and photoelectrons are ejected, reducing the transmitted flux of x-ray photons. The sudden increase in absorbance as the photon energy is increased occurs when the photon energy is equal to the binding energy (E_b) of a core electron, and is called the absorption edge. Absorption edges are characteristic of the absorbing atom. The edge is called a K-edge when the excited core level is the 1s level, and an L-edge for excitation from the 2s or 2p levels.

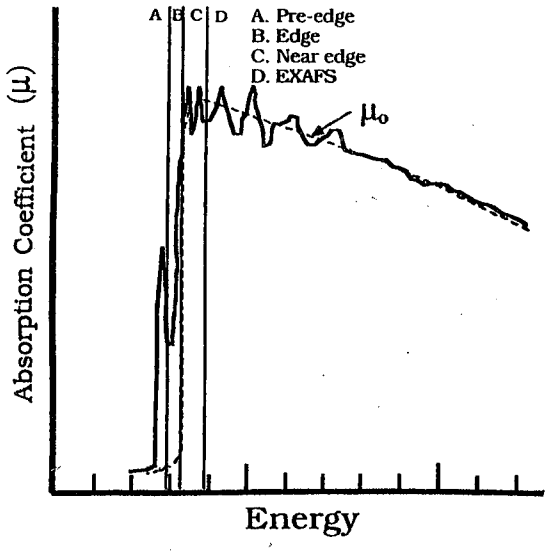

Figure 2.3 A Schematic diagram of different regions on the EXAFS and XANES spectrum of a solid

Fig 2.3, on the other hand, shows a typical absorption spectrum for a solid. It is clear that there is structure in the edge region, and extending well above it. The structure in the edge region and up to ~ 50 eV above it, is known as x-ray absorption near edge structure (XANES), whilst the region extending from the edge to 1000 eV, or more, above it is known as extended x-ray absorption fine structure (EXAFS). The structural features in the XANES region are due to the multiple scattering effects and bound state transitions. One of the first explanations for the EXAFS phenomenon was given by Kronig (7) who explained it as the result of the energy gaps at the Brillouin zone boundaries thus

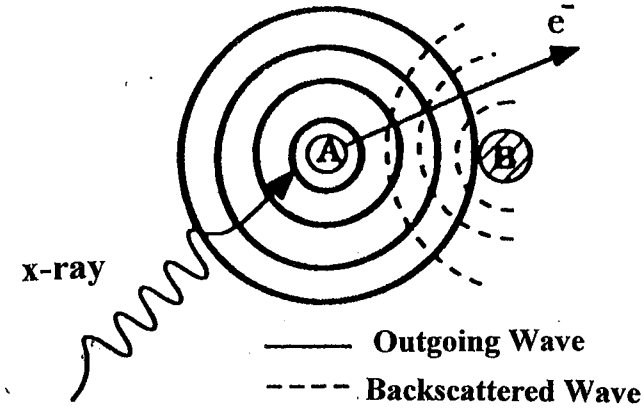

Figure 2.4 Absorbing process of an atom surrounded by neighbours

treating it as a long-range order phenomenon. Now it is realised that the EXAFS of condensed matter is in fact a short range order effect, which can be most simply explained with reference to fig 2.4.

When the incoming x-ray photon has sufficient energy to photo-ionise the absorber A, a photo-electron wave propagates from the absorber and this wave is backscattered by neighbouring atoms e.g. B. Interference between the two waves at A results in a modulation of the x-ray absorption cross section and hence oscillation in the absorbance. The probability of a core electron absorbing an x-ray photon depends on its initial and final state, where the initial state is the localised state defining the absorption edge, whilst the final state is the sum of the out-going and the backscattered waves.

2.3.2 EXAFS Theory

Over the years, an increasingly complex theoretical description of EXAFS has been developed and many factors have been added to account for physical processes which affect the EXAFS phenomenon. The true structural capabilities of the EXAFS technique were only realised when Sayers et al. (8) treated the atoms surrounding the absorbing one as a system of weak point scatterers. This short-range single electron scattering theory gave the technique the ability to solve the structure of disordered, as well as ordered systems. Lee and Pendry (9), and Ashby and Doniach (10) were amongst the many workers who have contributed immensely to formalising EXAFS theory. Stern (11) has treated the out-going and backscattered photoelectrons as spherical waves, whilst Gurman et al.(12) have developed a rapid, exact, curved-wave theory for EXAFS

calculations. To speed up calculation routines, a small atom approach (13) can be used. In order to identify the various contributions to the EXAFS oscillations, it is necessary to define the EXAFS function $\chi(k)$ as

$$\chi(k) = \frac{\mu - \mu_0}{\mu_0} \qquad (2.1)$$

Where $\mu_0(k)$ is the absorption cross-section of an isolated atom, and $\mu(k)$ is the absorption cross-section of an atom in a condensed environment. Based on the small atom approximation presented by Gurman (12,13), the EXAFS formalism for a K-edge is given in wave vector form as : k

$$\chi(k) = \sum_i \frac{N_i}{kr_i^2} |f(k)| exp(\frac{2r_i}{\lambda_i}) exp(-2k^2\sigma_i^2) sin[2kr_i + \Phi_i(k)] \qquad (2.2)$$

Where $k = [(8\pi^2 m/h^2)(h\nu - E_0)]$ is the photoelectron wave number, N_i is the number of backscattering atoms in a neighbouring shell at a distance r_i from the absorbing atom, $|f(k)|$ is the backscattering amplitude of atoms in the shell, λ_i is the mean free path of the photoelectron and $\Phi_i(k)$ is the total phase shift encountered by the photoelectron due to the absorber and backscatterer's potentials.

$$\Phi_i(k) = \phi_i(k) + 2\delta_l \qquad (2.3)$$

δ_l is the phase shift due to the absorber atom, whilst ϕ_i is the phase shift due to the backscattering atom. The reason for having twice the value of the phase shift due to the absorber is that the ejected photoelectron experiences the absorbing atom potential twice, when leaving the absorber, and when returning after being backscattered by the neighbouring atoms. The term, $exp(\frac{-2r_i}{\lambda_i})$ is an amplitude reduction term which

accounts for inelastic losses in the scattering process. $exp(-2k^2\sigma_i^2)$ is the Debye-Waller term where σ^2_i is the mean square variation in r^2_i which accounts for the thermal vibration and static disorder. It is clear from this expression that $\chi(k)$ is a summation of sine wave functions with $2kr_i$ as their period. This feature may be exploited in a simple analysis where a Fourier transform of this expression yields peaks corresponding to different shells of backscattering atoms.

2.3.3 EXAFS data analysis

To extract structural parameters; such as interatomic distances (bond length), number and type of backscattering neighbours from EXAFS spectra, a consistent data analysis procedure must be followed. The procedure includes E_0 setting, possible deglitching, pre- and post-edge background removal, edge normalisation, and extracting of the EXAFS signal $\chi(k)$. Once $\chi(k)$ has been determined, Then the curve fitting using a program such as EXCURV (14) is performed.

2.3.3.1 Pre-edge background subtraction and normalisation

As seen in figure 2.5a, to remove the pre-edge background, a low order polynomial is fitted and subtracted from the region before the edge. Post-edge background subtraction, involves the subtraction of the smoothly decaying atomic absorption function $\mu_0(E)$ from the EXAFS absorption coefficient $\mu(E)$. It is a common practice to approximate the smooth part of $\mu(E)$ from extrapolation of $\mu_0(E)$ at energies where the EXAFS has decayed to zero. Polynomial splines of the second or third order are typically used for background subtraction routines. After pre- and post-edge background

subtraction, the EXAFS is normalised by dividing by the absorption cross section of an isolated atom (μ_0), i.e. the post edge background.

2.3.3.2 EXAFS in wave vector form

A threshold energy, E_0 is set so that an expression of EXAFS can be made in terms of wave vector (k). An accurate value for E_0 should be chosen, since its value has a direct effect on the phase shift of the EXAFS oscillations, especially at low wave vector values. Lee and Beni (15) suggested that different E_0 values should be tried until the phase shift values agreed with the theoretical one. A widely used alternative method is of choosing the E_0 value as that of a good model compound with known structure (16-18). In this work, the E_0 used was that of the inflection point in the absorption edge. In earlier versions of the EXCURV analysis program, E_0 was treated as an iterative parameter until a good theoretical fitting for the experimental results was obtained. The change in value of E_0 in EXCURV92 (19) which is employed for data analysis in this work, is no longer a fitting parameter, since the phase shifts are more accurately determined than in previous versions of this program.

2.3.3.3 k-weighting

In fig. 2.5 b, an example of the k^3 weighted EXAFS of W L_3-edge of potassium tungstate is shown. To reduce the effect of the $1/r^2_i$ factor in equation 2.2, and the k dependence of the backscattering amplitude, the EXAFS is typically weighted by multiplying by k^2 or k^3. This weighting procedure is performed so that the small oscillations observed at high k values are made comparable in amplitude to the large

oscillations at low k values. Changes in weighting factor should not change the fitting parameters, which is a good test for the quality of the fitting.

2.3.3.4 Fourier transform

The EXAFS expression in wave vector form is made up of sinusoids with a phase and an amplitude. As shown in fig. 2.5 c, a Fourier transform of the EXAFS is given by

$$\phi(r) = \frac{1}{\sqrt{2\pi}} \int_{k_{min}}^{k_{max}} k^n \chi(k) exp^{(2ikr)}\, dk \qquad (2.4)$$

is thus, as was first suggested by Sayers et al (8), a radial distribution function, which exhibits peaks at the interatomic distances between the absorber and each of the backscattering shells. To optimise the fit, a Fourier filtering technique is often used to isolate each shell, before the data are back transformed to k-space where the amplitude and the phase fitting is carried out.

2.3.3.5 Fitting for the phase

An early method of analysis involved comparing the peak position in the Fourier transform of the measured EXAFS function for model compounds, with the known crystallographic parameters. The difference between the peak positions and the known nearest neighbour distance was attributed to the phase shift which was then used to correct the nearest neighbour distances obtained from the peak positions in the Fourier transform for the unknown material. A better, and now almost universal, method is to calculate phase shifts which are then checked by fitting data for model compounds. Once acceptable phase shifts have been obtained structural data for unknown materials

are obtained by fitting the observed EXAFS function in k-space. The accuracy of bond length determination may be within 0.01Å, whilst typically only 20% is possible for co-ordination number determination, due to correlation with the disorder term.

2.3.3.6 Fitting for amplitude

Fitting for the amplitude gives information about the type and the number of backscattering atoms in each shell. Identifying different species from the EXAFS spectrum is based on the variation of the backscattering amplitude for different atomic numbers. Teo and Lee (20) calculated the backscattering amplitude as a function of wave vector and showed that it is easier to differentiate between heavier elements than between lighter ones.

2.3.4 X-ray absorption near-edge spectroscopy (XANES)

The XANES region as seen in fig. 2.2 can be rich in structural information and contains strong oscillations. In this thesis, no mathematical expression will be given for the XANES region, only an account of the process and the physical essence of XANES is presented. Bianconi (21) defined the energy separating the XANES region from that of the EXAFS as the energy of the excited electron when its wavelength equals the bond length between the absorber and backscatterer.

A theoretical understanding of the electronic structure in condensed matter is achieved by studying the low-lying extended electron states (22). These states are responsible for bonding the system together and determine its electronic properties. Electron states giving rise to XANES include the unoccupied states from the Fermi level to the point where EXAFS starts.

As an example of importance of the XANES region in probing the structure of oxide films on metal electrodes (aluminium in this study), Chung et al. (23) have reported on the chromium species which incorporates into alumina oxide material grown anodically on aluminium at high potential from an aqueous electrolyte containing chromate ions. XANES studies for this system have provided the co-ordination around Cr (absorber) and its valency. Observations of Cr K-edge shift which is the result of changes in valency, presence of peaks before the edge, as well as a shape resonance which are associated with the Cr being in a tetrahedral co-ordination has led to the conclusion that both Cr (III) and Cr (VI) oxidation states are present in the alumina films. Also they have been able to explain the direction of the mobility of the incorporated Cr as a result of transformation caused by the field during film growth. Davenport et al. (24) have used in-situ XANES to monitor the changes in Cr valence states in passive films formed by polarising a ~ 20 Å Al- 12% Cr alloy. They found that Cr valence state can be changed reversibly without dissolving the 6 valent state.

In this thesis, XANES spectra of alumina model compounds with known structure are used in a qualitative manner to show different features of thin alumina oxide films prepared as described in this work. The method is called "finger-printing" and it can be used to give information about the local atomic environment of the absorber

2.3.5 EXAFS detection methods

EXAFS and XANES spectra are measured by various methods. The nature of the absorber, its concentration, and the experimental set-up determine the method chosen for EXAFS detection. In all EXAFS detection methods, the x-ray absorption coefficient

is measured either directly from the attenuation on passing through a sample, as in transmission, or by recording something that is proportional to the absorption, e.g. x-ray fluorescence or the electron (Auger, partial, or total) emission.

2.3.5.1 Transmission EXAFS

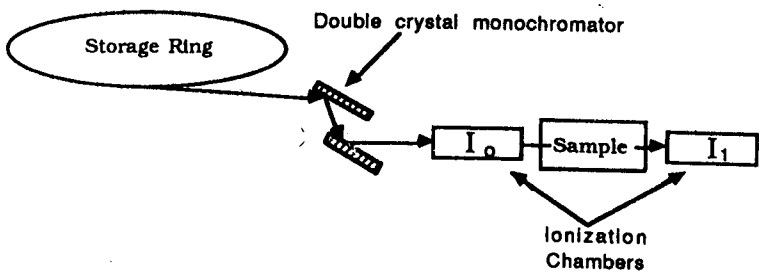

Figure 2.6 A transmission EXAFS arrangement

Transmission EXAFS is the only direct method for x-ray absorption coefficient measurement. It is based on the measurement of x-ray intensities before and immediately after the beam of photons has passed through the sample. Transmission EXAFS is mostly used for thin concentrated and uniform samples. Two ionisation chambers with high gain electrometers are used to measure the x-ray intensities, one after the monochromator for (I_0) measurement, and as seen in fig. 2.6, the second one after the sample for transmitted intensity (I_t). The following relation gives the transmitted intensity, I_t

$$I_t = I_0 \exp(-\mu x) \qquad (2.5)$$

where x is the sample thickness and μ is the linear x-ray absorption coefficient

$$\mu = 1/x \ln(I_0/I_t) \qquad (2.6)$$

Transmission EXAFS data are plotted as $\ln(I_0/I_t)$ versus E where E is the energy of the x-ray photons. Even though transmission EXAFS is easy and direct to measure, it is not

suitable for investigating passivating surface films, because these films overlie the metal substrate. Instead, it is possible to record EXAFS spectra of these films and surface layers by detecting something that is proportional to the x-ray absorption, arising from the relaxation of the excited absorber atom. These methods include fluorescence and electron yield which are both proportional to the absorption cross section in the EXAFS region. Alternatively, reflection EXAFS can be measured for very flat surfaces.

2.3.5.2 Fluorescence EXAFS

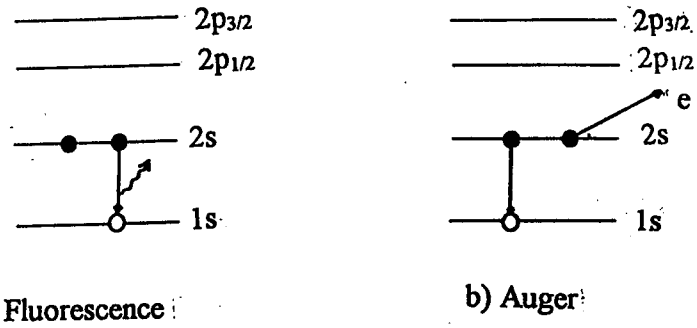

Figure 2.7 Atomic relaxation processes, a) fluorescence b) Auger

The transmission technique is inappropriate for dilute and/or thick samples and therefore, fluorescence is used as an alternative method to monitor EXAFS (25). Fig 2.7 shows the possible processes by which a core hole may be filled. Fluorescence is a radiative process where an atom relaxes from an excited state to the ground state by the release of photons. The photon energy is the difference in energy between the two shells Fluorescence can be detected by different means. For relatively concentrated samples, ion chambers can be used. However, ion chambers suffer from poor discrimination against scattered radiation, so to overcome this problem, solid state detectors are often

utilised. Filters are commonly used to keep out scattered radiation and thereby avoid saturation of the detectors. The fluorescence method is capable of investigating the structure of mono- or even submono-layer systems. This method has a good elemental sensitivity but it is not surface selective because x-rays have a large penetration depth and the fluorescence signal originates from deep in the material.

2.3.5.3 Electron yield EXAFS

Auger-, partial-, or total- electron yield can also be used to monitor EXAFS. Electrons emitted in EXAFS can only come from the surface and near-surface region because of their small mean free path (26,27). It should be noted that, x-ray fluorescence and electron emission (Auger) are always in competition. The dominance of one of these processes over the other is determined by the atomic number of the excited atoms. The branching ratio of these processes is such that electron yield is favoured at low energy (light elements), whilst fluorescence is favoured at high energy (heavy elements). Hence, electron yield EXAFS is useful in investigating the structure of surfaces and thin films.

The Auger electron yield used to monitor EXAFS is surface selective and for this reason it is employed in surface EXAFS (SEXAFS). A detector with energy discrimination capable of selecting only the Auger yield is used. A window can be used to separate the Auger emission from the dominant secondary electron yield (28). Auger-electron yield EXAFS is mainly used for probing the structure of surfaces.

In total electron yield EXAFS, all electrons emitted are recorded without regard to their energy. Auger-, photo-, as well as the inelastically scattered electrons. Total electron yield (TEY) was first used by Lukirskii and Brylov (29) to measure EXAFS

spectra, whilst Gudate and Kuntz (30) were the first to use synchrotron radiation sources to record EXAFS in this mode. Due to their mean free path, photoelectrons detected in TEY-EXAFS originate from and near the surface region, so it has a good sensitivity and greater surface selectivity than other modes. TEY-EXAFS has a sampling depth of ~ 100 Å. Electron yield is suitable for measuring EXAFS for thin surface films of low Z elements such as the passive films on aluminium, because of its surface sensitivity and selectivity and also the electron yield sampling depth is comparable to the thickness of the films. Jones and Woodruff (31) showed that TEY-EXAFS is suitable for analysing the structure of alumina films.

2.3.6 Reflection EXAFS (ReflEXAFS)

Total reflection EXAFS is valuable in solving the local structure of flat reflecting surfaces. The surface sensitivity of this method may be explained by considering the x-ray optics (32,33). When the refractive index is slightly less than 1, which it is for a metal for example, total external reflection is possible. The refractive index is given by

$$\eta = 1 - \delta - I\beta \qquad (2.7)$$

where

$$\delta = 1/2\pi\,(e^2/mc^2)\,(N_0\rho/A)\,[Z+\Delta f]\,\lambda^2 \qquad (2.8)$$

and

$$\beta = \lambda\mu/4\pi \qquad (2.9)$$

where (e^2/mc^2) is the electron radius, $(N_0\rho/A)$ is the number of atoms per unit volume, N_0 is Avogadro's constant, ρ is the density, A is the atomic weight, Z is the atomic number, λ is the wavelength of the x-ray photon, $[Z+\Delta f]$ is the real part of the scattering factor, f is the imaginary part of the refractive index, this factor is related to the linear

absorption coefficient, μ. The critical angle θ_c for total reflection of an x-ray beam from a smooth surface which is derived from Snell's law, is.

$$\theta_c = \sqrt{2\delta} \qquad (2.10)$$

The critical angle is of the order of a few hundred millidegrees, In ReflEXAFS, the ratio of the reflected and incident intensities is measured as a function of energy (34). The physical process leading to ReflEXAFS is complicated further because the reflectivity is a complex function of the angle of incidence, energy, and the refractive index. The penetration depth of this technique is ~ 20 Å, so it is highly a surface selective technique.

2.4 X-ray Photoelectron Spectroscopy (XPS)

2.4.1 Introduction

Photoelectron spectroscopy (PS) is a technique where photons are absorbed by atomic species at or near the surface region. As a result of this absorption process, photoelectrons acquire energy and are ejected into the vacuum. The kinetic energy of these electrons is analysed by the use of an electron energy analyser. The energy of the incident radiation determines the type of electron states that are probed. When helium lamps are used as the source of the incident photons, to excite states in the valence band, the technique is called ultraviolet photoelectron spectroscopy (UPS). When x-ray line sources such as Al $K\alpha$, Mg $K\alpha$ are the source of the incident photons, core level states are excited and the technique is called x-ray photoelectron spectroscopy (XPS) (35),. which is used to probe the electronic structure of materials.

Because of the small mean free path of the emitted photoelectrons, XPS is a surface specific technique. These emitted photoelectrons have a specific binding energy which makes XPS capable of identifying chemical species on the surface. Also XPS is used to characterise the chemical environment surrounding the absorbing atom in different phases including surfaces and thin films on solids (36-38). An important area of XPS application is the measurement of chemical shifts. These shifts can be used to gain information about oxidation states and charge transfer for different chemical bonds in molecules and solids. Recent developments in synchrotron radiation sources have made it possible to perform XPS measurements at different energies with a better intensity and resolution than that achieved with a conventional x-ray source.

2.4.2 Theory of XPS Process

In XPS, if the incident photons have sufficient energy $h\upsilon$ [Mg K_α (1253.6 eV) or Al K_α (1486.6 eV)] to ionise an atom, an electron which is bound to the solid with binding energy B_E, escapes the solid. The kinetic energy E_k of the emitted photoelectrons is given the conservation of energy

$$E_k = h\upsilon - B_E + \phi_s \qquad (2.11)$$

In this equation ϕ_s is the spectrometer work function, the value of $h\upsilon$ is known and the kinetic energy of the ejected electron can be measured by an electron energy analyser, thus B_E can be deduced from equation 2.11.

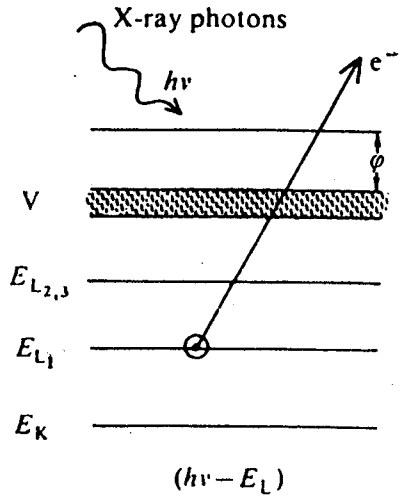

Figure 2.8 Physical process of the XPS

The physical process which leads to XPS is seen schematically in fig. 2.8. In this example, an electron from an L_1 state absorbs an incoming x-ray photon with energy $h\upsilon$, then the electron which was bound to the atom in the solid with binding energy E_b, is released into the vacuum. As the x-ray photon energy is scanned by the use of a crystal monochromator, a peak is recorded for the electron state.

The XPS spectrum is dominated by an intense sharp emission peaks. As seen above, these peaks are the result of the transition from the core state of the atomic species on the surface to the continuum. The energy of the emission peak is determined primarily by the energy of the core states. When the absorbing species are surrounded with other elements like oxygen in oxides, the position of the emission peak is shifted because the core state has a different energy and this shift is called the chemical shift. Physically, chemical shift appear as the result of the relaxation shift due to the core level

creation (photoemission) which is accompanied by other electrons relaxing to lower energy states, and thus screening the hole created. Tabulation of chemical shift data for different atomic species in different compounds with known structural parameters are used (fingerprinting). XPS spectra may be complicated further by the presence of other features including, inelastic loss "tails" due to the weak absorption of the incident x-rays and multiple plasmons losses.

2.4.3 Electron Energy Analysers

Electron energy analysers are used to measure the number of electrons within a defined energy range. The recording of XPS spectra requires the use of a sensitive electron detector with good energy resolution. Such detectors typically operate on the basis of electrostatic deflection where two parallel plates with different potentials create a field between equally spaced constant potential surfaces. Electrons entering the analyser with different kinetic energy will travel different distances through the field resulting in their separation. To reduce the effect of energy spread caused by the angular spread of the ejected electrons, an analyser capable of focusing electrons is desirable.

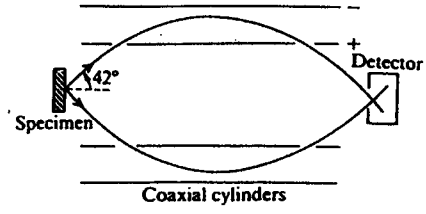

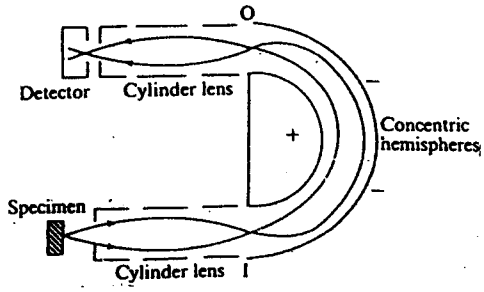

Figure 2.9 Schematic diagram of cylindrical mirror analyser (CMA) and concentric hemispherical analyser (CHA)

The cylindrical mirror analyser (CMA), and the concentric hemispherical analyser (CHA) are two types of electron energy analyser that achieve this. Their design, which is shown in fig. 2.9, is widely used in surface spectroscopy techniques. It is always desirable to have a high sensitivity and high resolution, but in reality it is a compromise situation, where good resolution would result in lowering the sensitivity. In electron energy analysers, the resolving power is determined by geometrical factors, whilst the sensitivity depends on $\Omega / 2\pi$ which is the fractional solid angle and 2π is the total solid angle.

References

(1) Greef R, Peat R, Peter LM, Pletcher D, and Robinson J; in "Instrumental Methods In Electrochemistry" Ellis Horwood Limited Publishers (1985)178
(2) As in reference 1, p. 212
(3) Long, G. G., Charger, J., and Kuriyama, M., in "Passivity of Metals and Semiconductors"., ed. M. Froment, Amsterdam Elsevier, (1983)139
(4) Samant, M. G., Borges, G. L., Gordon, J. G., Melroy, O. R., and Blum, L., J. Am. Chem. Soc., **109**(1987)5970
(5) McBreen, J., O'Grady, J. E., and Pandya, K. I., J. Power Sources, **22**(1988)303
(6) Lu, F., Salita, H. N, Baltruschat, H., and Hubbard, A. T., J. Electroanal. Chem. and Interfacial Electrochemistry, **222**(1987)305
(7) Kronig, R. del, Z Phys., **75**(1932)468
(8) Sayers, D. E., Stern, E. A., and Lytle, F. W., Phys. Rev. Lett., **27**(1971)1204
(9) Lee, P. A. and Pendry, J. B., Phys. Rev. B, **11**(1975)2795
(10) Ashby, C. A., and Doniach, S., Phys. Rev. B, **11**(1975)1279
(11) Stern, E. A., Phys. Rev. B, **16**(1979)3027
(12) Gurman, S. J., Binsted, N., and Ross, I., J. Phys. C, **17**(1984)143
(13) Gurman, S. J., J. Phys. C, **21**(1988)3699
(14) Gurman, S. J., Binsted, N., and Ross, I., J. Phys., Solid State Phys., **19**(1986) 1845
(15) Lee, P. A., and Bemi, G., Phys. Rev. B, **15**(1977)2682
(16) Hayes, T. M., Sen, P. N., and Hunter, S. H., J. Phys. C, **9**(1976)4357
(17) Cramer, S. P., Dawson, J. H., Hodgson, K. O., and Hager, L. P., J. Am. Chem. Soc., **100**(1978)7282
(18) Tullius, T., Frank, P., and Hodgson, K. O., Proc. Nat. Acad. Sci., USA, **75**(1978)4069
(19) Binsted, N., Campbell, J. W., Gurman, S. J., and Stephenson, P. C., "SERC Daresbury Laboratory EXCURV92 Program", (1991)
(20) Teo, B. K., and Lee, P. A., J. Am. Chem. Soc., **101**(1979)2815
(21) Bianconi, A., App. Surf. Sci., **6**(1980)392
(22) Faulkner, J. S., Prog. Mater. Sci., **27**(1982)3
(23) Chung, S. W. M., Robinson, J., Thompson, G. E., Wood, G. C., and Isaacs, H. S., Phil. Mag. B-, **63**(1991)557
(24) Davenport, A. J., Isaacs, H. S., Frankel, G. S., Schrott, A. G., Jhanes, C. V, and Russak, M. A., J. Electrochem. Soc., **138**(1991)337
(25) Heald, S. M., Keller, E., and Stern, E. A., Phys. Lett., 103A(1984)155
(26) Hasse, J. Applied Phys. A, **38**(1985)181
(27) Landman, U., and Adams, D. L., J. Vac. Sci. Tech., 14(1977)466
(28) Stohr, J., Johnsson, L. I., Brennan, S., Hecht, M., and Miller, J. N., Phys. Rev. B, **22**(1980)4052
(29) Lukirski, A. P., and Brylov, I. A., Soviet Phys-Solid State, **6**(1964)169
(30) Gudate, W., and Kunz, C., Phys. Rev. Lett., **29**(1972)169
(31) Jones, R. G., and Woodruff, D. P., Surf. Sci., **114**(1982)83
(32) James, R. W., "The Optical Principles of the Diffraction of X-rays", London, Bell, (1948)

(33) Bilderback, D. H., SPIE Proc., **315**(1982)90
(34) Martens, G., and Rabe, P., Phys. Stat. Solidi A, **58**(1980)415
(35) Siegbhan, K., Nordling, C., Fahlman, A., Nordberg, R., Hamrin, K, Hedman,, J., Johnsson, G., Bergmark, T., Karlsson, S., Lindgren, I, and Lindberg, B, in "ESCA, Atomic, Molecular, and Solid State Structure Studies by Means of Electron Spectroscopy". Almqvist and Wiksells Boktryckeri Ab. Stockholm, 1967
(36) Turner, D. W., Baker, C., Baker, A. D., and Brundle, C. R., "Molecular Photoelectron Spectroscopy". Wiley Interscience, London, 1970
(37) Apker, L, Tafi, E., and Dickey, J., Phys. Rev., **74**(1948)1462
(38) Eastman, D. E., in "Techniques of Metals Research VI".(E. Passaglia. ed), Interscience, New York, (1972)413
(39) Eastman, D. E., in "Proceeding of the IV International Conference on Vacuum Ultraviolet Radiation Physics". Hamburg, (1974), (E. E. Koch et al. eds.), Pergamon-Vieweg., (1975)417

3. Chapter Three Experimental Details

3.1 Introduction

In this chapter, details of the preparation of aluminium metal samples as a bulk material and as films on glass microscope slides are outlined. The electrolytes, electrodes, and the potentiostat used for growing passivating alumina layers on aluminium surfaces are also described.

Since the aim of this work is to investigate the structure of the passive alumina films, a powerful and direct structural technique capable of analysing disordered and amorphous systems, as well as crystalline ones, is required. To obtain structural information about the alumina films in this study, x-ray absorption spectroscopy (XAS) was employed. Extended x-ray absorption fine structure (EXAFS), x-ray absorption near edge structure (XANES) and reflection EXAFS (ReflEXAFS) were used to determine the structure of alumina films on aluminium. Total electron yield and total external reflection EXAFS and XANES spectra were collected on the SOXAFS station on beamline 3.4 at Daresbury synchrotron radiation source (SRS), whilst station 9.2 was used to collect fluorescence EXAFS at the L_3 edge of tungsten in alumina films. The experimental apparatus used for collecting EXAFS, XANES, and ReflEXAFS spectra reported in this thesis are outlined and a brief description of x-ray sources, and in particular the synchrotron radiation source at Daresbury is presented.

X-ray photoelectron spectroscopy (XPS) was used to characterise the chemical constituents of the oxide layers on aluminium. Different aspects of XPS including the

apparatus, scans performed, data analysis, depth profiling and other related matters are described.

3.2 Sample Preparation

3.2.1 Aluminium metal bulk sample preparation

The samples used in this study were cut from a 99.9999% purity sheet of aluminium metal formed by the zone refining technique (Péchiny). To ensure a reproducible working electrode surface with no imbedded impurities, a pre-treatment process was required. Aluminium samples of 1, 2, and 3 cm^2 were cut, mounted by sticking them to a disk made of resin, and ground flat using SiC paper. Because aluminium is a soft metal, a special mechanical polishing routine was used to polish the aluminium electrodes. A mirror-like aluminium surface finish could be achieved when a set of 30μm, 6μm, and a 3μm oil based polishing liquids was used. Diamond based liquids were not used because they scratched the aluminium surface at the end of each polishing routine. Instead a colloidal silica was used as an abrasive material, in conjunction with a soft cloth for the final finish. The surfaces of the aluminium metal samples were pre-treated by the Forest Products Laboratory (FPL) process (1,2). This process involved; de-greasing by immersion in acetone for ~ 20 minutes, rinsing in distilled de-ionised water (D-D water), drying in nitrogen gas, before cleaning and etching in a solution containing $Na_2Cr_2O_7.H_2O$,H_2SO_4, and H_2O in a 1:10:30 ratio by weight (3). The specimens were then thoroughly rinsed in D-D water and dried with nitrogen gas prior to electrochemical or chemical treatment. On completion of the experimental treatment, the samples were rinsed and dried in the same manner as described above. Then the

samples were stored in a desicator under vacuum at room temperature until their transfer to Daresbury Laboratory for x-ray absorption analysis.

3.2.2 Aluminium film sample preparation

Samples for ReflEXAFS measurements were prepared as thin films of aluminium on glass by evaporating 99.997% purity aluminium wire onto a glass microscope slide in a vacuum chamber (Ion. Tech. Ltd. Teddington, UK). The base pressure of the chamber was maintained at 10^{-6} Torr, using an oil diffusion pump aided by a rotary pump. Glass microscope slides were cleaned by immersion for 1 hour in solution of Decon-90 detergent for degreasing. Distilled de-ionised water was used to rinse the slides and nitrogen gas was used to dry them. The clean microscope slides were placed in the vacuum chamber, whilst the aluminium wire was placed in a tungsten wire basket. The tungsten basket was electrically heated leading to the evaporation of the aluminium wire and the consequent deposition of aluminium film on the glass slides. The same treatment (immersion, passivation) procedure as for the aluminium bulk samples was followed. It is noted that under certain conditions of water pH and potential, the aluminium film were completely or partially washed away. Such samples were unsuitable for investigations by the ReflEXAFS technique.

3.3 Electrochemical Techniques

In this experiment, a three electrode electrochemical cell (3) was used along with an instrument to supply and vary the applied potential to the working electrode as shown in fig. 3.1.

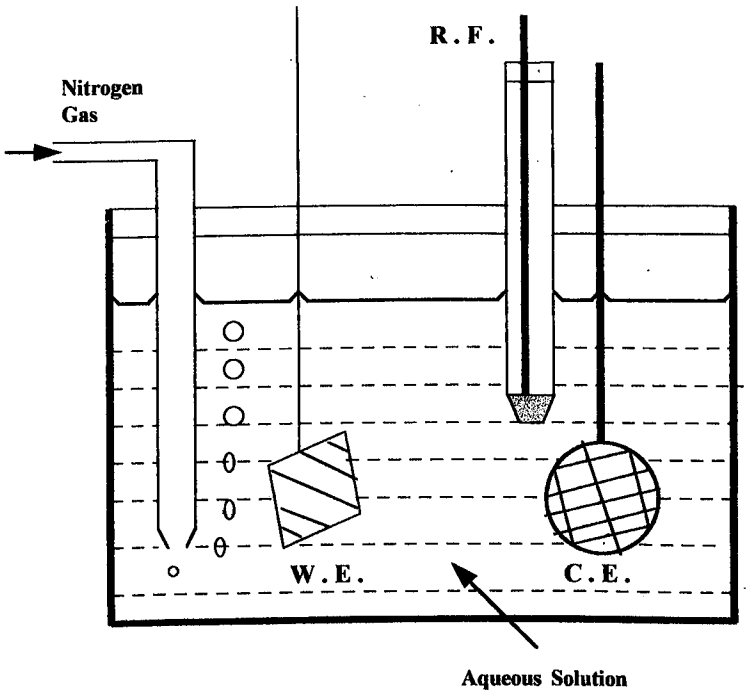

Figure 3.1 Electrochemical cell used in polarisation experiments

The cell comprises a Pyrex glass beaker with a PTFE cover through which the working, reference, and counter electrodes, as well as the nitrogen gas supply, entered. Nitrogen gas was bubbled through the solution to displace dissolved oxygen. Aluminium metal samples were connected to the potentiostat by an aluminium wire. The counter, or secondary electrode (C.E.) used was a platinum mesh, whilst the reference electrode was a saturated calomel electrode (SCE). The reference electrode was placed in a separate compartment with a glass frit in the bottom to minimise the engress of chloride ions into the main part of the cell. The glassware used for the electrolyte solutions was cleaned by soaking in solution of Decon-90 detergent as a degreaser followed by rinsing in distilled deionised water. The electrolyte solutions were prepared from Na_2SO_4 (Analar Reagent) and distilled deionised water, and their pH adjusted to the desired value by the addition of a small amount of NaOH or H_2SO_4.

The working and the counter electrodes were arranged parallel to ensure that the current on the working electrode was uniform. Immersion and immersion/polarisation of aluminium was performed in de-oxygenated solutions as a result of nitrogen bubbling in the solution which also served as an agitator of the solution. This was done to minimise the local build-up of reaction products and to limit changes in the pH of the solution near the working electrode surface. Immersion and polarisation were carried out at room temperature. Prior to polarisation, samples were immersed in the electrolyte for 40 minutes for the surface to reach equilibrium. The equilibrium potential (known as the corrosion potential) was measured and any subsequent polarisation started from this value.

The potentiostat used in this experiment was DT 2101 (Hi-Tek. Inst) along with a waveform generator type PPR1 (Hi-Tek. Inst.) to apply and vary the potential of aluminium electrodes. The polarisation curves were recorded by the use of an *X-Y* recorder (PL4 J.J. Lloyds Inst.).

Aluminium bulk and film samples were treated by immersion for different periods of time in deoxygenated water adjusted to pH 2, 7 and 10. During the immersion nitrogen gas was bubbled into the solution. The electrochemically treated samples were first immersed as described above, then a potentiodynamic sweep was started from the corrosion potential to different anodic and cathodic values in the range of - 2.17 V to + 2.5 V. A sweep rate of 5 mV/s was used throughout the polarisation experiments.

3.4 Synchrotron based experimental techniques

3.4.1 Synchrotron radiation facility at Daresbury Laboratory

In this section, the role of synchrotron radiation sources in providing high intensity x-ray sources is considered. Experimental station, namely, 9.2 EXAFS station and 3.4 SOXAFS stations are described. Different aspects of these station as well as data collection and analysis are outlined.

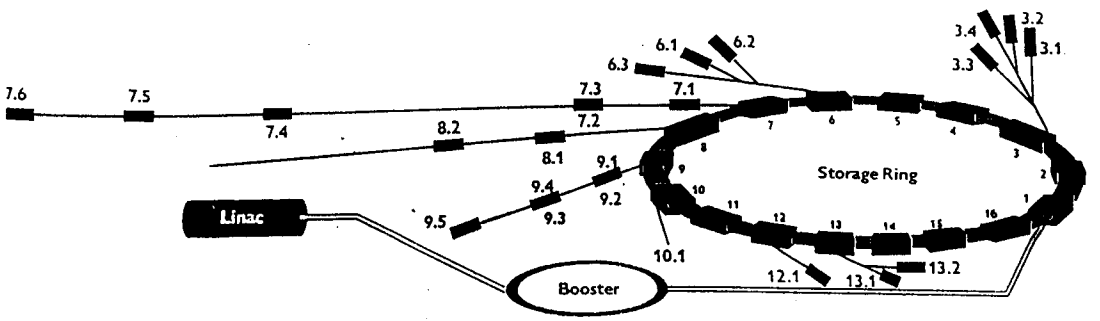

Figure 3.2 layout of the SRS at Daresbury

It was not until the 1950's that the role of synchrotron radiation as a light source for the development of soft x-ray spectroscopy, was realised (4).

The synchrotron radiation source SRS at Daresbury seen schematically in fig. 3.2, was the first dedicated radiation source to be used as a research tool. Fig. 3.2 displays different elements of the SRS at Daresbury.

A hot cathode is used to produce electrons which are accelerated to 12 MeV in the linear accelerator (LINAC), they are then injected into the booster synchrotron where their energy is increased to 600 MeV. The final energy of the electrons reaches 2 GeV in the storage ring. To make the electrons follow a circular path in an evacuated tube,

sixteen dipole magnets are used. A high power radio frequency (RF) accelerator system is used to boost the energy of the electrons to 2 GeV as well as to compensate for the energy

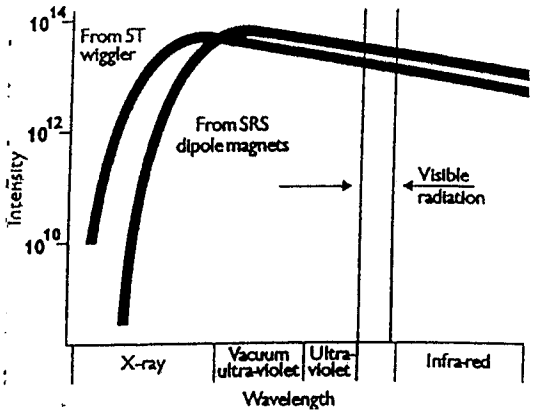

Figure 3.3 Distribution of the Emitted radiation of the SRS

lost by the emitted synchrotron radiation. On average electrons have a 20 hours lifetime in the 96 m circumference storage ring.

Fig. 3.3 shows different radiation regions of radiation (x-rays, ultraviolet, infrared) produced from the 5 Tesla Wiggler and the SRS dipole magnets, displayed as intensity as a function of wavelength. Traditionally the radiation in all beamlines has been produced by the dipole magnets of the storage ring and thus has the same spectral features. Recently, insertion devices which are periodic magnetic structures assembled in the straight part of the ring have been used to produce radiation of different properties at different beamlines determined by the experimental requirements. Wigglers and undulators are two forms of the insertion devices. As seen in fig 3.3, the radiation spectrum emitted by the 5 Tesla wiggler of the SRS at Daresbury is shifted to shorter

wavelengths. Undulators being interference devices produce a sharp peaked and discontinuous spectrum.

3.4.1.1 EXAFS station 9.2 of the SRS

Station 9.2 was used to collect fluorescence-EXAFS above the tungsten L_3 edge to investigate the environment around the tungsten which is incorporated into thick alumina films anodically formed on aluminium polarised to 100 V in tungstate electrolyte.

This station shown in fig. 3.4 (5) is a versatile instrument for glancing angle x-ray absorption spectroscopy and reflectivity EXAFS.

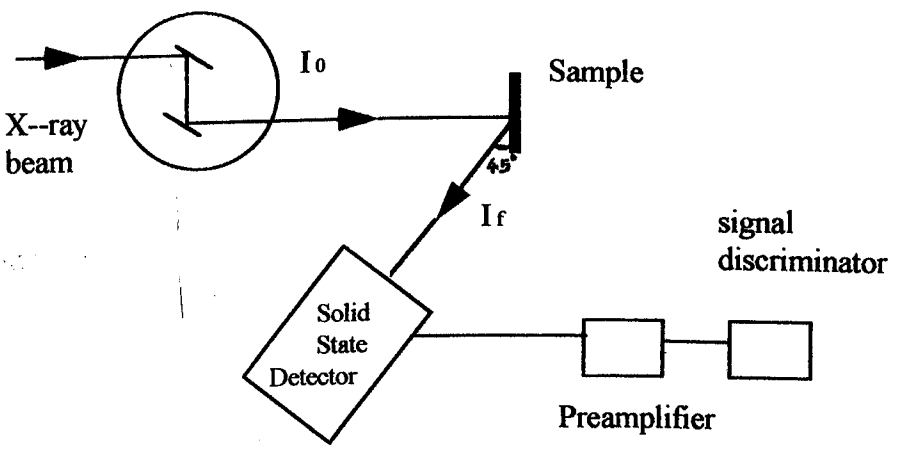

Figure 3.4 layout of station 9.2 of the SRS at Daresbury

The instrument comprises: basic frame/optical bench, collimation system, sample stage, and a computer control system. The whole instrument sits on a motorised table, so that it can be adjusted with respect to the beam position. The sample stage is made up of a large two-axis goniometer and a specimen holder.

By changing the angular position of a mirror, a beam of x-rays was focused and its high energy cut-off was adjusted to help remove harmonics from the monochromatic beam. The intensity of the incident beam (I_0) was measured by the use of an ionisation chamber made of stainless steel and filled with a mixture of Xenon and Helium gases. The chamber was connected to a power supply operated at 300 V and the ratio of the two gases was set so that only a maximum of ~ 20% of the incident beam was absorbed.

The beam was made monochromatic by the use of two Si(220) single crystals configured as a double crystal monochromator. The second crystal of the monochromator arrangement was used to provide harmonic rejection and maintain the direction of the beam. After the monochromatic beam strikes the sample, fluorescence EXAFS above the L_3 tungsten edge was measured by an array of 12 Germanium solid state detectors positioned at 45° to the sample in the plane of the storage ring. Solid state detectors are chosen for fluorescence EXAFS measurement because of their excellent discrimination level. The angle of 45° was chosen for the detector position to minimise the effect of scattered radiation. The signals from the solid state detectors go through an electronic arrangement including a preamplifier and a signal discriminator. Fluorescence EXAFS scans of tungsten L_3-edge were started at ~ 10000 eV which is pre-edge and was continued beyond the edge (10200 eV) up to 11100 eV. Conventional transmission spectra were also recorded for a tungsten foil (5μm) and for potassium tungstate. Four fluorescence EXAFS spectra were collected for the tungsten L_3 edge in alumina films which is the subject of structural characterisation.

3.4.2 Soft X-ray station on beamline 3.4 of the SRS

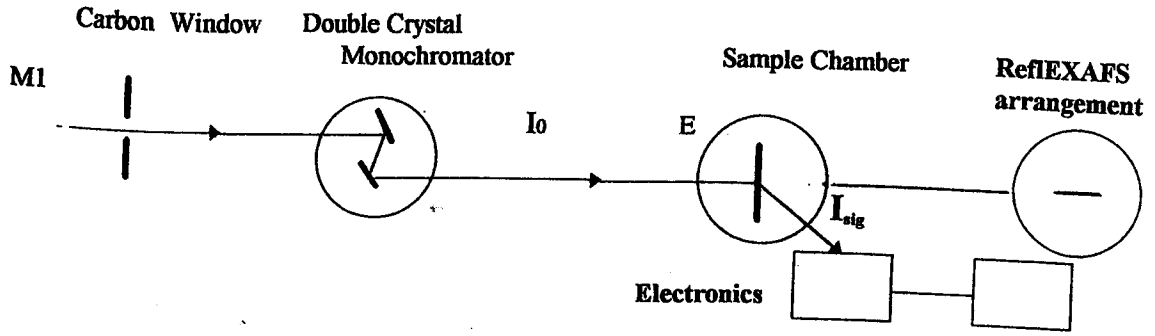

Figure 3.5 SOXAFS station layout

The soft x-ray beamline (station 3.4) of the SRS at Daresbury was developed for EXAFS studies covering materials with low energy absorption edges within range of 0.5-5 keV (6). The station layout is shown schematically in fig. 3.5 including the mirror, the double crystal monochromator, and the HV sample chamber.

M1 is a toroidal Cr-coated mirror which deflects and focuses the beam in the vertical plane. Through appropriate choice of glancing angle at the mirror, the mirror acts also as a low pass filter, cutting off high energy radiation and thereby protecting the thermally sensitive monochromator crystals (made of materials like quartz and beryl). The 4000 Å thick carbon window is used for two purposes; firstly to separate the monochromator from the UHV part of the beamline. Secondly to screen out the VUV and UV part of the radiation which can lead to an increase in the background signal. Two valves positioned on either side of the carbon window are used to protect against pressure differences.

In figure 3.5, F represents a choice of either a 250 μm beryllium or a 1.5 μm aluminium filter. These filters are inserted in the beam's path to remove UV radiation. The energy of the radiation incident upon the sample was determined using a double crystal monochromator fitted with a pair of (1010) quartz crystals. The two monochromator crystals were mechanically linked, whilst the first crystal could be rotated, the second could be both rotated and translated. The first element of the monochromator was water cooled to reduce thermal effects whilst the second crystal could, if necessary, be "de-tuned" by rotating slightly from the bragg condition to reduce the harmonic component in the incident beam. Generally however the high energy cut-off of the focusing mirror was set such that there was no harmonic component in the energy ranges studied.

To measure I_0, the intensity of the x-ray beam after passing the monochromator, a 0.5 μm beryllium foil was used. The I_0 signal was measured as the drain current on the beryllium foil by a picoammeter capable of measuring currents in the range of 10^{-12} A. The total electron yield signal, I_{sig}, was measured as the drain current of the sample. A Kiethley 427 current amplifier was used and because of the very low signal measured all of the electronics were operating at the limit of their sensitivity.

The sample chamber E shown in fig.3.5 included a multiple stage sample holder which held up to 10 samples on special plates made of stainless steel or aluminium. The samples were stuck onto the plates by a conducting copper foil, and slotted into the side of the sample holder. The separation of the centres of the samples was 15.5 mm. A mechanism was provided so that any sample on the sample holder could be positioned in the path of the x-ray beam. For beam centering, a plate coated in an x-ray sensitive

phosphor was loaded into the lowest slot of the sample holder. The sample holder arrangement and the vacuum pumps used throughout the station were designed with the intention of fast pump-down time, as well as efficient use of the synchrotron source. A Balzers 330 ls^{-1} turbomolecular vacuum pump was employed to achieve a base pressure of $7x10^{-7}$ -10^{-8} Torr in the sample chamber in a short period of time. X-ray beam size at the sample was adjustable and it had dimensions of ~ 5 x 0.2 mm^2.

As seen in Fig. 3.5, the SOXAFS can be utilised to measure the EXAFS in the total reflection mode. To perform ReflEXAFS experiments, the sample arrangements, E, has to be pulled out of the beam path.

3.4.2.1 Data collection and analysis

Control and movement of the double crystal monochromator, as well as the recording of the measured I_0, and I_{sig} were performed by the use of a computer. EXAFS and XANES spectra could be divided into many regions. Depending on the relative importance of the region measured, the number of energy points, and the time for measurements at each point could be set accordingly. Other scan parameter; such as start and end of the scan, number of regions, and the number of scans could be pre-set as well.

Scans started around 1520 eV which is 40 eV before the aluminium K edge and continued until 1820 eV which is close to the Si K-edge at 1832 eV. This limit is set by the presence of Si in the quartz monochromator crystals. In EXAFS scans, the energy was incremented in 1 eV steps for the pre- and the post edge regions whilst a step of 0.5 eV used for the edge region. In XANES spectra, the energy was increased by the same value except for the edge region where 0.2 eV was used for good resolution and to

observe any structural features in the edge region. EXAFS scans took ~ 55 minutes on average, whilst XANES required ~ 25 minutes. Multiple EXAFS scans for the same sample were necessary for good data analysis. The data collected by the use of the SOXAFS station was transferred to another computer where the analysis was carried out.

3.4.3 ReflEXAFS apparatus on beamline 3.4 at Daresbury

3.4.3.1 Introduction

In this section a description of the newly built and fitted arrangement on the 3.4 beamline (SOXAFS station) enabling the performance of ReflEXAFS at phosphorus, silicon, sulphur, and aluminium K-edges is given (7,8).

3.4.3.2 Apparatus description

The same beamline elements shown in fig. 3.5 for total electron yield TEY-EXAFS were used for the grazing angle EXAFS set-up with the sample holder pulled out of the x-ray beam path.

The ReflEXAFS apparatus as shown in the schematic diagram of fig. 3.6 has two ionisation chambers to measure the incident and reflected beam intensities, and a sample table with variable position and variable angle of reflection. The ReflEXAFS chamber was separated from the rest of the SOXAFS station by a thin polymer window.

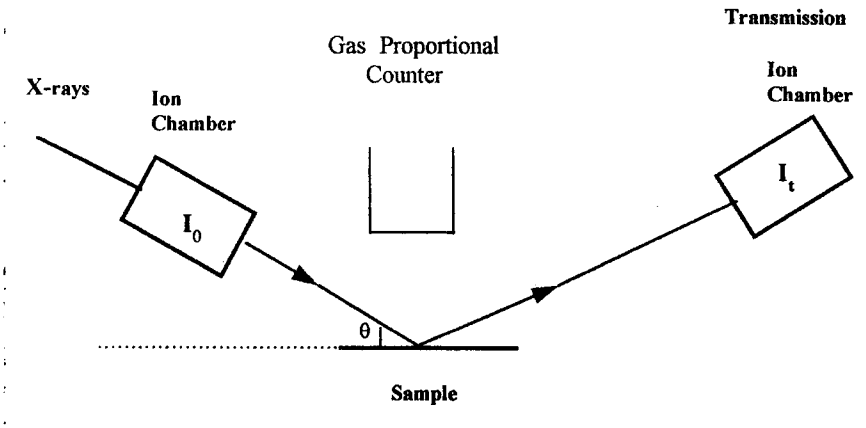

Figure 3.6 Schematic diagram of the ReflEXAFS apparatus

To carry out ReflEXAFS measurements, beam and sample alignment was essential. The front slit was vertically adjusted to be in line with the beam. This was done by moving the slit until a maximum signal was recorded by the front ion chamber. Next, the rear slit vertical position was aligned, with the sample table retracted from the beam line, by vertical movement until a maximum signal was recorded by the rear ion chamber. At this stage, the x-ray beam in the experimental arrangement was aligned. The sample alignment was performed to make the sample surface parallel to the beam and the sample rotation axis to coincide with the mid-point of the beam. This procedure was carried out by measuring the signal at the rear ion chamber as the sample stage was scanned in the rotational and vertical directions. This was performed with the help of a the LabView (9) programme run on a Macintosh computer. Once a maximum signal was recorded in the rear ionisation chamber by rotating the sample, the sample stage was raised to cut out 50% of the x-ray beam. This alignment procedure was carried out several times in an iterative manner. Then, the rear slit was replaced by a beam stop.

The function of the beam stop was to block the direct x-ray beam from entering the rear ion chamber.

The reflectivity was then recorded as a function of the angle of the incidence. This enabled the critical angle ϕ_c to be determined. All ReflEXAFS spectra were recorded at angles less than the critical value.

3.4.3.3 ReflEXAFS data collection and analysis

ReflEXAFS scans were carried out in the same manner as for the TEY-EXAFS, using the same computer and control unit of station 3.4. ReflEXAFS spectra were collected for each of the differently treated aluminium film samples. Analysis of the ReflEXAFS data was performed in the same manner as for the total electron yield EXAFS of passivating alumina films.

3.5 X-ray photoelectron spectroscopy (XPS)

3.5.1 Introduction

In this work, XPS spectra were measured for films naturally formed on aluminium metal exposed to air, and the films formed by immersion in 0.05 M Na_2SO_4 electrolyte with different pH values. Also thin layers on aluminium formed by anodic and cathodic polarisation to different voltages in the same electrolyte were investigated by XPS

3.5.2 Sample Treatment

Bulk aluminium metal bulk samples of 1 cm^2 area were mechanically polished in the same manner with those used for EXAFS and XANES studies. Then they were either exposed to air, immersed in aqueous solutions at pH 2, 7, or 10, or immersed and

cathodically or anodically polarised. They were then quickly removed from the solution, rinsed in distilled de-ionised water, and dried by nitrogen gas. They were then mounted on a sample stub and transferred to the XPS spectrometer for data collection.

3.5.3 XPS apparatus

The XPS spectrometer used in this study was a VG type with an ESCALAB-5 analyser and Mg and Al Kα x-rays sources. The apparatus had a separate introduction chamber for fast pump-down time, and a sample chamber containing the main elements, including the source and analyser. A schematic diagram of the ESCALAB-5 is shown in figure 3.7.

A concentric hemispherical (CHA) type analyser was used with the VG-XPS spectrometer in this study to measure XPS. Kuyatt and Simpson (10) have shown that the resolution of the CHA for equal entrance and exit apertures is given by

$$\text{Resolution} = r/R \qquad (3.1)$$

where r is the radius of the entrance and exit aperture

R is the mean radius of the analyser

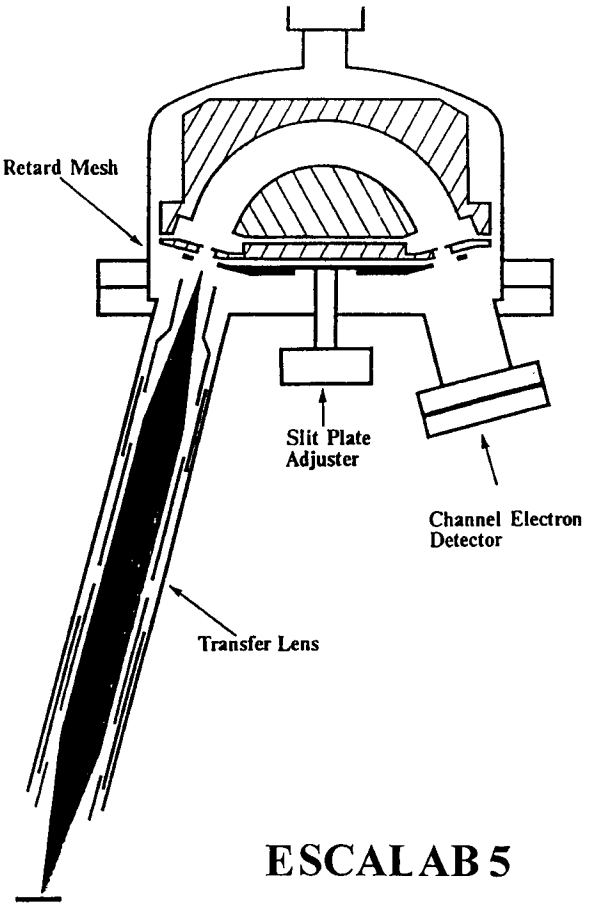

Figure 3.7 layout of the VG-XPS spectrometer

Therefore, the resolution of the analyser can be increased by reducing the aperture size. The lens system consists of two Einzel lenses. The lens potential was varied in proportion to the kinetic energy of the electron to be analysed. The specimen was mounted at a distance from the analyser so that an optimal resolution and intensity were obtained. The operating regime used in the ESCALAB-5 kept the retardation potential constant whilst the lens potential was varied.

3.5.4 Data collection and analysis

Wide energy XPS scans were performed on the "as received" aluminium samples after each treatment to identify the species present in the oxide film formed on its surface. The samples were placed on the end of a transfer system in the introduction chamber and the chamber evacuated to the same pressure as the main chamber HV conditions, of ~ (10^{-7}- 10^{-8}) mbar required for the XPS measurements.

Layer by layer depth profiling of the films was achieved by the use of sputtering with an argon ion gun. The argon gun was typically operated at 2 keV.

Alumina oxide films are insulators and as they lose electrons through the photo emission process a charge starts to build on their surfaces. There are many ways by which the effects of this charge build-up can be corrected. The method used in this work, was to measure the shift in the binding energy of the 1s state of the C atoms. Aluminium surface contamination with carbon is the result of its exposure to CO and CO_2 found in abundance in the laboratory environment during handling and transfer to the XPS introduction chamber. The binding energy (E_b) of the C 1s should have a value of 284.6 eV. Any deviation from this value should be corrected for. The C 1s line was measured in every scan to check whether there was a charge build-up. For better statistical accuracy in exact determination of the binding energy and its shift, in some cases up to 10 narrow scans with an average time of ~12 minutes for each scan were collected and averaged. An energy step of 0.1 eV was used in these scans.

A curve fitting program was used for deglitching, and background subtraction. The curve fitting program also allowed binding energy determination, and peak integration. The Al 2p state due to aluminium and the oxide, C 1s, as well as, the O 1s were measured in the range of 1400-1425 eV, 1190-1215 eV, and 940-970 eV respectively.

References

(1) Davis GD, Sun TS, Ahearn JS, and Venables JD, J Materials Science, **17** (1982)1808

(2) Eichner, H. W., Schowalter, W. E., Forest Product Laboratory, Madison, WI, Report No. 1813(1950)

(3) Greef R, Peat R, Peter LM, Plecher D, and Robinson J; in "Instrumental Methods In Electrochemistry", Ellis Horwood Limited Publishers (1985)357

(4) Tomboulian DH and Hartman P, Phys. Rev., **102**(1956)1423

(5) Daresbury Laboratory report, DL/SCI/P598E

(6) LabView from National Instruments, 6504, Bridge Point Parkway, Austin, TX 78730-3030, USA

(7) McDowell AA, West JB, Greaves GN and Van der Laan G, Rev. Sci. Instrum., **59**(1988)843

(8) Roper MD, Buksh PA, Kirkman IW, Van der Laan G, Padmore HA, and Smith AD, Rev. Sci. Instrum, **63**(1992)1822

(9) Kirkman IW and Buksh PA, Rev. Sci. Instrum., **63**(1992)869

(10) Kuyatt, C. E., and Simpson, J. A., Rev. Sci. Instrum., **38**(1967)103

4. Chapter Four Fluorescence EXAFS of Tungsten in Alumina Films

4.1 Introduction

As has already been described when aluminium is anodised at large positive potentials, an anodic oxide film grows. It is now well established that in certain electrolyte solutions, ionic species from the solution are incorporated into the oxide film (1,2). These species may change the oxide film properties and can influence their solubility/stability. One feature which makes investigating these species economically rewarding is that in some instances they may cause a big reduction in the corrosion rate which is a desirable property.

In this chapter, a first attempt to investigate the local structure around tungsten incorporated into anodic alumina films on aluminium polarised at 100 V in tungstate aqueous solution by the use of the EXAFS technique, is reported.

4.2 Electrolyte Species Inclusion into Anodic Film

In general, anodic alumina films grow as the result of ionic species movement under the influence of the electric field across the film. The outward movement of Al^{3+} ions and the inward movement of O^{2-} and OH^- happens across the pre-existing air formed film and it is driven by the high electric field (3) The oxide film grows at the oxide/solution

and metal/oxide regions respectively. Inert gas markers, for example xenon, are used to determine the transport number of each species. During oxide film growth under high current efficiency, the transport number of the cation was found to be 0.4 (4). If the current density and the solution pH are reduced, the cation transport number is reduced as well since it is possible in such conditions that Al^{3+} is directly ejected into the solution.

To determine whether electrolyte anions are immobile or if mobile the direction of their mobility, an inert gas (xenon) layer may be deposited onto the metal surface before anodisation and used as a reference marker (5,6). After anodisation, transmission electron microscopy studies of ultramicrotomed alumina film sections are carried out to determine the presence and the direction of mobility of the incorporated species as well as the Al^{3+}, O^{2-}, and the OH^- (7,8). The direction of mobility of the incorporated species is determined by reference to the location of the inert gas marker after anodisation and the use of differential electron beam induced crystalisation of the ultramicrotomed sections of alumina in transmission electron microscope. Xenon is used as a marker layer, because it is immobile during anodic film growth and it is easy to distinguish in the transmission electron micrograph. In these micrographs, incorporated electrolyte species appear darker than the xenon layer, because they have a higher atomic number. Rutherford backscattering spectroscopy was used to determine the composition and density of the film. Dell'Oca and Young (9) have revealed that the incorporation of electrolyte species influences the ionic transport processes during anodic film growth. It has been shown that (3) species from borate electrolytes were immobile, those from phosphates electrolytes were inwardly mobile, and those of tungstate electrolytes were

outwardly mobile. The electrolyte anions mobility was attributed to the electric field effect in transforming these species. In the case of outward mobile electrolyte species, such as tungsten, it is believed that the anion adsorbs at the film/solution region at first, then it is trnsformed into an outwardly mobile species by the effect of the electric field. Even though the exact nature of the transformation process is not well known, where it may occur at the adsorption stage or after incorporation, but the end result is a positively charged and outwardly mobile cation. The level of electrolyte species incorporation depends on the type of electrolytes used and the anodisation voltage.

4.3 EXAFS study of Tungsten Incorporated into Alumina films

Traditionally, electron microscopy or XPS has been used to show whether an electrolyte anion was incorporated into the oxide film after anodisation and the direction of mobility. However, electron microscopy can not be used to resolve the local structure of incorporated species. In the case of aluminium anodised in aqueous tungstate electrolyte at 100 V, a thick barrier-type morphology film grows on its surface with the incorporation of tungsten. The EXAFS technique was used to resolve the local structure around the tungsten species incorporated into alumina oxide, because of its capability in resolving short range order systems.

4.4 Tungsten and Oxygen Phase Shifts Determination

The accurate determination of structural parameters from the EXAFS results depends on the use of an exact and reliable phase shifts for the central absorbing atom, as well as the

backscattering atoms in different shells. The procedure followed in this work to obtain reliable phase shifts for tungsten and oxygen was to calculate tungsten and oxygen phase shifts in EXCURV92, then test their reliability by using them to fit tungsten foil and K_2WO_4 model compounds. Once these phase shifts were proven reliable, they were then used to fit fluorescence EXAFS above the W-L_3 incorporated into the alumina films on aluminium anodised at 100 V in tungstate electrolyte.

Since the tungsten incorporated into the anodic oxide film is likely to be surrounded by oxygen atoms, phase shifts due to oxygen atoms were calculated in EXCURV92. Potassium tungstate was used as a model compound to check the reliability of the calculated oxygen phase shift. Based on the phase shift transferability for the same pair of absorber and backscatterer, the phase shifts calculated and tested by fitting the EXAFS of the model compounds can be used for theoretical fitting of the experimental EXAFS of the oxides with unknown structure. Transmission EXAFS of W-Foil

4.5 Transmission EXAFS of W- Foil

A transmission EXAFS spectrum of the tungsten foil above the L_3-edge (10200 eV) was measured on station 9.2 of the SRS at Daresbury and the raw spectrum is shown in fig. 4.1 a.

The experimental EXAFS spectrum was theoretically fitted, where the phase shift for the absorbing W was calculated by treating the central (absorbing atom) as a relaxed core state on the assumption that the relaxation process for the central atom was of the

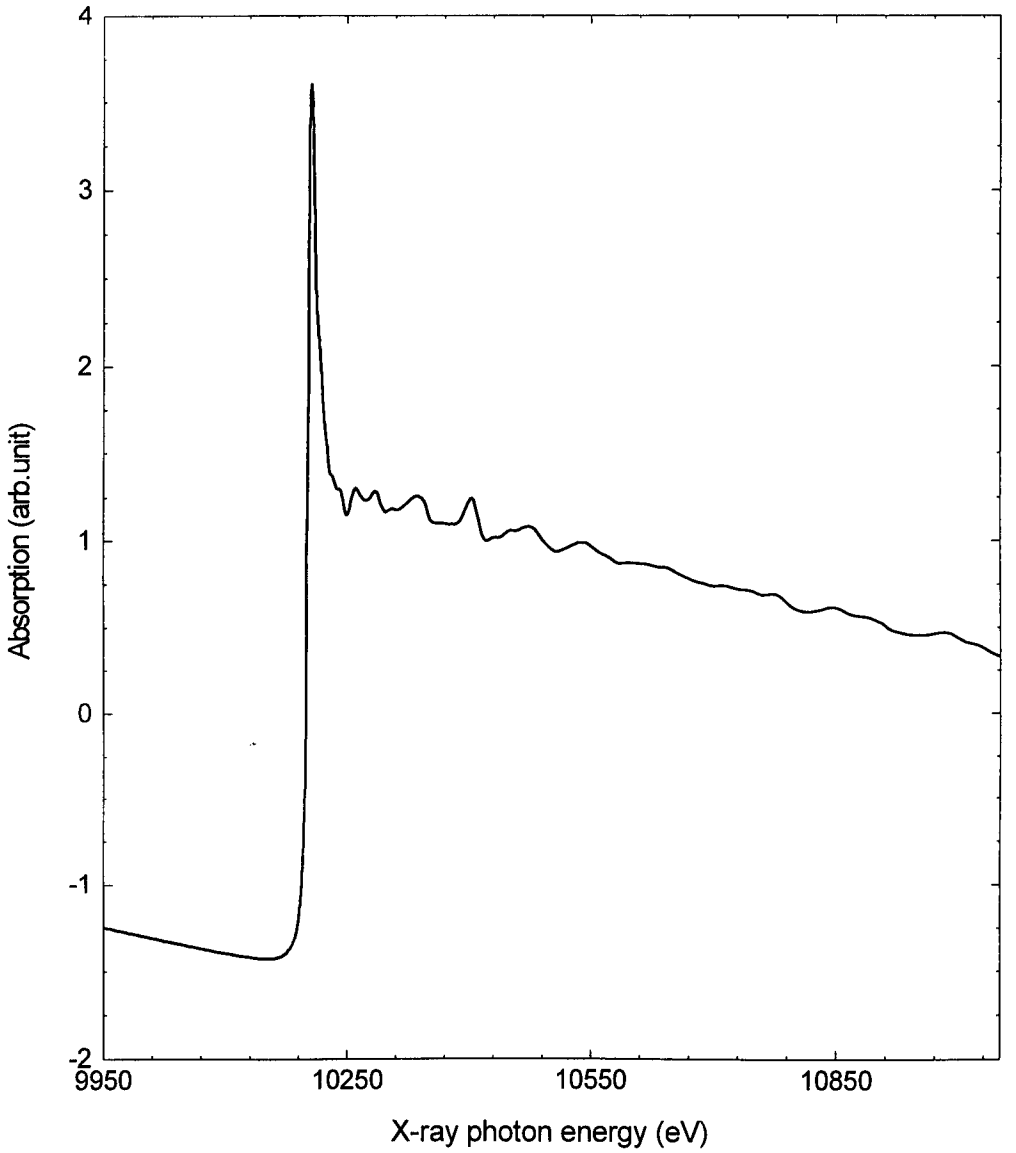

Figure 4.1 a Transmission EXAFS of L_3 of tugnsten foil.

2p core hole. The calculated phase shifts were used in the theoretical fitting of the experimental EXAFS spectrum. The fitting of the experimental EXAFS curve was performed for the first 3 shells of backscattering W atoms where published crystallographic values for the bond length distance and co-ordination number for each shell was used as starting for the EXAFS fitting. In metallic tungsten foil, the absorbing tungsten atom is co-ordinated by 8, 6, and 12 atoms as the number of W backscatterer in the first, second, and third shell respectively with a bond lengths of 2.75 Å, 3.186 Å, and 4.507 Å in the same order (10). Tungsten structural parameters were determined from x-ray diffraction technique. In EXCURV92, E_0 [chapter 2 (2.3.3.2)] is not a fitting parameter and at the same time, the Fermi energy is used as a fitting parameter and changes in its value can effect the EXAFS fitting. Fig. 4.1 b show the k weighted EXAFS and its Fourier transform.

The bond length values for the first three tungsten backscattering shells obtained from this fitting were 2.74 ± 0.005 Å, 3.16 ± 0.008 Å, and 4.48 ± 0.01 Å respectively with the same number of coordinating tungsten atoms in those three shells as given in reference 9. From these structural results, it can be concluded that the phase shift calculated in EXCURV92 for tungsten is reliable and can be used to account for the phase variation due to tungsten in unknown structure.

4.6 Transmission EXAFS of W-L_3 in Potassium Tungstate

Potassium tungstate (K_2WO_4) which has known structural parameters from x-ray diffraction was used as a model compound. This sample was prepared at the Physics

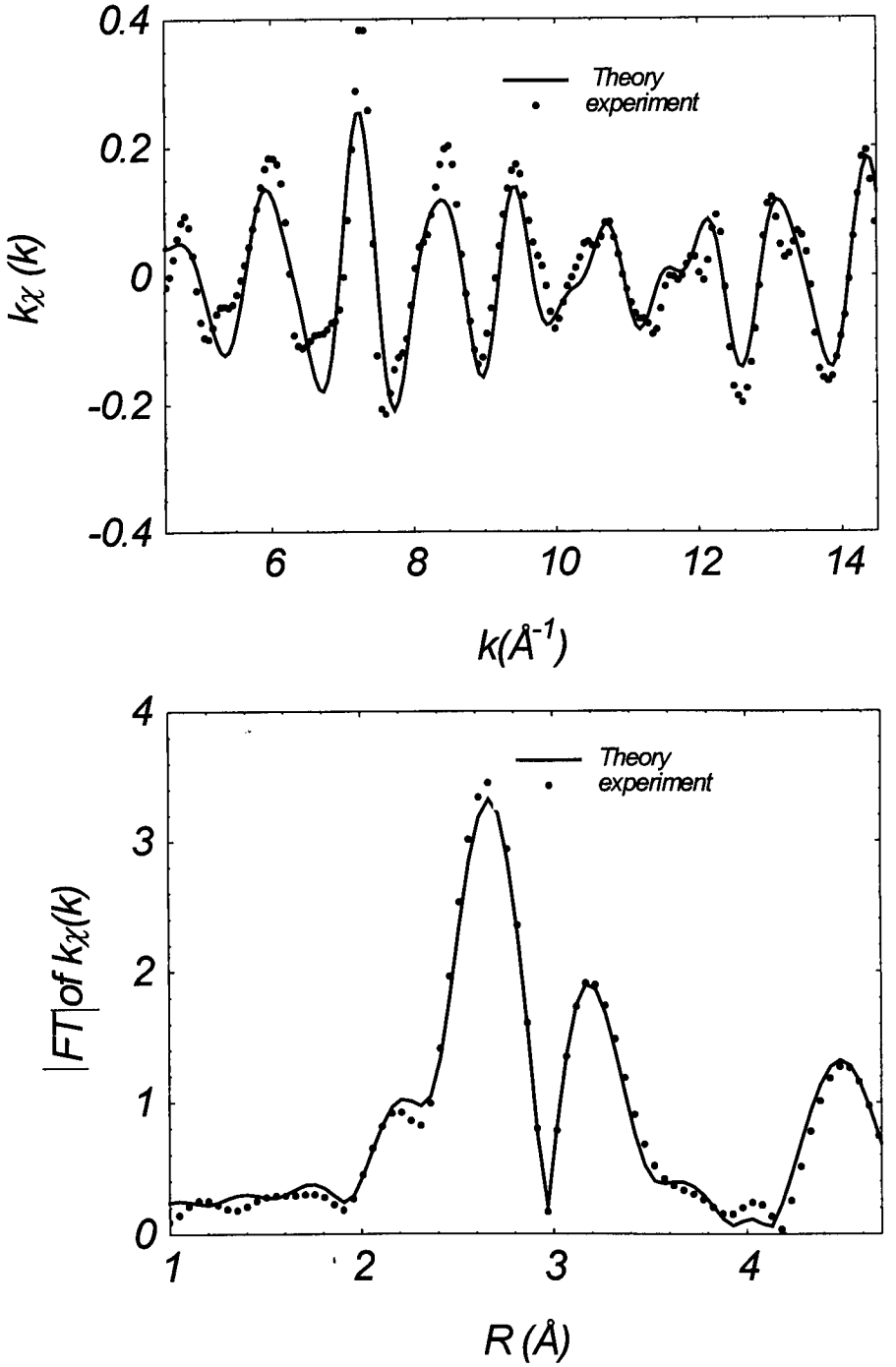

Fig. 4.1 *b*, k weighted EXAFS of W-L_3 and the Fourier transform

Department, University of Warwick, as has been described by Pettifier (11). Transmission EXAFS was measured around the L_3-edge (10200 eV) of tungsten in potassium tungstate and was used to check the phase shift for oxygen as the backscatterer atom. The raw transmission EXAFS spectrum measured above the L_3 of K_2WO_4 is shown in fig. 4.2a. Pre- and post-edge subtraction as well as EXAFS function transformation into K-space is shown in fig. 4.2 b.

Again, EXAFS analysis was carried out as in the previous section. In this case, the phase shifts for oxygen were calculated in EXCURV92. As a start for the EXAFS data fitting, crystallographic parameters for K_2WO_4 were used, where the W-O bond length was 1.79 ± 0.002 Å and a co-ordination number of 4 ± 0.2 (four oxygen atoms surround each tungsten atom) (11). Fig 4.2c shows the k^3 weighted transmission EXAFS spectrum for K_2WO_4 as well as the Fourier transform showing a single shell of oxygen atoms. The bond length distance for the oxygen shell obtained from the EXAFS in this work was 1.79 ± 0.01 Å and the number of oxygen atoms co-ordinating the absorbing tungsten was found to be 4.0 ± 0.65. As can be seen in fig. 4.c, good theoretical EXAFS fit for the experimental spectrum was established in this case. One of the reasons behind this good theoretical fit, is the reliable phase shifts for tungsten and oxygen calculated in EXCURV92. It should be mentioned that a combination of approximation accounting for the ground state and the potential exchange as Von-Bart and Hedin-Lundqvist were used to provide a calculation route for the potentials that the photoelectron experiences when leaving the absorbing atom and when it is backscattered. From the EXAFS structural results presented in the last two sections for

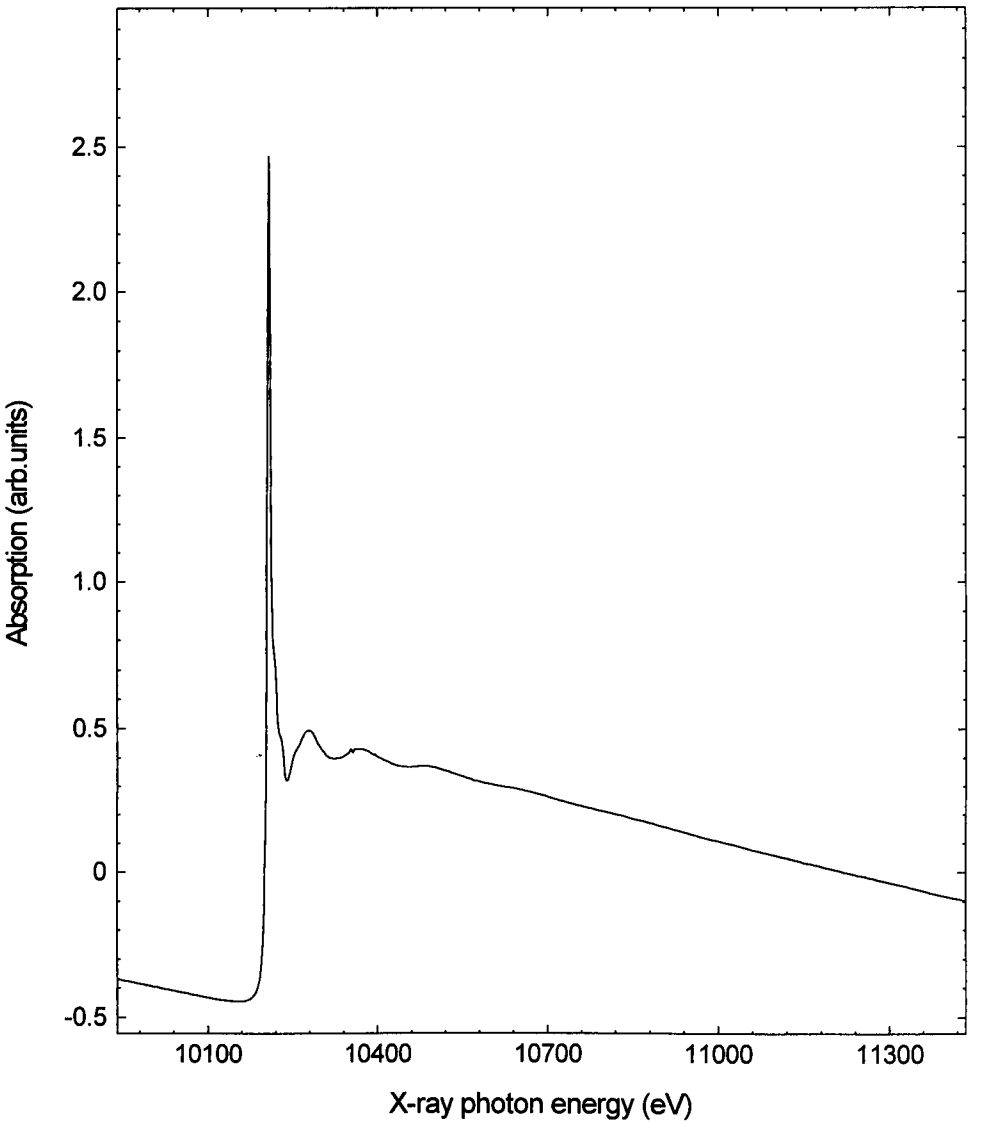

Figure 4.2 a Transmission EXAFS spectrum of W in potassium tungstate

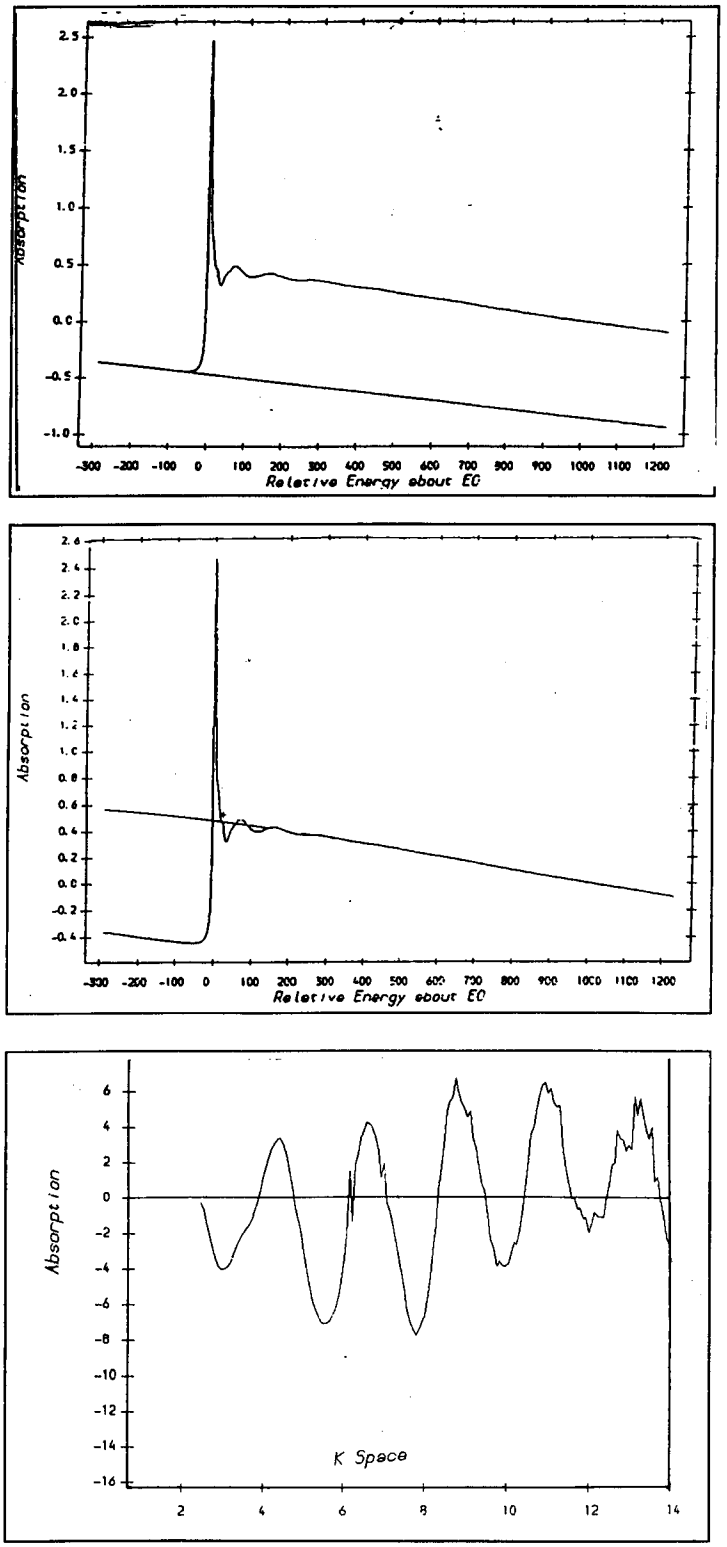

Figure 4.2 b Pre- and post-edge subtraction as well as EXAFS function transformation into K-space.

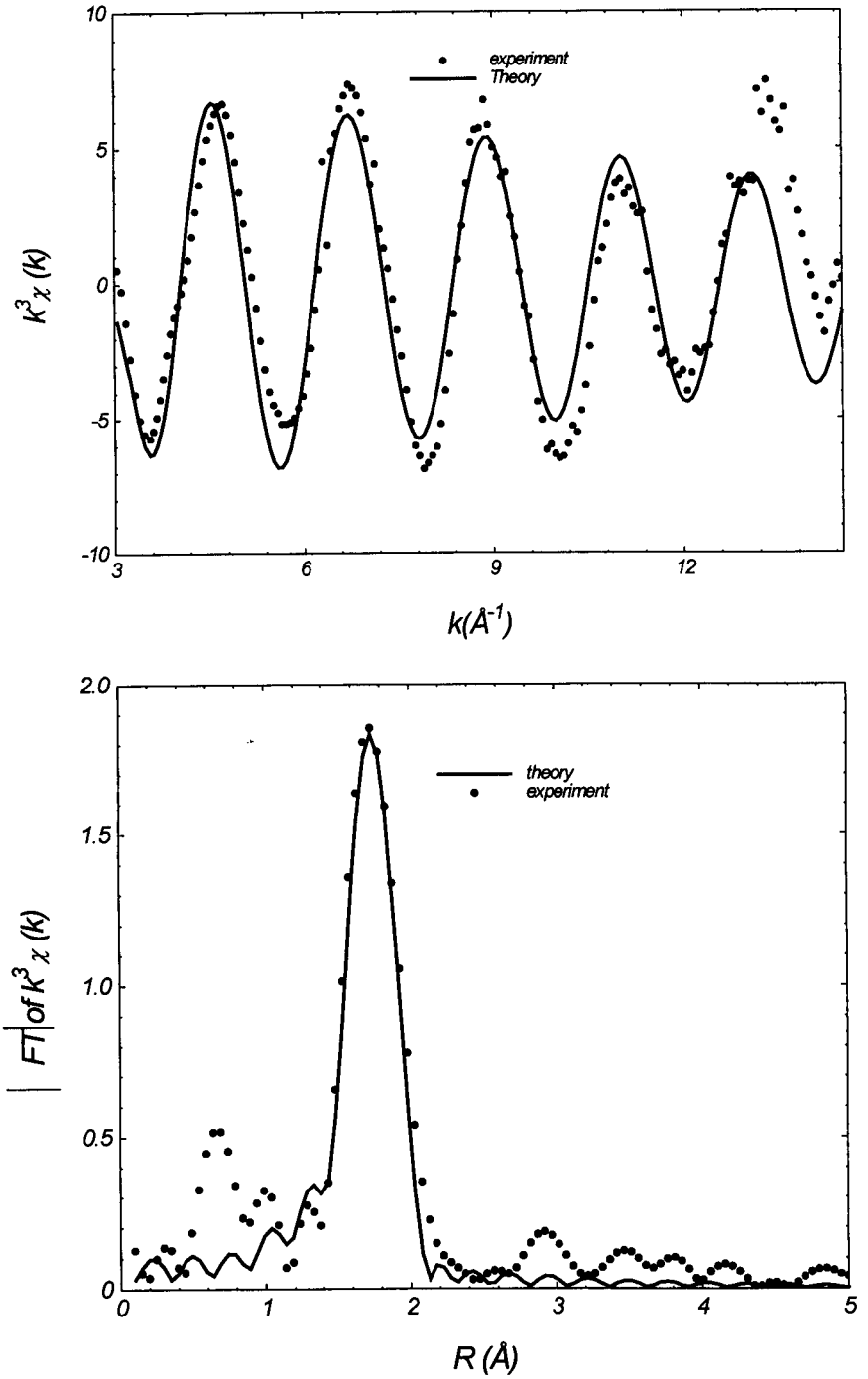

Fig 4.2, c k^3 weighted EXAFS of W-L_3 in K_2WO_4, and the Fourier transform.

W-foil and potassium tungstate, it is reliable to employ the W and O calculated phase shifts, to be used to analyse the structure around incorporated tungsten in alumina films.

4.7 Fluorescence EXAFS of W-L3 Incorporated in Anodic Alumina Films

In this section, EXAFS spectra recorded in fluorescence mode above the L_3-edge for tungsten incorporated from tungstate electrolyte into anodic alumina films formed on aluminium by polarisation to 100 V, are presented in attempt to characterise the local structure around incorporated tungsten. Fluorescence was chosen to record EXAFS in this case because of its suitability for dilute systems. To improve the signal to noise ratio in the experimental data, four W-L_3 fluorescence spectra were collected and summed and are shown in fig. 4.3 a.

For the EXAFS data analysis stage, EXCURV92 was used to find a best fit theoretical curve for the experimental EXAFS results, after background subtraction. The phase shifts of the tungsten absorbing atom and that of the backscattering oxygen atom which were calculated in EXCURV92 and tested by fitting the EXAFS of the model compounds and their structural parameter were used in the fitting of the EXAFS of the incorporated tungsten. The k^3 weighted experimental EXAFS of tungsten in alumina film and its Fourier transform and the corresponding best fit are presented in fig. 4.3 b.

The local structure around tungsten incorporated species in alumina oxide is defined through the bond length between the absorber and backscatterer W-O in this case and also the number of oxygen atoms around the absorbing tungsten. The W-O

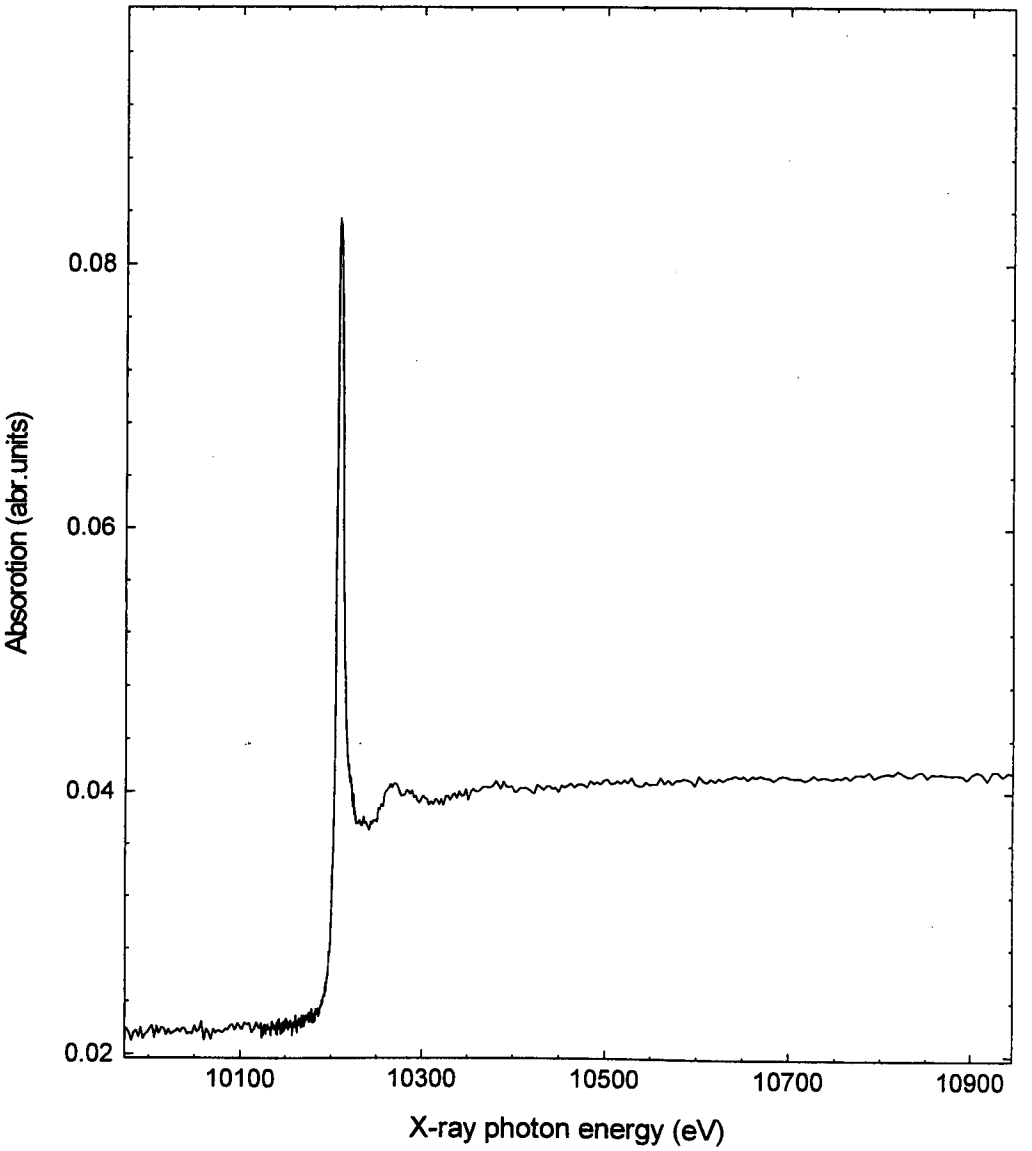

Figure 4.3 a Fluorescence EXAFS spectra of W-L_3 incorporated in anodic alumina film formed on aluminium at 100 V in tungsten electrolyte.

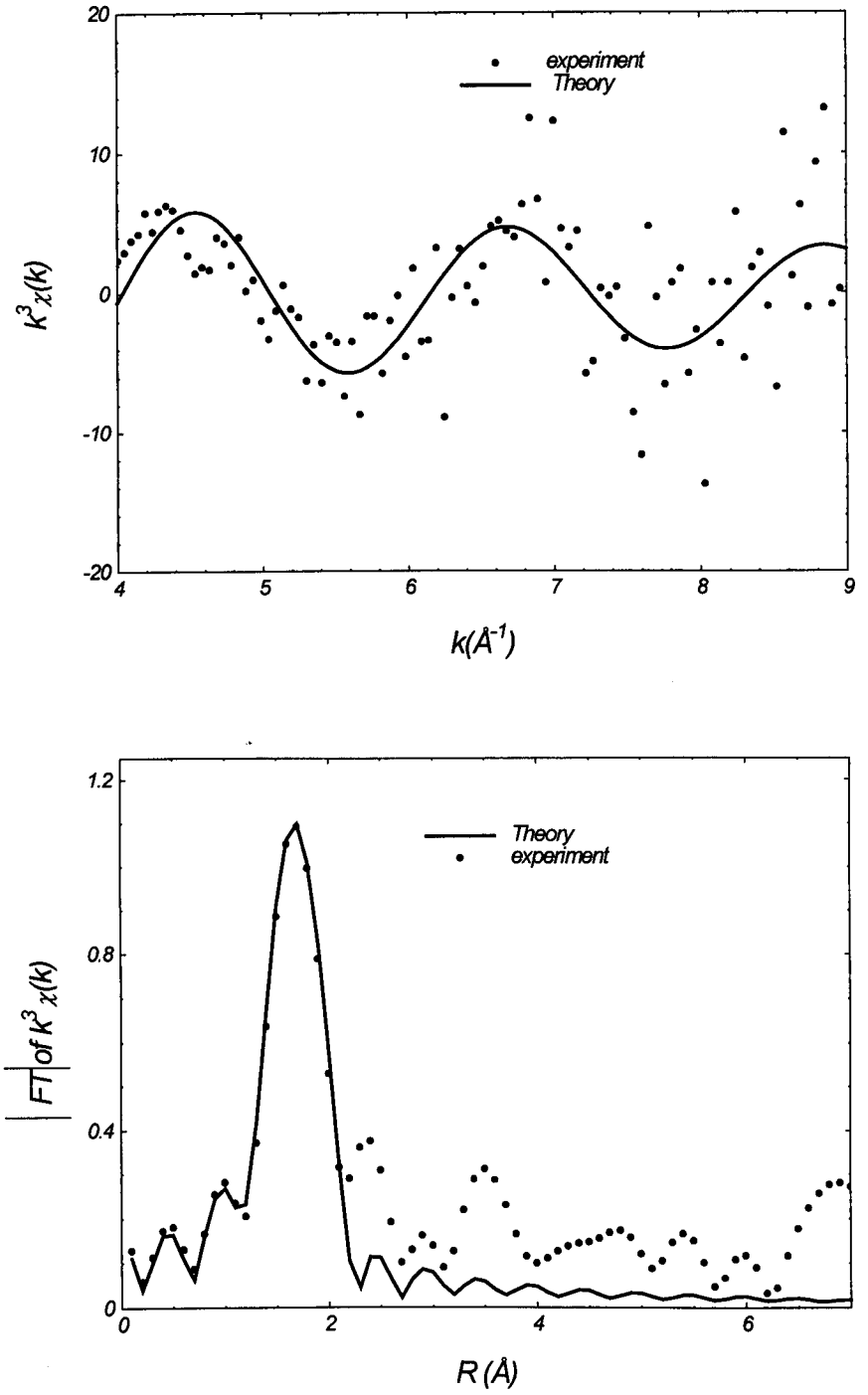

Fig. 4.3, b k^3 weighted EXAFS and the Fourier transform of tungsten incorporated into alumina oxide films.

bond length obtained from the EXAFS fitting was found to be 1.79 ± 0.01 Å and tungsten was co-ordinated by 4 oxygen.

4.8 Discussion of Results and Conclusions

In this chapter, it has been shown that EXAFS technique recorded in fluorescence mode has been, for the first time, used to investigate and resolve the local structure around tungsten electrolyte species incorporated into alumina anodic film.

From this study, it is obvious that tungsten species incorporate into the alumina films formed during the polarisation of aluminium in tungstate aqueous electrolyte at 100 V. The EXAFS results around tungsten L_3 has revealed that only one shell with four oxygen atoms are surrounding the absorbing tungsten atom at a distance of 1.79 ± 0.01. The ability of EXAFS technique in determining the local structure around electrolyte species, is due to the improvement in the calculation routine used in EXCURV92 to calculate the phase shift for the absorber and the backscatterer

The structure around the tungsten incorporated in alumina can be explained in terms of the bond length and the co-ordination number reported for this system. Tungsten incorporated in this case has a short range order and it is tetrahedrally co-ordinated by oxygen. The second explanation is based on the idea that tungsten may be incorporated as a part of the anodic alumina structure.

In view of the local structure of incorporated tungsten resolved in this study, where tungsten is tetrahedrally co-ordinated by oxygen, tungsten exists in WO_4^-, even though these could not be the entities which are moving outward under the influence of the

field. It could be that tungstate is moving outward, because it is linked to the alumina structure in some way that it is dragged outward.

It can be concluded that during anodisation, tungsten species when incorporated into the oxide film, are transformed under the influence of the high field and are outwardly mobile. The previous statement implies that tungstate species are transformed by some mechanism into a positively charged species which move outward with the egress of Al^{3+} species. As the tungstate species are initially adsorbed at the oxide/ solution interface, tungstate becomes positive through the loss of its oxygen. This stripping process eventually leads to the production of W metal cation which is positively charged and outwardly mobile under the field.

It is clear from the capabilities of the EXAFS technique in elucidating the local structure around tungsten electrolyte incorporated species which has been applied for the first time to investigate such systems. EXAFS technique can play an important role in determining directly the local structure of many incorporated species in different systems.

References

(1) Randall, J. J., Bernard, W. J., and Wilkinson, R. R., Electrochim. Acta., **10**(1965)183

(2) Skeldon, P., Shimizu, K., Thompson, G. E., and Wood, G. C., Thin Solid Films, **123**(1985)127

(3) Thompson, G. E., Xu, Y., Skeldon, P., Shimizu, K. Han, S. H., and Wood, G. C., Phil Mag. **55**(1987)651

(4) Skeldon, P., Shimizu, K., Thompson, G. E., and Wood, G. C., Surf. Interface Anal., **5**(1983)252

(5) Pringle, J. P. S., J. Electrochem. Soc., **119**(1972)482

(6) Pringle, J. P. S., Ibid, **120**(1973)398

(7) Shimizu, K., Thompson, G. E., and Wood, G. C., Thin Solid Films, **88**(1982)255

(8) Shimizu, K., Thompson, G. E., and Wood, G. C., Thin Solid Films,**77**(1981)313

(9) Dell'Oca, C. J., and Young, C. Y., J. Electrochem. Soc., **117**(1970)1548

(10) Stahe, J. S., and Straumemis, M. E., J. Appl. Phys., **42**(1971)3288

(11) Pettifier, R. F., PhD. Thesis, Physics Department, The University of Warwick, (1978)

(12) Koster, A. S., Koools, F..X. N. M.., and Riek, G. D., Acta. Cryst, B, **25**(1969)1704

5. Chapter Five Electrochemistry and XPS Results and Discussion

5.1 Introduction

In this chapter, polarisation curves of pure aluminium in aqueous solutions at various pH's, in bulk and evaporated film forms, are presented to characterise their electrochemical behaviour and to monitor passivating oxide film growth on aluminium. Al 2p, O 1s, and C 1s XPS spectra of oxide films on aluminium are also presented as a function of film depth. These spectra are used to probe the relative film thickness and to provide information about their composition.

5.2 Polarisation of aluminium

The corrosion potential measured for pure aluminium left to equilibrate for about an hour in de-aerated aqueous solutions at various pH's was found to be ~ -1.05 V at pH 2, ~ -1.45 V at pH 7, and ~ -1.6 V at pH 10. All potentials measured and reported in this work were made relative to the saturated calomel electrode (SCE) used as a reference electrode.

5.2.1 Polarisation Curves of Aluminium Bulk

The electrochemical behaviour of aluminium bulk samples polarised in aqueous solutions of 0.05 M Na_2SO_4 as the electrolyte at pH 2, pH 7, and pH 10 are presented in figure 5.1.a, b, and c.

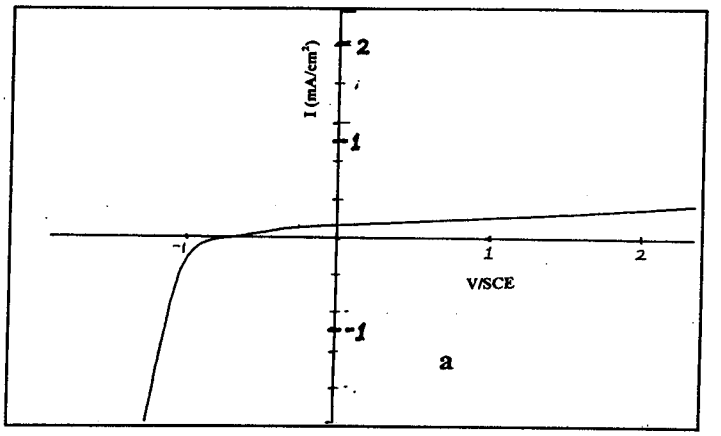

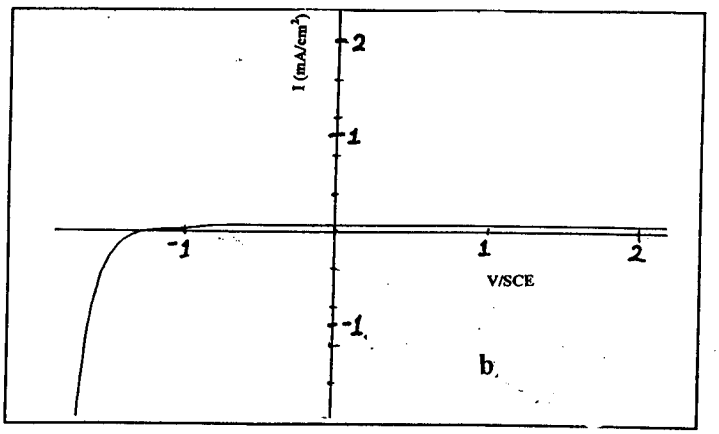

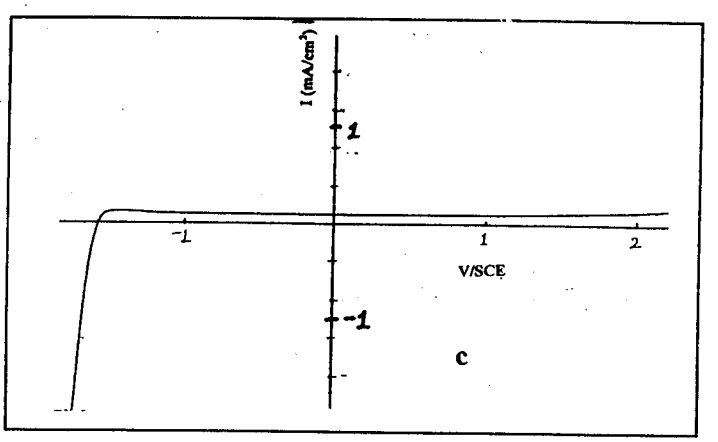

Figure 5.1 a, b, and c Polarisation curves of aluminium in 0.05 M Na2 SO4 at pH 2, 7, and 10

Curves a, b, and c in figure 5.1 were obtained by immersing aluminium metal in water at pH 2, 7, and 10 respectively for ~ 40 minutes at the corrosion potential. Then a potentiodynamic sweep was performed in each case between -2.2 to + 2.5 V at a sweep rate of 5 mV/s. It is clear from the curve in figure 5.1 a, that oxide growth on aluminium bulk in water at pH 7 was progressive, indicated by the increase in current as the potential was anodically increased resulting in film thickening. The polarisation curve shown in figure 5.1 c is for aluminium in aqueous media at pH 10, where on the anodic side, current density is maintained at a small value which denotes the passivity region, as the potential was increased, the oxide film becomes thicker. At cathodic potentials, the solution pH in the vicinity of aluminium becomes alkaline resulting from hydrogen evolution and this may lead to different electrode processes. In these conditions the aluminium surface film may become unstable. From these figures, it is seen that an increase in the aluminium electrode potential did not result in oxygen evolution. No major, or abrupt behaviour was noticed on all of these curves.

5.2.2 Polarisation Curves of Evaporated Aluminium Films

In this case only one polarisation curve is presented, that of pure aluminium prepared as films on a microscope slide polarised in pH 10 by sweeping the potential from - 1.9 V to + 2.9 V at a sweep rate of 5 mV/s. This curve is shown in figure 5.2.

Aluminium films in pH 2 and 7 were not capable of withstanding the immersion and polarisation conditions. As a result, aluminium films were flaked and when they were polarised abrupt current density changes was observed due to increases in the aluminium surface area which was exposed to the solution. To avoid this washing off,

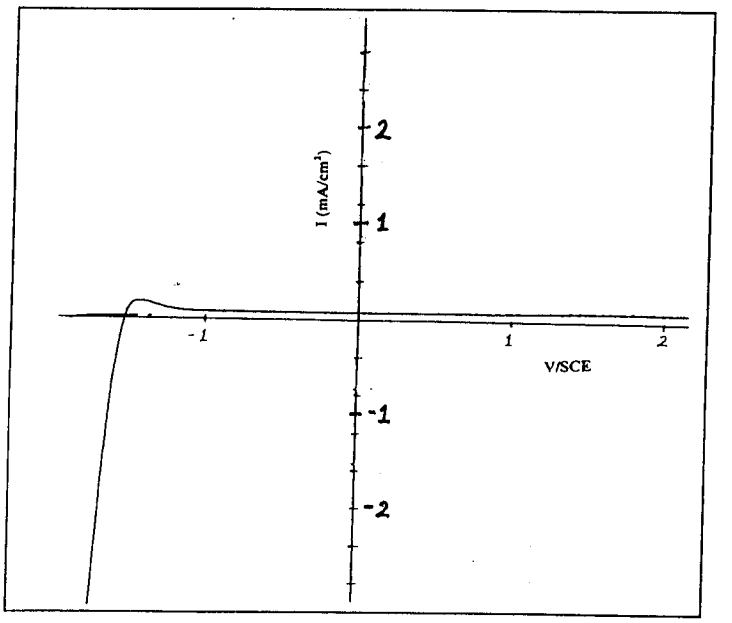

Figure 5.2 *Polarisation curve of aluminium evaporated films in aqueous solutions at pH 10*

aluminium films which are intended to be polarised should be treated as soon as introduced into the solution. Only the polarisation curve for an aluminium film in pH 10 is prresented in fig. 5.2. There are no features on this curve.

5.3 XPS Results of Thin Films on Aluminium

5.3.1 Introduction

XPS spectra of oxide films formed on aluminium by exposure to air or moisture (air-formed films), immersion in aqueous solutions and by anodic and cathodic polarisation to different voltages are reported in this section. The binding energy, area under the peak for the Al 2p transition due to metallic and oxidised aluminium, were measured for the films formed as will be explained in following sections. These values are presented in a tabulated form, along with the binding energy of the C 1s, and O 1s. XPS measurements were carried out at various depths resulting in an intensity depth profile and the raw spectra are shown in a graphical form.

5.3.2 Data Collection and Analysis

XPS spectra were collected with the pressure in the sample chamber maintained at 10^{-8} Torr. Detailed scans were carried out to determine the peak position and the area under the peak (intensity) of each transition. Furthermore, each state was measured after argon ion sputtering of the samples for a definite time, resulting in a depth profile, A large amount of contamination especially by carbon is expected on the surface of the "as received" specimen. The binding energy E_b due to the metallic Al 2p and the aluminium in the oxide were determined. A curve fitting programme was used to determine the Al

2p peak position which gives its kinetic energy and its area, which facilitates binding energy determination of each transition, and an estimation of the relative thickness of the film. The C 1s transition was measured to check if there is a charge build up on the sample surface after being bombarded with x-rays. For all XPS spectra measured in this work, the C 1s transition energy was corrected to 284.6 eV (1) which is the widely accepted value.

All XPS data are plotted as a function of sputtering time showing the Al 2p transition of aluminium and oxide. Sputtering was performed until the Al in oxide peak disappeared indicating that the oxide has been removed. In some cases as will be indicated, removing all of the aluminium oxide was not possible where a little shoulder was left after the sputtering. The Al 2p transition of aluminium metal originates from the metal where there is no charging, so it does not require correction. Depth profile XPS data are presented to show the existence and the relative thickness of aluminium oxides in each treatment. It should be noted that the Al 2p, O 1s, and C 1s transition states originate from the near surface, because the mean free path for the photoelectrons is very small.

Fig 5.3 a, b, and c shows an example of XPS raw data analysis where linear background subtraction and two Lorentzian equations were used to fit the peak due to the aluminium metal and that of the aluminium oxide. The accuracy in the Al 2p binding energy determination is ± 0.1 eV.

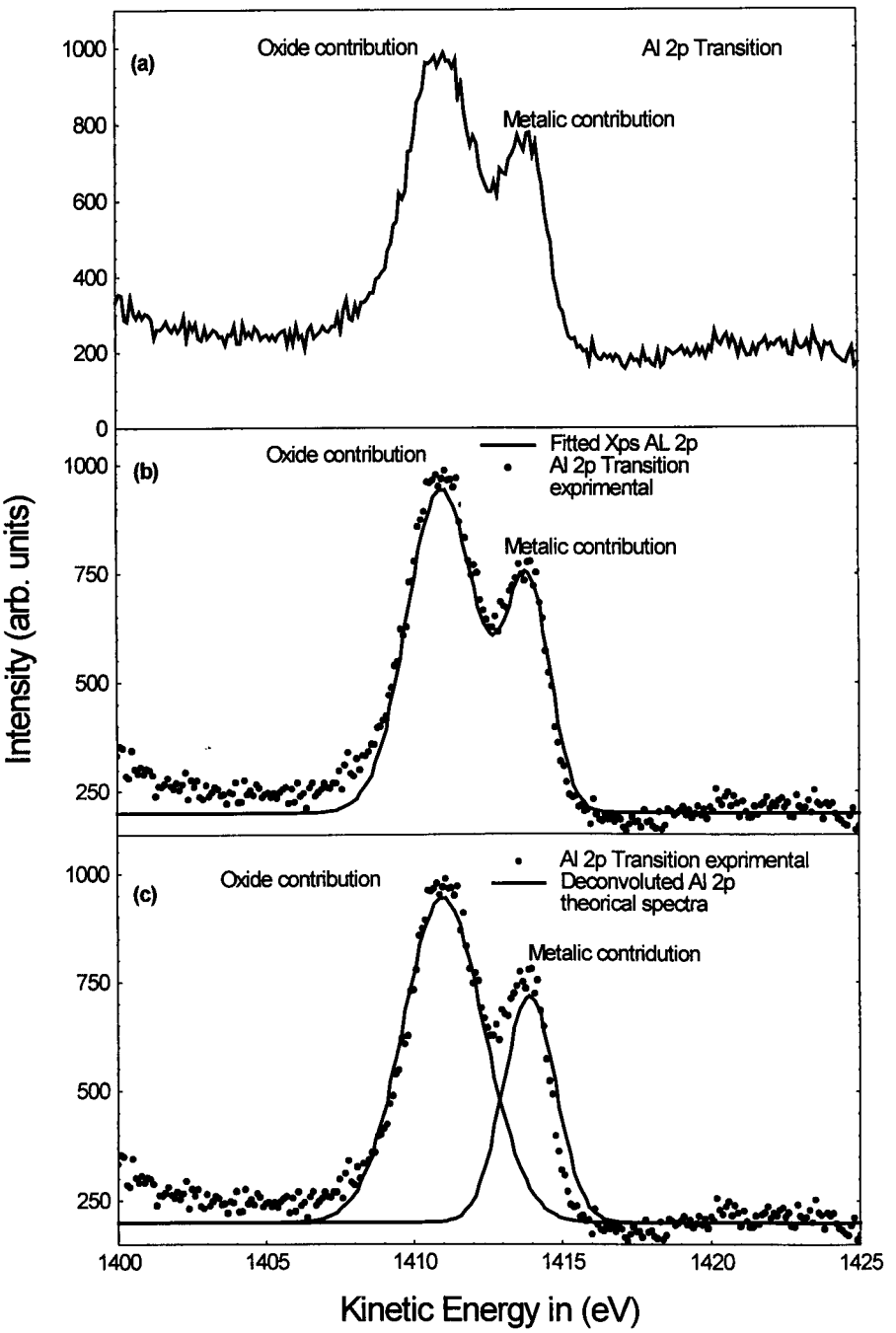

Fig 5.3 a, b, and c raw XPS Al 2p transition, theoretical fit , and background subtracted deconvoluted peaks respectively

5.3.3 XPS of Air-Formed Films

In this section, XPS results of an air-formed oxide film on 1 cm^2 aluminium bulk sample mechanically polished as described in chapter three is presented. The binding energy values of Al 2p due to aluminium and oxide along with their areas under the peak as well as that of O 1s, and C 1s are reported in table 5.1.

Time of sputtering	Binding energy, E_b of Al 2p, O 1s, and C 1s transitions in eV				Charge corrected Al 2p oxide in eV	Al 2p oxide peak area	Al 2p metal peak area
	Al 2p oxide	Al 2p metal	O 1s	C 1s			
As received	75.0	72.8	532.5	284.9	74.8	500	400
5 min.	75.0	72.8	532.5	284.9	74.7	510	325
15 min.	74.5	72.7	532.5	284.9	74.2	870	1100
35 min.	74.8	72.8	532.1	284.8	74.6	750	1300
75 min.	-	72.8	532.0	284.8	-	-	2100

Table 5.1 XPS depth profile of an air- formed film on aluminium

From table 5.1, the oxide film in this case is thin with the aluminium metal 2p transition apparent in the "as received" sample. A charge corrected binding energy range of 74.2 -74.8 eV for Al 2p oxide and 72.7-72.9 eV of the metallic 2p state were recorded. Comparable intensities for the metal and the oxide were measured for the as received, sample but as sputtering starts the intensity due to the aluminium oxide diminishes.

It is evident from the XPS spectra in figure 5.4 and the binding energy of Al 2p transition in table 5.1 that the structure of this oxide film is uniform and does not change at various depths. Also there is no shift in C 1s transition, which confirms that there was no charging on the specimen's surface. From figure 5.4, it took only 2 cycles of argon beam sputtering for the oxide signal to diminish dramatically and this indicate that the film is thin.

5.3.4 XPS of Alumina Oxide Film on Aluminium in Boiling water

In this treatment the oxide film formed is known to be of a crystalline pseudoboehmite phase and it was prepared by immersing a piece of aluminium in boiling distilled de-ionised water for ~30 minutes.

Time of sputtering	Binding energy, E_b of Al 2p, O 1s, and C 1s transitions in eV				Charge corrected Al 2p oxide in eV	Al 2p oxide peak area	Al 2p metal peak area
	Al 2p oxide	Al 2p metal	O 1s	C 1s			
2 min.	78.4	-	535.8	284.9	78.1	2500	-
7 min.	79.4	-	536.7	285.1	78.9	2800	-
37 min.	80.3	-	537.7	285.0	79.9	2850	-
82 min.	80.8	-	538.3	284.9	80.5	3200	-
107 min.	80.7	-	538.3	285.0	80.3	2500	-

Table 5.2 XPS depth profile of thick oxide film on aluminium in boiling water, ion gun at 4 keV

From table 5.2 and figure 5.5, it is clear that the Al 2p peak due to the thick oxide is the only detectable feature. The Al 2p transition of the metal was not seen even after many sputtering cycles. A large range of Al 2p binding energies of the oxide 76.1 - 80.8

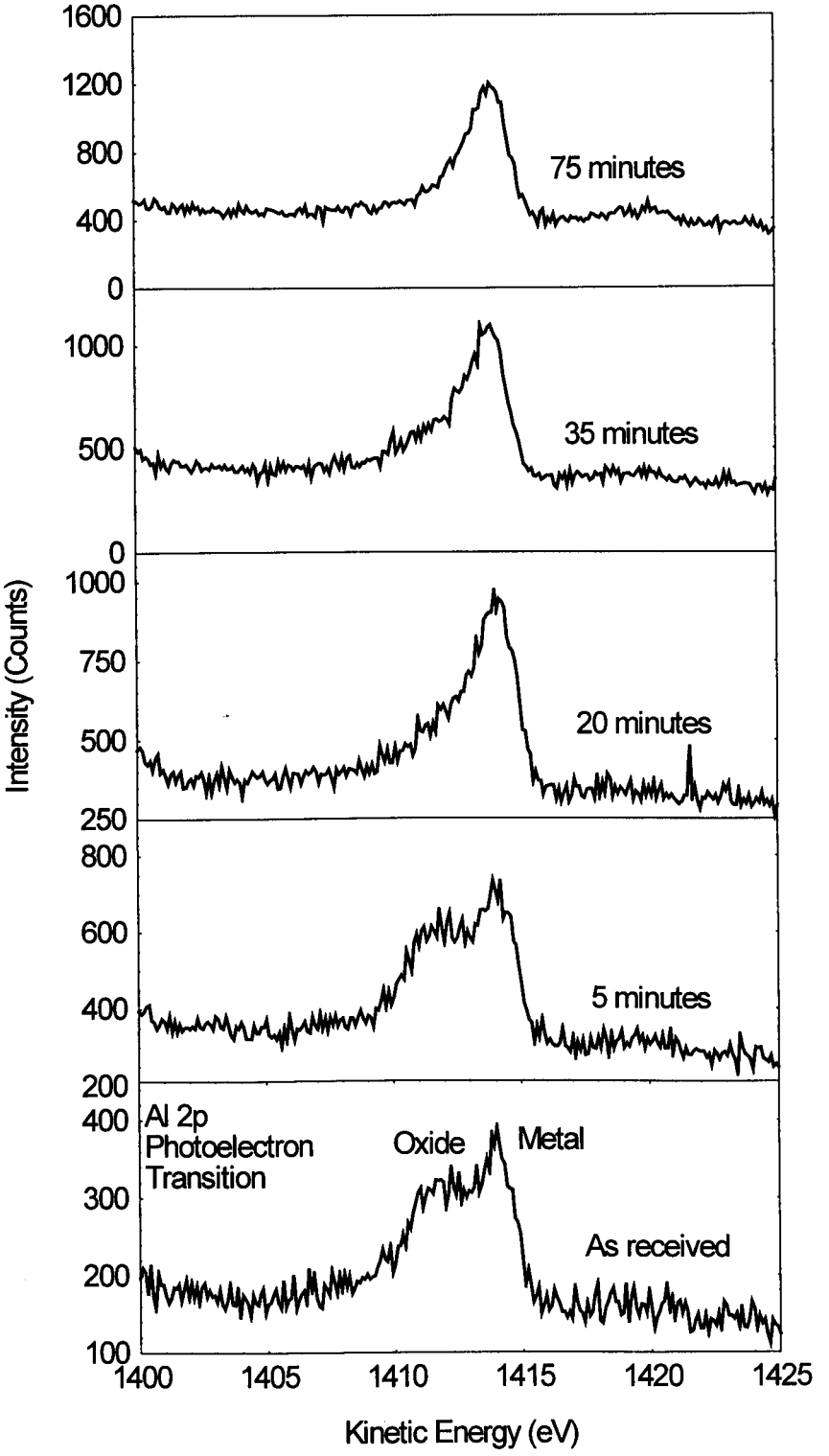

Fig 5.4 The depth profile of XPS Al 2p transition of air- formed film onAluminium

eV was recorded, with large intensity. This indicates that this oxide which has a crystalline psuedoboehmite phase is too thick for any aluminium metal signal to be detected.

It is seen in figure 5.5 that after 7 minutes of argon ion sputtering, the Al 2p oxide peak position was shifted to lower kinetic energy and stayed constant. The oxide film is thick and even after 107 minutes of sputtering, the oxide signal was still the dominant feature in this spectrum.

5.3.5 XPS of Anodic Oxides on Aluminium in Water at Different pH's

In this section, XPS results at various depths of films on aluminium polished, etched and immersed in de-aerated aqueous solution at pH 7, 10, and 2 respectively for ~ 2 hours are presented. The binding energies of Al 2p transition for aluminium metal and oxide and its charge corrected value, O 1s, and C 1s and the intensities of these peaks are also given in the relevant tables. The figures presented in the next sections are indicative of the presence and the relative amount of the film on aluminium in each case. The data presented in the figures are raw data.

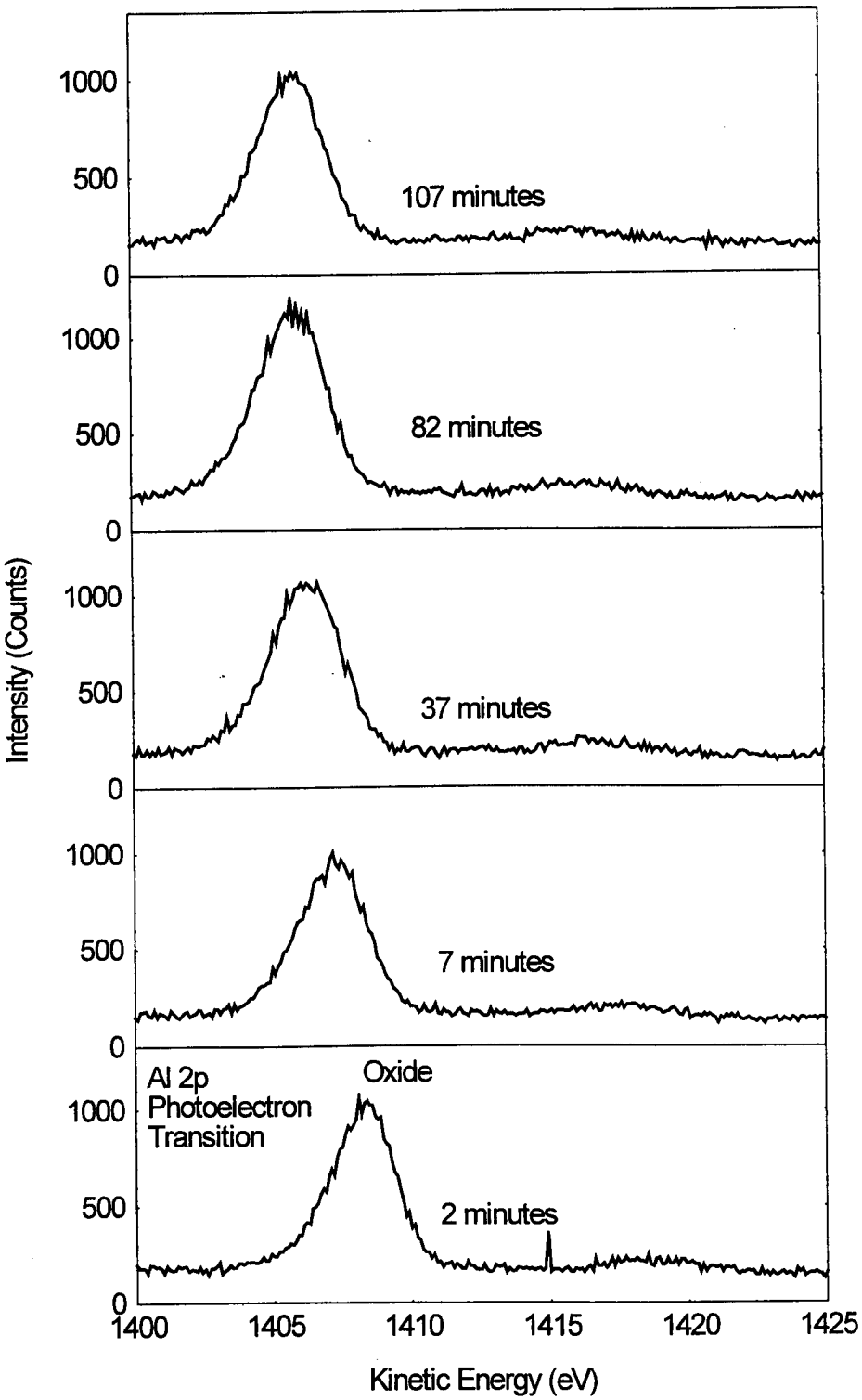

Fig 5.5 The depth profile of XPS Al 2p transition of oxide film on aluminium in boiling water, ion gun at 4keV.

5.3.5.1 pH 7

Time of sputtering	Binding energy, E_b of Al 2p, O 1s, and C 1s transitions in eV				Charge corrected Al 2p oxide in eV	Al 2p oxide peak area	Al 2p metal peak area
	Al 2p oxide	Al 2p metal	O 1s	C 1s			
As received	75.7	72.9	533.6	286.2	74.1	1000	400
4 min.	75.7	72.8	532.5	284.9	75.5	2200	1100
10 min.	75.3	72.9	532.7	285.0	74.9	1500	1500
22 min.	75.1	72.9	532.8	284.9	74.8	1200	1900
40 min.	-	72.8	532.6	284.8	-	-	2100

Table 5.3 XPS depth profile of oxide film on Al in aq. sol. pH 7, ion gun at 2 keV

The binding energy of Al 2p oxide is 74.1-74.9 eV except for one value where it was 75.5 eV, and E_b for the metal is 72.8-72.9 eV. An XPS depth profile of the Al 2p transition for aluminium and oxide is plotted in figure 5.6. This film resembles the air formed one. Even after several sputtering cycles, it was not possible to remove the oxide contribution completely where a shoulder like feature was left on the oxide side. This small residual oxide contribution is most likely caused by oxygen which disassociated from water in the XPS sample chamber.

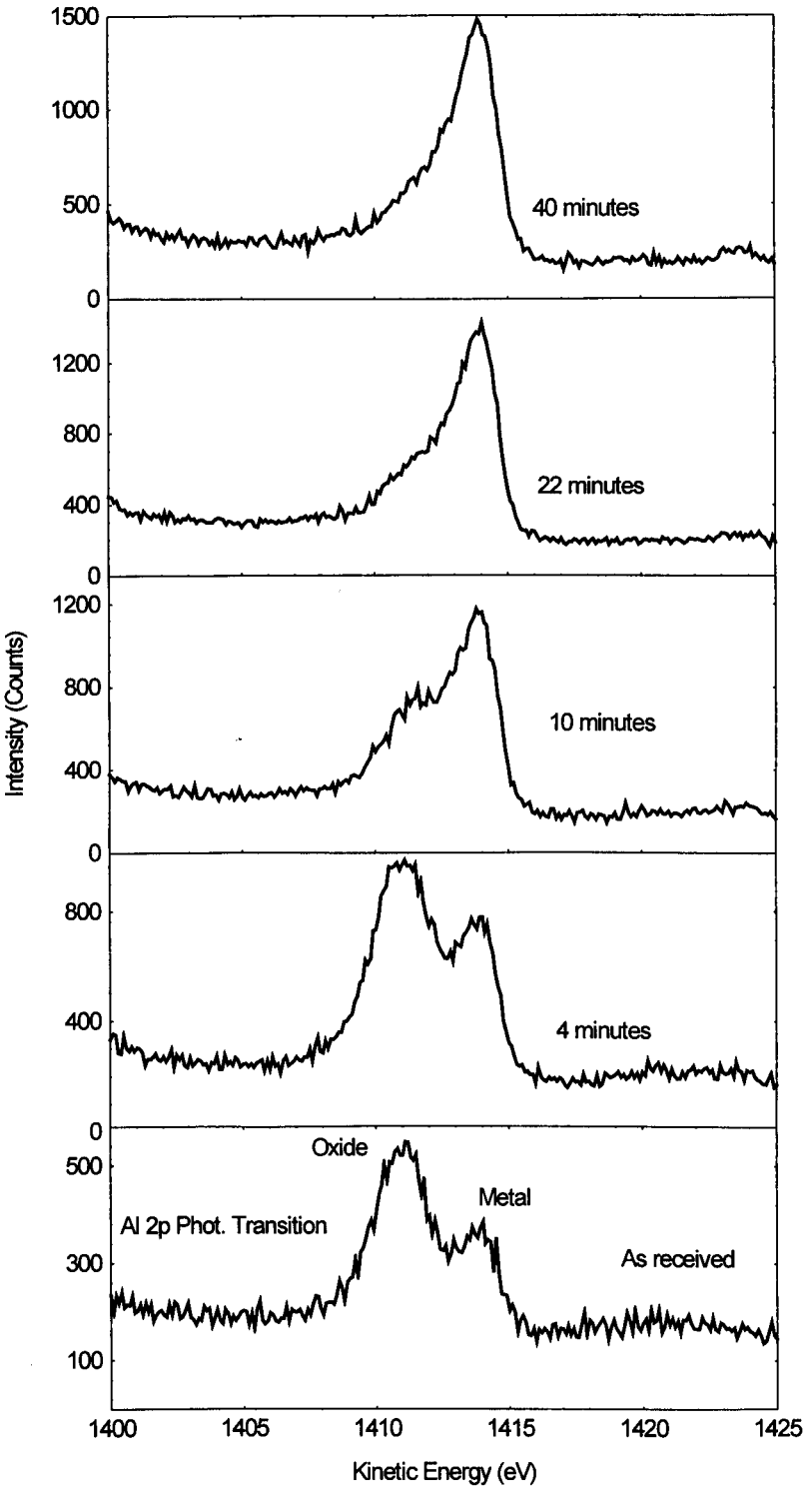

Fig 5.6 The depth profile of XPS Al 2p transition of anodic oxide film on aluminium in aq. sol. at pH 7

5.3.5.2 pH 10

Time of sputtering	Binding energy, E_b of Al 2p, O 1s, and C 1s transitions in eV				Charge corrected Al 2p oxide in eV	Al 2p oxide peak area	Al 2p metal peak area
	Al 2p oxide	Al 2p metal	O 1s	C 1s			
As received	76.1	-	534.1	286.9	73.8	1100	-
18 min.	75.7	72.9	532.9	284.8	75.5	2300	450
52 min.	75.3	72.8	532.8	284.6	75.3	1500	1000
76 min.	74.9	72.8	532.5	284.7	74.8	1000	2000
86 min.	-	72.8	532.5	284.7	-	650	2200

Table 5.4 XPS depth profile of oxide film on Al in aqueous solutions at pH 10.

In table 5.4, the Al 2p transition due to oxide is the dominant feature in the XPS spectra. In fig. 5.7, the intensity of Al 2p transition of the aluminium metal and oxide are plotted showing the difference in intensity as a function of sputtering time. The binding energy of the Al 2p transition of aluminium is 72.8 - 72.9 eV and for the oxide 73.8- 75.5 eV. The oxide film in this case is uniform. Figure 5.7 presents depth profiled Al 2p transition intensity for the metal and the oxide and their variation as a function sputtering time.

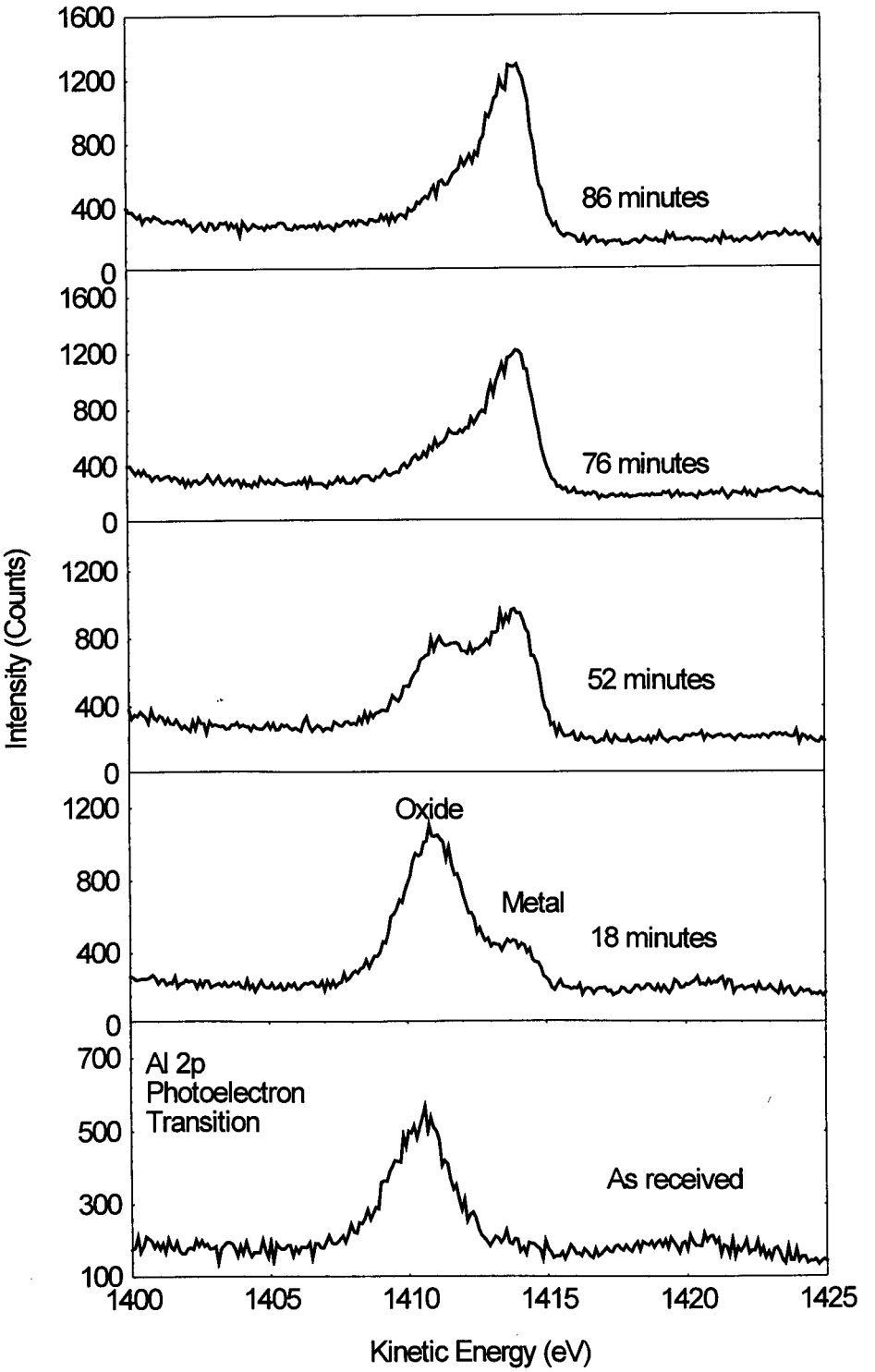

Fig 5.7 The depth profile of XPS Al 2p transition of oxide on aluminium in aq. sol. at pH 10, ion gun at 2 keV

5.3.5.3 pH 2

Time of sputtering	Binding energy, E_b of Al 2p, O 1s, and C 1s transitions in eV				Charge corrected Al 2p oxide in eV	Al 2p oxide peak area	Al 2p metal peak area
	Al 2p oxide	Al 2p metal	O 1s	C 1s			
As received	75.3	72.9	533.3	286.1	73.8	740	230
3 min.	75.3	72.8	532.7	284.9	75.0	1400	700
12 min.	75.1	72.8	532.7	285.0	74.7	1300	780
35 min.	74.7	72.7	532.7	285.1	74.2	650	1200
48 min.	-	72.8	532.6	285.1	-	-	2000

Table 5.5 XPS of sputtered oxide film on aluminium in pH 2 aq. sol., ion gun at 2 keV

The binding energy of the Al 2p transition of the oxide is 73.8-75 eV, and that for aluminium is 72.8 eV. Very small C 1s shift and uniformity in the Al 2p line energy is observed .

In this case, Al 2p transition of the metal is the dominant feature and a small oxide contribution was observed for the as received and up to 12 minutes of sputtering. Al 2p of aluminium in metallic and oxidised state are plotted as a function of sputtering time as shown in fig. 5.8.

5.3.6 XPS of Oxide Films on Aluminium Polarised in Aqueous Solution at pH 2

Oxide films formed on aluminium polarised to +2.5 V/SCE in pH 2 were characterised by the use of XPS. The relative thickness and binding energy of Al 2p, O 1s, and C1s, as well as their intensities are reported.

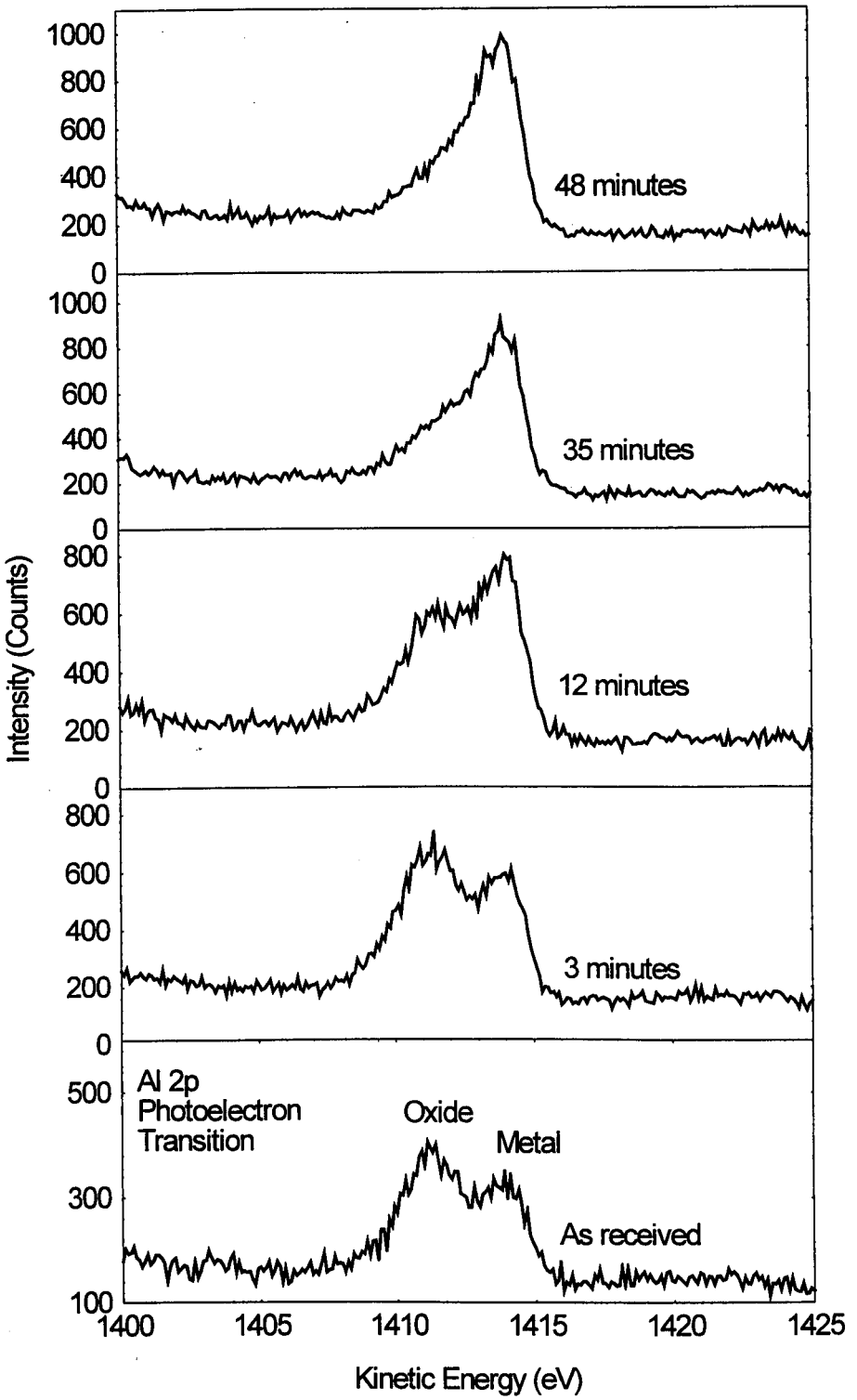

Fig 5.8 The depth profile of XPS Al 2p transition of oxide film on aluminium in pH 2, ion gun at 2 keV.

5.3.6.1 +2.5 V/SCE

XPS spectra measured for the as received and after each sputter of aluminium polarised in water at pH 2 to +2.5 V/SCE and the results are reported in table 5.6,

Time of sputtering	Binding energy, E_b of Al 2p, O 1s, and C 1s transitions in eV				Charge corrected Al 2p oxide in eV	Al 2p oxide peak area	Al 2p metal peak area
	Al 2p oxide	Al 2p metal	O 1s	C 1s			
As received	77.8	-	535.6	288.4	74.0	250	-
16 min.	75.4	72.9	532.9	284.6	75.4	970	160
26 min.	75.0	72.8	532.7	284.7	74.9	670	680
41 min.	75.0	72.7	532.7	284.7	74.9	400	800
56 min.	-	72.8	532.5	284.6	-	-	1250

Table 5.6 Depth profile of XPS of Al polarised to +2.5 V/SCE in pH 2, ion gun at 4 keV

The binding energy of the Al 2p transition of aluminium is 72.7-72.9 eV and that of the oxide is 74-75.4 eV. A large C 1s binding energy shift is apparent from table 5.6. It took 16 minutes of sputtering time for a signal from the aluminium metal to be detected. The Al 2p transition intensities of the metal and oxide are shown in figure 5.9. In this figure, the film looks thick and it took 18 minutes for a metallic signal to be recorded.

Figure 5.9, shows depth profile of the oxide film formed as a result of anodic polarisation of aluminium to + 2.5 V in acidic aqueous solutions. Different sputtering times were used and the Al 2p transition for metal and oxide are presented.

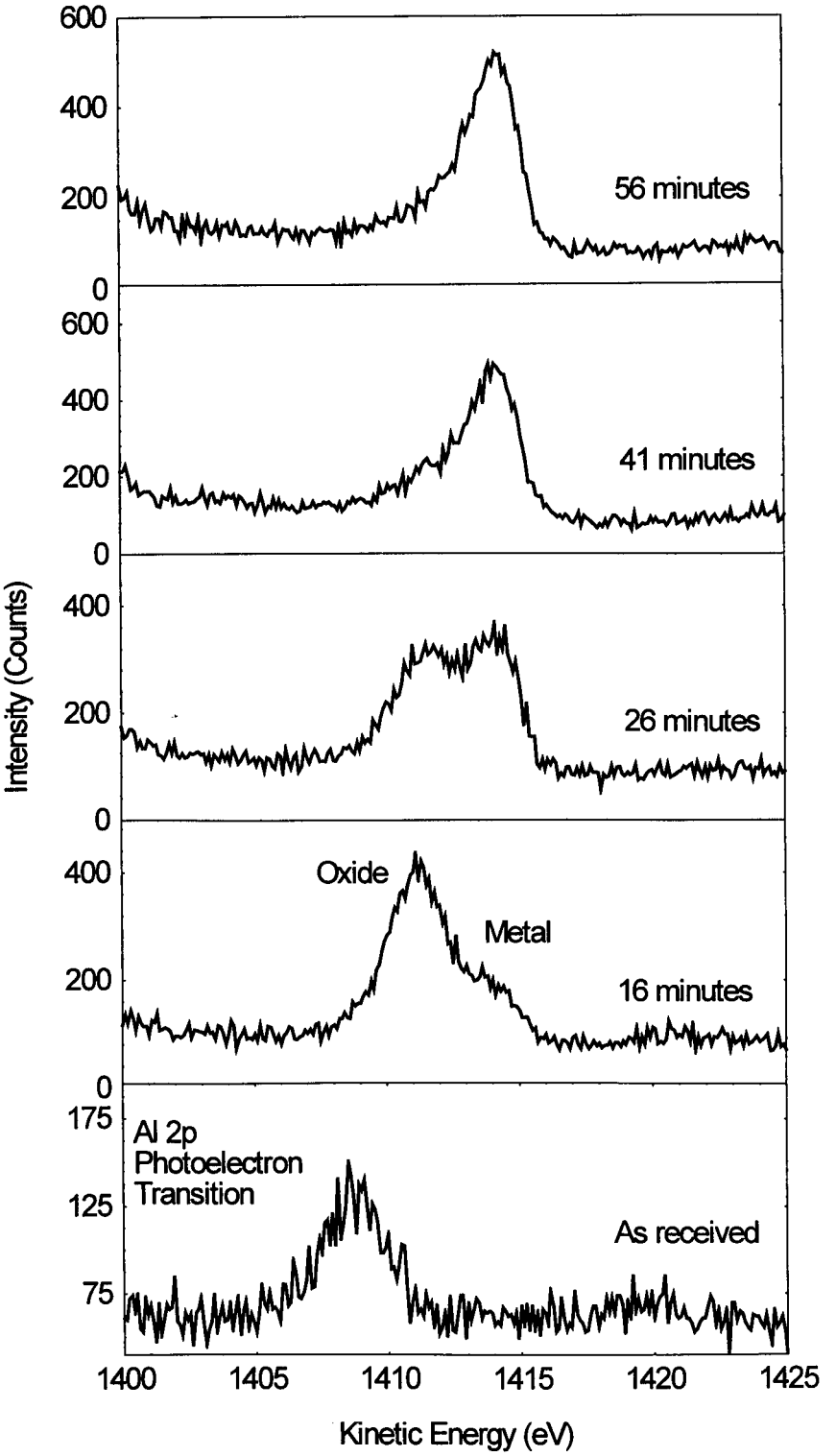

Fig 5.9 The depth profile of Al 2p XPS of oxide film on Al in water at pH 2 to +2.5 V, ion gun at 4 keV

5.3.7 XPS of Films on Aluminium Polarised in Aqueous Solution at pH 7

XPS spectra measured at different depths for anodic oxide films formed by anodic and cathodic polarisation of aluminium to +2.5 V/SCE and -2.2 V/SCE respectively, in aqueous solution at pH 7 are presented. As in previous cases, binding energies and other parameters are tabulated, whilst raw data graphs are used to show the relative thickness of each component of the oxide each

5.3.7.1 +2.5 V/SCE

Time of sputtering	Binding energy, E_b of Al 2p, O 1s, and C 1s transitions in eV				Charge corrected Al 2p oxide in eV	Al 2p oxide peak area	Al 2p metal peak area
	Al 2p oxide	Al 2p metal	O 1s	C 1s			
8 min.	76.8	-	534.5	285.9	75.5	940	-
47 min.	75.5	72.9	533.2	284.6	75.4	750	250
57 min.	75.2	72.7	532.9	284.3	75.4	400	600
72 min.	74.7	72.7	532.7	284.4	74.9	300	800
112 min.	-	72.6	532.7	284.6	-	-	1100

Table 5.7 XPS of Al polarised to +2.5 V in water at pH 7, ion gun at 4 keV

It can be seen in table 5.7 that the binding energy of metallic aluminium is in the range of 72.2-72.9 eV and for Al oxide is 74.6-75.7 eV. The intensity of aluminium oxide 2p transition is noticeable even after a few cycles of Argon sputtering, which indicate that the aluminium oxide is thick. The intensity of the aluminium metal and oxide is shown in figure 5.10. From this figure, it is clear that the oxide film is thick

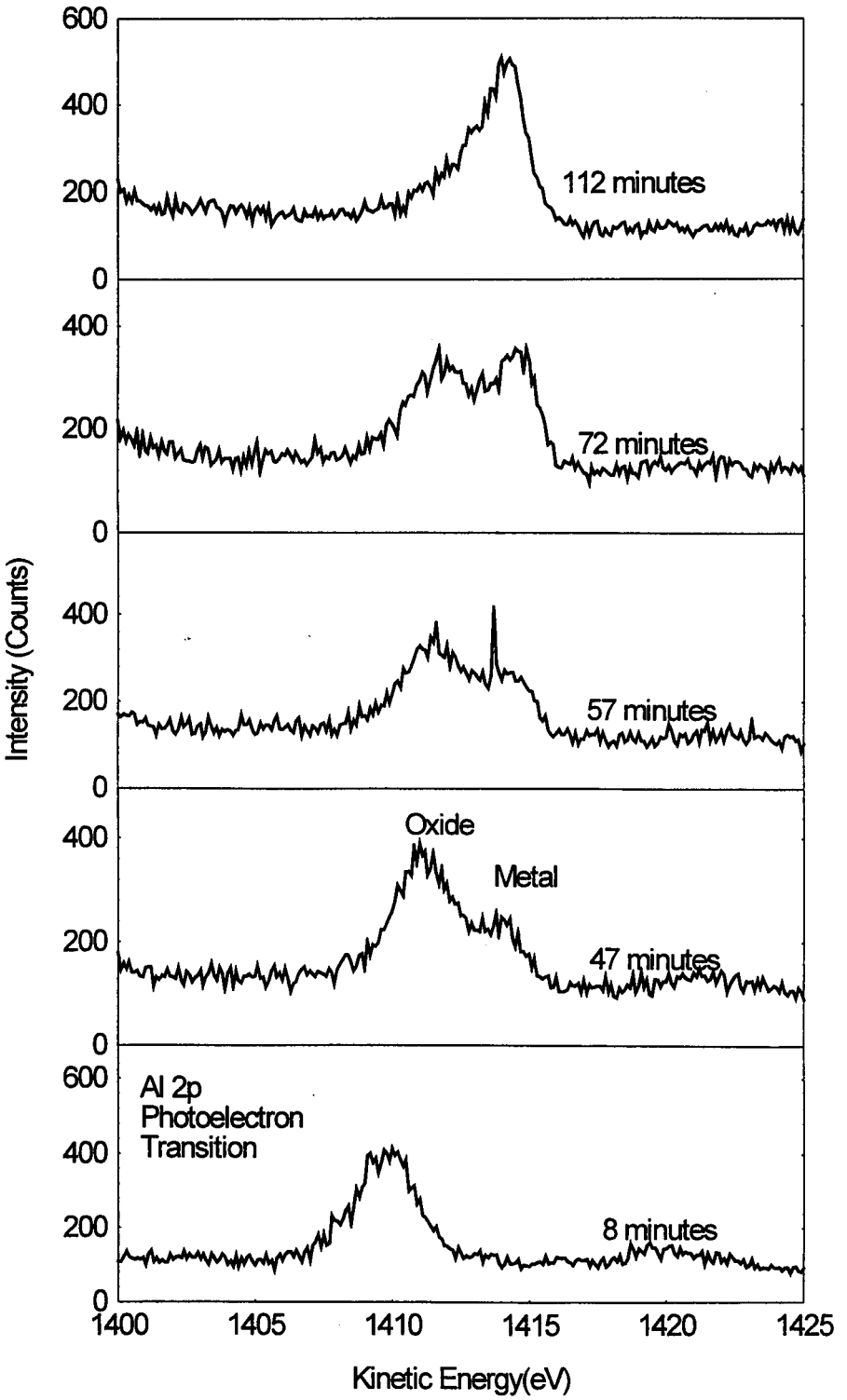

Fig 5.10 The depth profile of XPS of oxide film on Al polarised to +2.5 V/SCE in aq. sol. at pH 7, ion gun at 4 keV.

where it took almost 50 minutes of sputtering to notice the aluminium metal peak. Also the Al 2p peak measured after 8 minutes sputtering has a lower kinetic energy.

5.3.7.1 -2.2 V vs SCE

Time of sputtering	Binding energy, E_b of Al 2p, O 1s, and C 1s transitions in eV				Charge corrected Al 2p oxide in eV	Al 2p oxide peak area	Al 2p metal peak area
	Al 2p oxide	Al 2p metal	O 1s	C 1s			
As received	75.0	72.6	533.5	285.9	73.7	360	300
2 min.	74.6	72.4	532.8	284.6	74.6	800	450
7 min.	74.7	72.4	532.8	284.6	74.7	850	650
22 min.	74.7	72.5	532.8	284.6	74.7	300	850
47 min.	-	72.9	533.0	285.0	-	-	1200

Table 5.8 XPS Al 2p transition of oxide film on Al polarised in pH 7 to -2.2 V/SCE, ion gun at 4 keV

Polarising aluminium to -2.2 V in aqueous solution at pH 7, does not lead to the thickening of the pre-existing film. This conclusion is made on the basis of the binding energy of Al 2p transition due to the metallic (72.4-72.9 eV) and oxidised (73.7-74.9 eV) aluminium reported in table 5.8 as well as the E_b for O 1s and complemented by the absence of any charging on the oxide surface As it can be seen from figure 5.11, which displays the Al 2p transition intensity of the metal and oxide measured after various sputtering cycles, the film formed in this case is thin. It only took about 16 minutes of argon ion sputtering to remove the oxide film on aluminium.

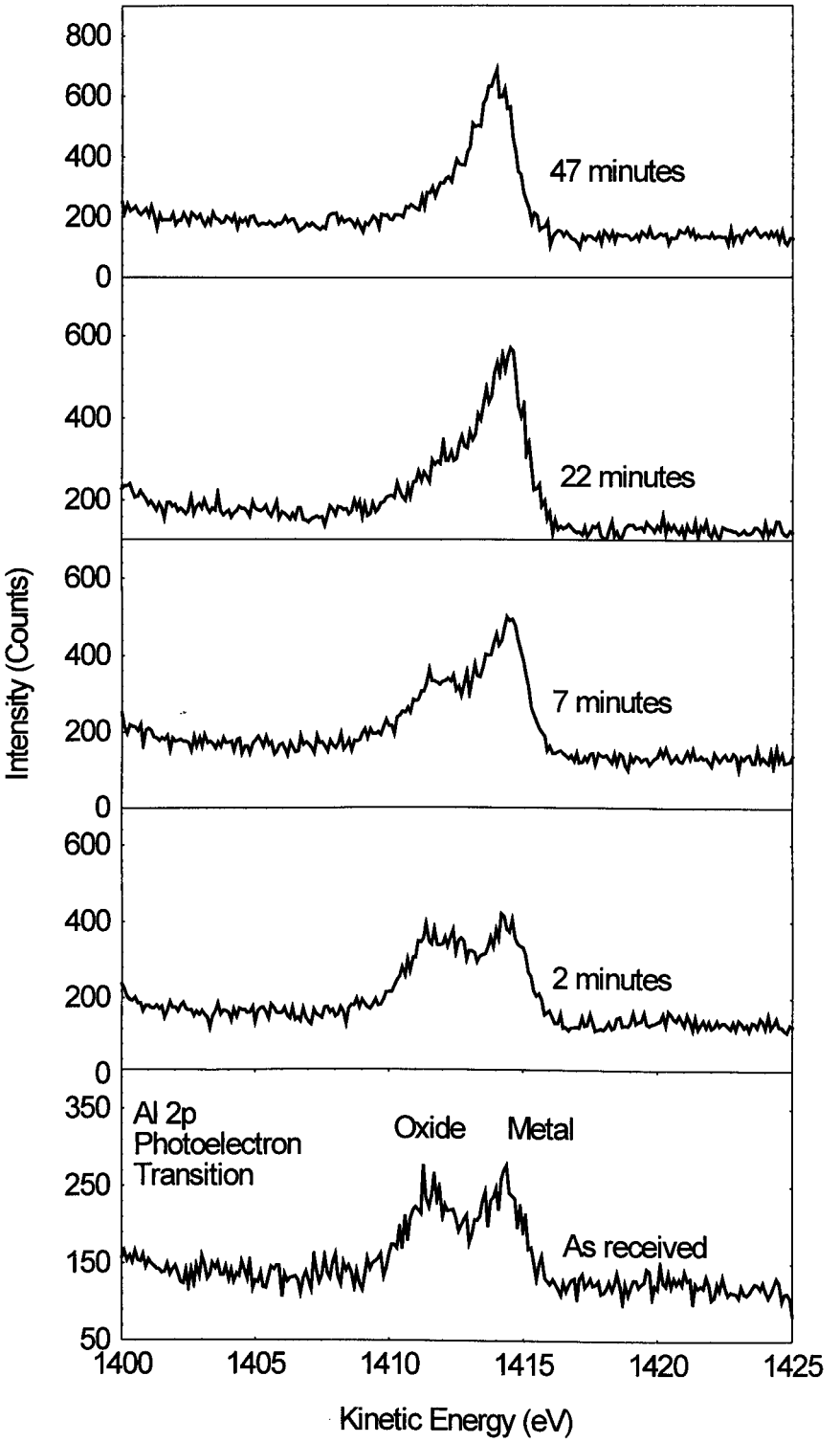

Fig 5.11 The depth profile of Al 2p transition intensities of Al polarised to -2.2 V/SCE in pH 7 aqueous solution

5.3.8 XPS Results of Films on Aluminium Polarised in pH 10

An aluminium electrode was anodically polarised to + 0.9 V in 0.05 M Na_2SO_4 electrolyte at pH 10 and the XPS results at different depths are presented in a tabulated and figure form.

5.3.8.1 +0.9 V/SCE

Time of sputtering	Binding energy, E_b of Al 2p, O 1s, and C 1s transitions in eV				Charge corrected Al 2p oxide in eV	Al 2p oxide peak area	Al 2p metal peak area
	Al 2p oxide	Al 2p metal	O 1s	C 1s			
As received	77.4	-	535.4	287.7	74.3	420	-
6 min.	75.5	72.8	533.4	284.7	75.4	1150	150
16 min.	77.3	74.9	535.2	286.5	75.4	800	600
26 min.	-	74.0	534.4	286.1	-	-	1150
51 min.	-	73.9	534.4	286.1	-	--	1500

Table 5.9 *XPS Al 2p of oxide film on Al in pH 10 polarised to +0.9V, ion gun at 4 KeV*

The binding energy of the Al 2p of the oxide was 77.4 eV and the C 1s showed about 3 eV shift from its value when there is no charging on the surface (284.6 eV). It took ~ 7 minutes of sputtering with the ion gun at 4 keV for the aluminium metal peak to be detected.. The binding energy of metallic aluminium for this oxide is in the range 72.8 - 74.9 eV and that of the oxide is 74.3- 75.4 eV.

Al 2p metal and oxide intensities in the as received form and after each sputtering are presented in figure 5.12. It can be seen form this figure that after the first sputtering cycle, the peak position tends to higher kinetic energies and after that the peak position stays the same.

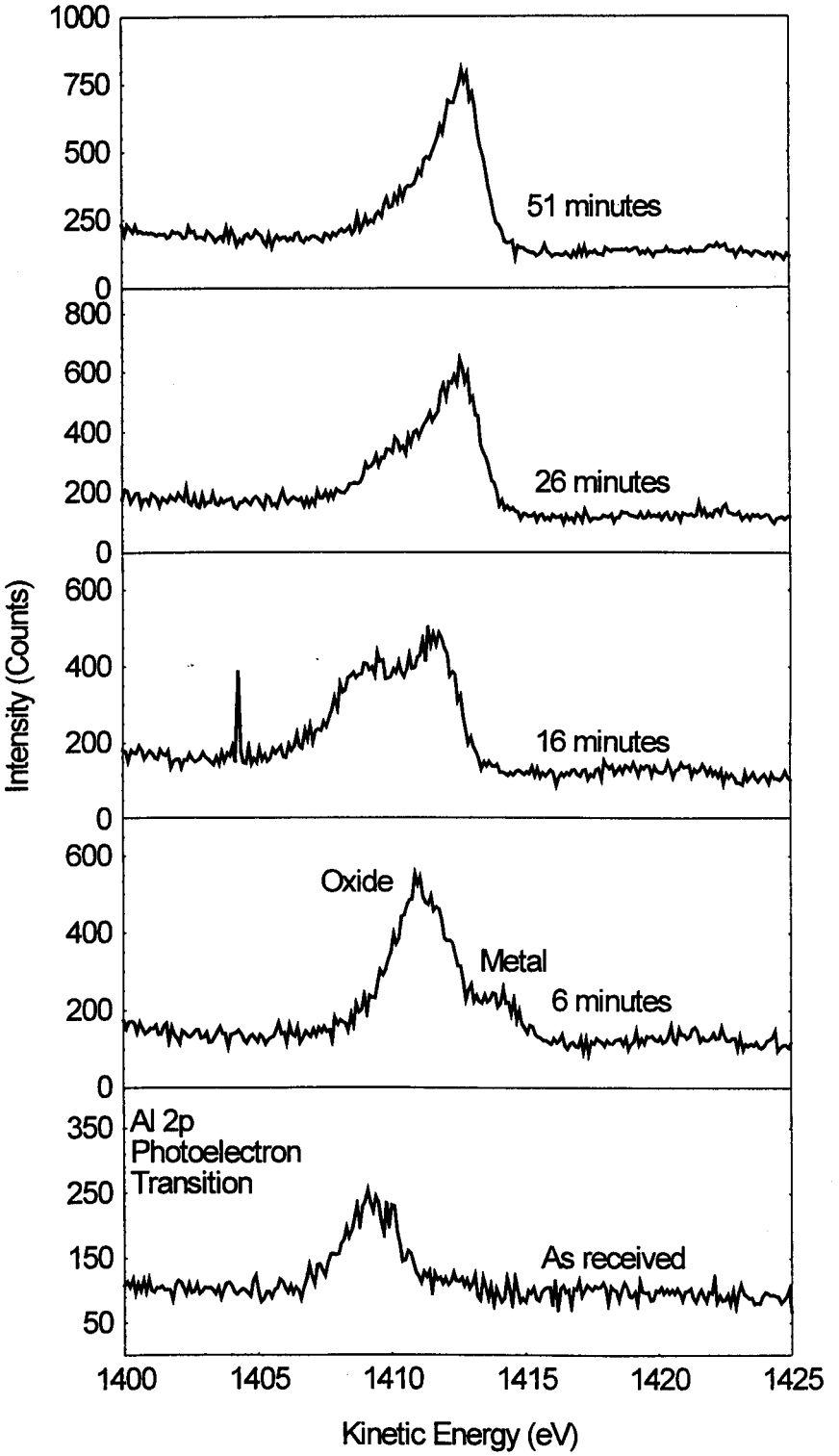

Fig. 5.12 The depth profile of XPS Al 2p transition of oxide film on aluminium in pH 10 polarised to +0.9V, ion gun at 4 keV.

5.4 Summary and Discussion

5.4.1 Electrochemistry Results

In this study current-potential curves were measured to monitor the growth of passive films formed by anodic and cathodic polarisation of pure aluminium, as bulk and a film in aqueous solutions as a function of pH and voltage. The potentiodynamic sweep of aluminium in water as seen from the polarisation curves in aqueous solutions at pH 2, 7, or 10, generally have no features and as expected, no oxygen evolution was observed at anodic potentials. The corrosion potential measured in this work for aluminium in aqueous media at various pH's agree with those reported by Craig et al. (2) and also reported by Moshier et al. (3). Based on this, it can be concluded that the electrochemical reactions are of the same nature, so as a consequence, the end product of the polarisation of aluminium in water at various pH's is the same as those prepared by Moshier et al. (3). The electrochemical results presented in fig. 5.1 a, b, and c and fig. 5.2 indicate that aluminium film samples behave in the same manner as those in bulk form. This can lead to the conclusion that the passivating layers anodically formed on aluminium surface in both forms are identical. So XPS, XANES, EXAFS, and REFLEXAFS results of these films which will be presented and discussed in chapter 6, are valid for aluminium in both forms.

5.4.2 XPS Results

XPS measurements were carried out to identify if electrolyte species incorporate into the passivating films on aluminium during formation by immersion or polarisation in water with 0.05 M Na_2SO_4 added electrolyte. Moshier et al. (3) have indicated that some of

the electrolyte species incorporate into thin anodic films on aluminium. From the XPS measurements carried out in this study, no traces of any of the species (Sulphur and Sodium) of the electrolyte were detected in these films and this is expected since the amount of added electrolyte is small and also low voltage level to which the polarisation was carried out.

From the value of E_b of C 1s given in the tables, in general, no charging on the passivating aluminium oxide layers was noticed in this study. The shift in the binding energy of the Al 2p oxide peak can be used as an indicator of the film having being in a different chemical and structural environment.

Based on the binding energy and the thickness of the film observed in tables 5.3, 5.5 and figures 5.6, 5.8, films formed by aluminium immersion for ~ 2 hours in aqueous media at pH 2 and 7 are as thick as the air formed film. There was no change in the C 1s value which indicate that there was no charging of the surface. Hence, there was no thickening of the pre-existing air-formed film and this proves that sample removal from the solution and the film's exposure to high vacuum in the XPS chamber does not introduce any changes in the film. This observation has also been made by Moshier et al.(3). This also proves that ex-situ investigations of passivating layers on aluminium using XPS in this chapter and XAS in the next chapter is valid.

Table 5.6 and figure 5.9 shows that anodic oxide films on aluminium in acidic aqueous electrolytes at pH 2 to +2.5V is relatively thick where the uncorrected E_b of 77 eV indicates some charging on the film's surface. This result agrees with the finding of Moshier et al. (3). It took few sputtering cycles for the Al 2p transition in metallic state to be detected. From figure 5.11 and table 5.8, cathodic polarisation of aluminium in

neutral aqueous solutions to -2.2 V/SCE does not lead to the thickening of the initial air oxide film. Again relying on the oxide and metallic Al 2p state, it is evident from figure 5.12 and table 5.9 that the oxide film formed on aluminium polarised to +0.9 V/SCE in aqueous media at pH 10 is thick

Fuggle et al. (4) has suggested that O 1s has a binding energy of 532.4 eV for oxygen in aluminium oxide. The values measured and reported in this investigation for O 1s in oxide films on aluminium agree very well with this value except in the case of oxides on aluminium in boiling water (538 eV) and that of aluminium polarised to + 0.9 V in pH 10 (535 eV), which could be an oxyhydroxide phase (see chapter 6).

The binding energy separation between the Al 2p of the charge corrected oxide and the metal was given as 2.6-3.7 eV (5,6) and the metallic 2p transition state was reported to be 71.8 eV. For the XPS depth profile data reported from this work, the metallic and oxide energy separation of Al 2p was found to be 2.1-2.7 eV and the E_b of the metallic Al 2p was 72.8 eV except for the film on aluminium in pH10 polarised at +0.9V where a value of ~ 74.8 was recorded. Different binding energy values for metallic Al 2p are given in the literature (7) 72.72 eV, (8) 72.85 eV, and (9) 72.84 eV.

In general the electrochemistry and XPS data presented in this chapter for anodic passivating oxide layers on aluminium, agree with the work reported by Moshier et al.(3) about under which polarisation conditions, a film forms and its relative thickness. From table 5.5, the charge corrected binding energy of the Al 2p of oxide film produced by immersing aluminium in boiling water for ~ 30 minutes was found to be 80 eV and it is known that the structure of this oxide is a pseudoboehmite crystalline phase. Whilst all the charge corrected E_b of Al 2p due to oxidised Al reported in this study for thin

passivating layers on aluminium formed as specified in this thesis, was found to be ~ 74 eV. Comparing the two Al 2p oxide E_b values, it is clear that the anodic oxide films on aluminium do not resemble the pseudoboehmite structure which was suggested by Moshier (3). The binding energy of the O 1s reported in this thesis, leads to the same conclusion where the binding energy of the O 1s for passivating films on aluminium was found to be ~ 532.8 eV, whilst that of the pseudoboehmite was ~ 538.0 eV. Also from the binding energies of the Al 2p and the O 1s of each film formed on aluminium and measured at various depths, it is clear that these films have a homogeneous structure all the way through..

References

(1) ASRM Standards on Surface Analysis, ASTM, Philadelphia, PA., (1986)
(2) Craig, H. L., and Scott, J. R., J. Matter., **4**(1969)540
(3) Moshier W. C., Davis, G. D., and Ahearn, J. S., Corro. Sci., **27**(1987)785
(4) Fuggle, J. C., Warson, L. M., Fabian, D. J., and Affossman, S., Sueface Science, **41**(1975)61
(5) Strohmeier, B. R., Surf. Interfaces Anal., **15**(1990)51
(6) Ocal, C., Bascurco, B., and Ferrer, S., Surf. Sci., **157**(1085)233
(7) Wagner, C. D.,Passoja, D. E. Hillery, H.F.Kinsiky, T. G., Six, H. A., Jansen, W. T., and Taylor , J. A. J. Vac. Sci. Technol., **21**(1982)933
(8) Talyor, J. A., J. Vac. Sci. Technol., **20**(1982)751
(9) Allgeyer, D. F., and Pratz, E. A., Surface and Interfaces Analysis, **18**(1992)465

6. Chapter Six EXAFS, XANES, and ReflEXAFS of Thin Passivating Films on Aluminium

6.1 Introduction

As has been discussed in chapter one, techniques such as, XPS, electron microscopy, and x-ray, neutron and electron diffraction are not capable of resolving passivating oxide films structure. X-ray absorption spectroscopy fulfils this requirement and was used in this study to characterise the structure of passive films on aluminium.

All of the EXAFS, XANES, and ReflEXAFS spectra presented in this chapter were measured above the aluminium K-edge (1560 eV) using station 3.4 SOXAFS of the SRS at Daresbury.

6.2 Model Compounds

To extract structural information from the EXAFS spectra measured above the aluminium K-edge for oxide films formed as explained in this study, phase shifts must be used. The need to correct for the phase shifts arises from the fact that the emitted photoelectrons experiences the potential of the backscattering atom once and that due to the absorbing atom twice. Accurate bond length determination depends on the use of reliable phase shifts for the species involved. As was explained in chapter 2, there are many ways to obtain phase shifts and the one adopted in this work is the same as the method used in chapter four.

Model compounds are chemical materials with known structures usually determined by the use of x-ray diffraction technique. In this study, aluminium metallic foil was

used as a model compound to test the phase shift for aluminium Alpha alumina was chosen to be the model compound to test the phase shift due to oxygen species. The transmission EXAFS spectrum for aluminium film, measured about the aluminium K-edge is presented in fig. 6.1. Also, an EXAFS spectrum for alpha alumina model compound is given in fig. 6.2, showing the absorption as a function of photon energy.

The EXAFS experimental data presented for aluminium and alpha alumina have to be theoretically fitted to determine the structural parameters. One of the main ingredients of resolving the structure of the passivating films on aluminium is to calculate the phase shifts due to the species present in the oxide film. The phase shift calculation for aluminium and oxygen was carried out in EXCURV92 programme. In this programme, these calculation are based on the muffin tin approximation for the potential. Hedin-Lundqvist method was used to calculate exchange potential where an analytical approximation to the self energy (1) was employed. The Von-Bart (2) approximation was used to calculate the ground state.

Once the phase shifts were calculated, they were used and along with the model compound crystallographic structural parameters, to fit the experimental EXAFS spectra. Bond length distances, number of atoms in each shell, Debye-Waller factor, type of atoms in each shell, E_f, which is the difference in energy between the vacuum level and the absorption edge being measured, are parameters used to fit the EXAFS spectrum..

The structural parameters of the best fit and those of the experimental EXAFS spectrum for aluminium foil, along with the accuracy of their determination, are listed

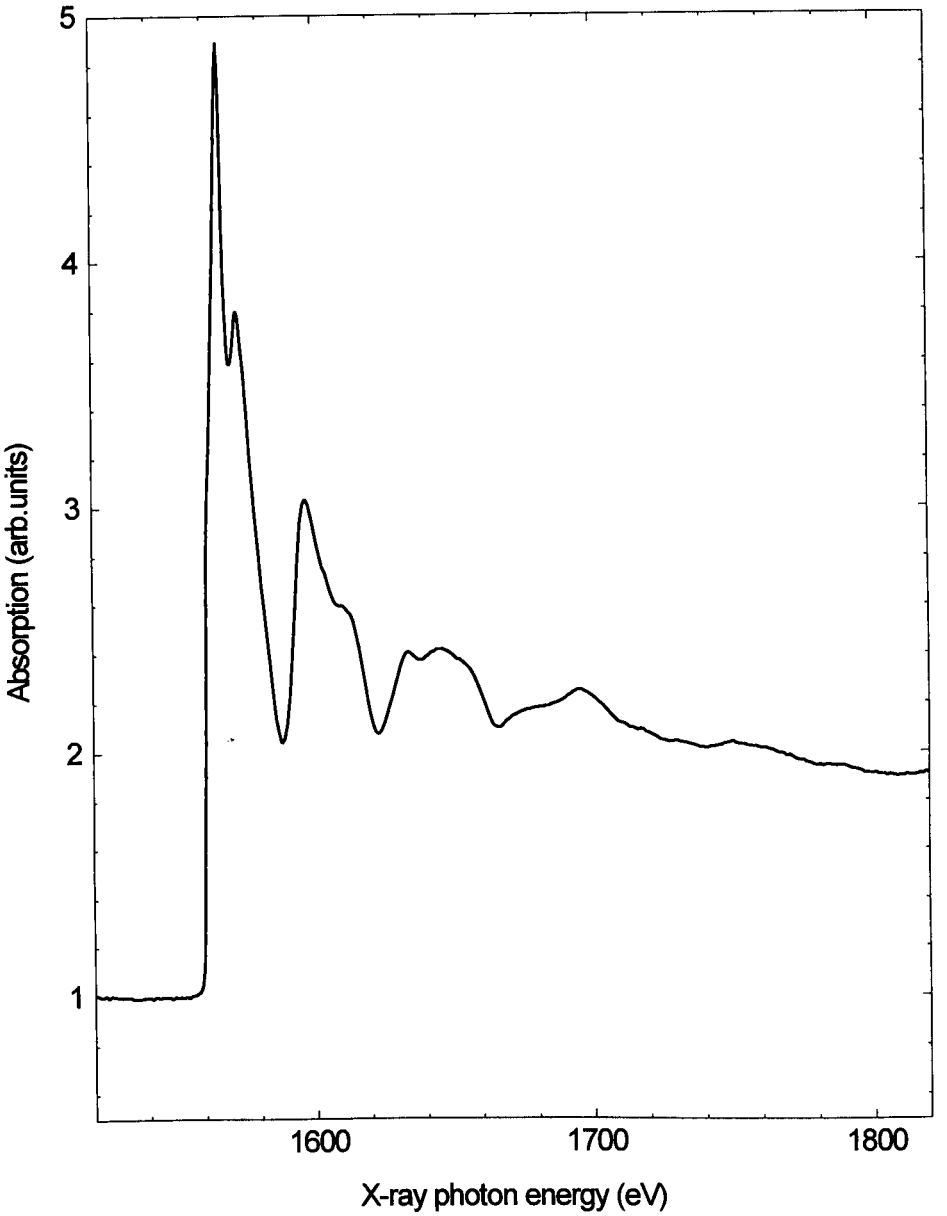

Figure 6. 1 EXAFS spectrum of aluminium foil measured in transmission mode above the aluminium K-edge

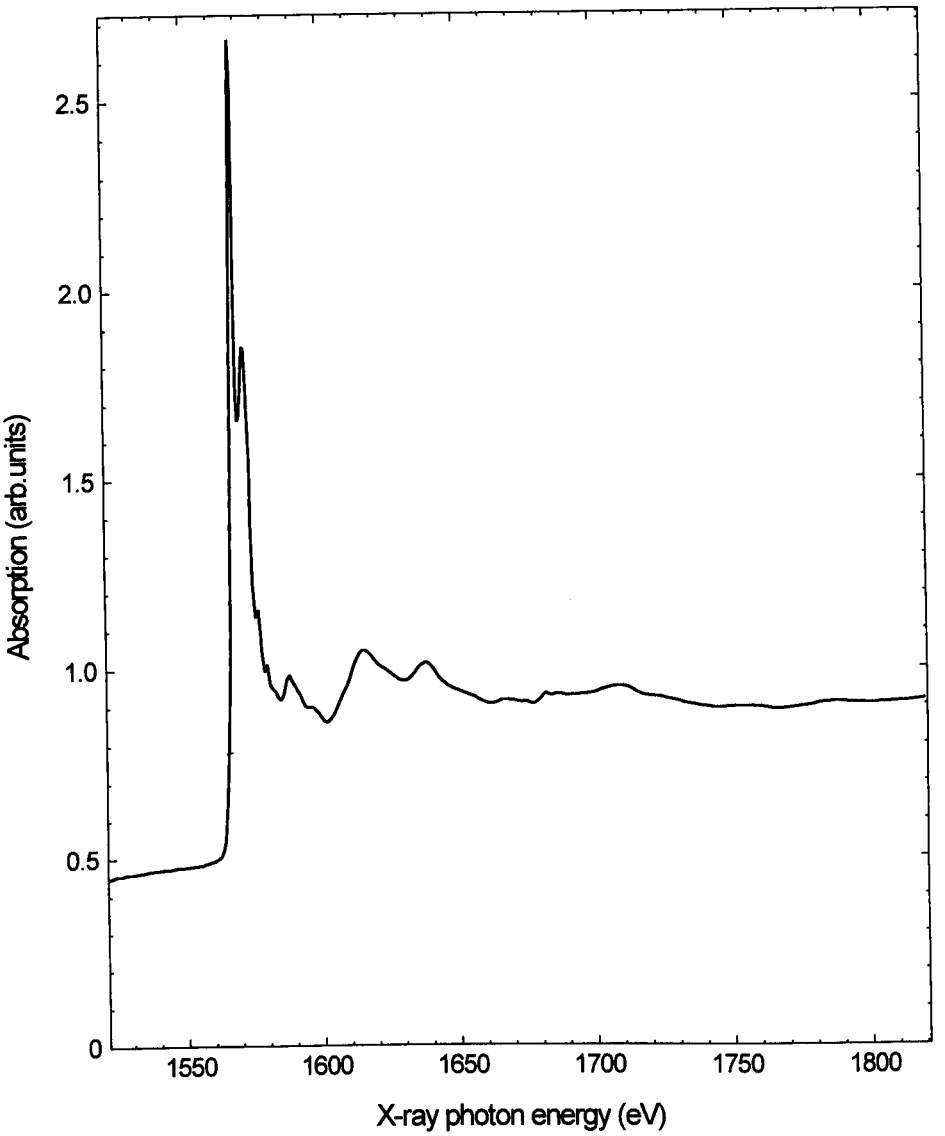

Figure 6. 2 EXAFS spectrum of alpha alumina model compound measured in total electron yield above the aluminium K-edge

in table 6.1 along with the crystallographic structural parameters (3), and the fits is shown in figure 6.3.

Shell No.	Type of Atom	Experimental Co-ordination Number	Crystallographic Co-ordination No.	Experimental Bondlength R/Å	Crystallographic Bond-length R/Å	Deby-Waller Factor $2\sigma^2/Å^2$
1	Al	12.4±1.4	12	2.83±0.003	2.863	0.013±0.002
2	Al	6.3±1.9	6	4.01±0.02	4.05	0.05±0.015
3	Al	17.3±5.2	24	5.91±0.01	5.95	0.03±0.006

Table 6.1 Structural parameters of the first three shells of aluminium atoms surrounding the absorbing aluminium atom.

Fig. 6.3 shows the theoretical fit for aluminium experimental EXAFS function above the Al K-edge. The same procedure was employed to calculate the phase shift for oxygen and then was used with crystallographic structural parameters to produce the best theoretical fit for the EXAFS spectrum of alpha alumina. Table 6.2, presents the structural parameters obtained from the fitted experimental EXAFS and that of the crystallographic data. Figure 6.4, presents the experimental and theoretical fit of the EXAFS function weighted by k^3 as well as the Fourier transform of alpha alumina.

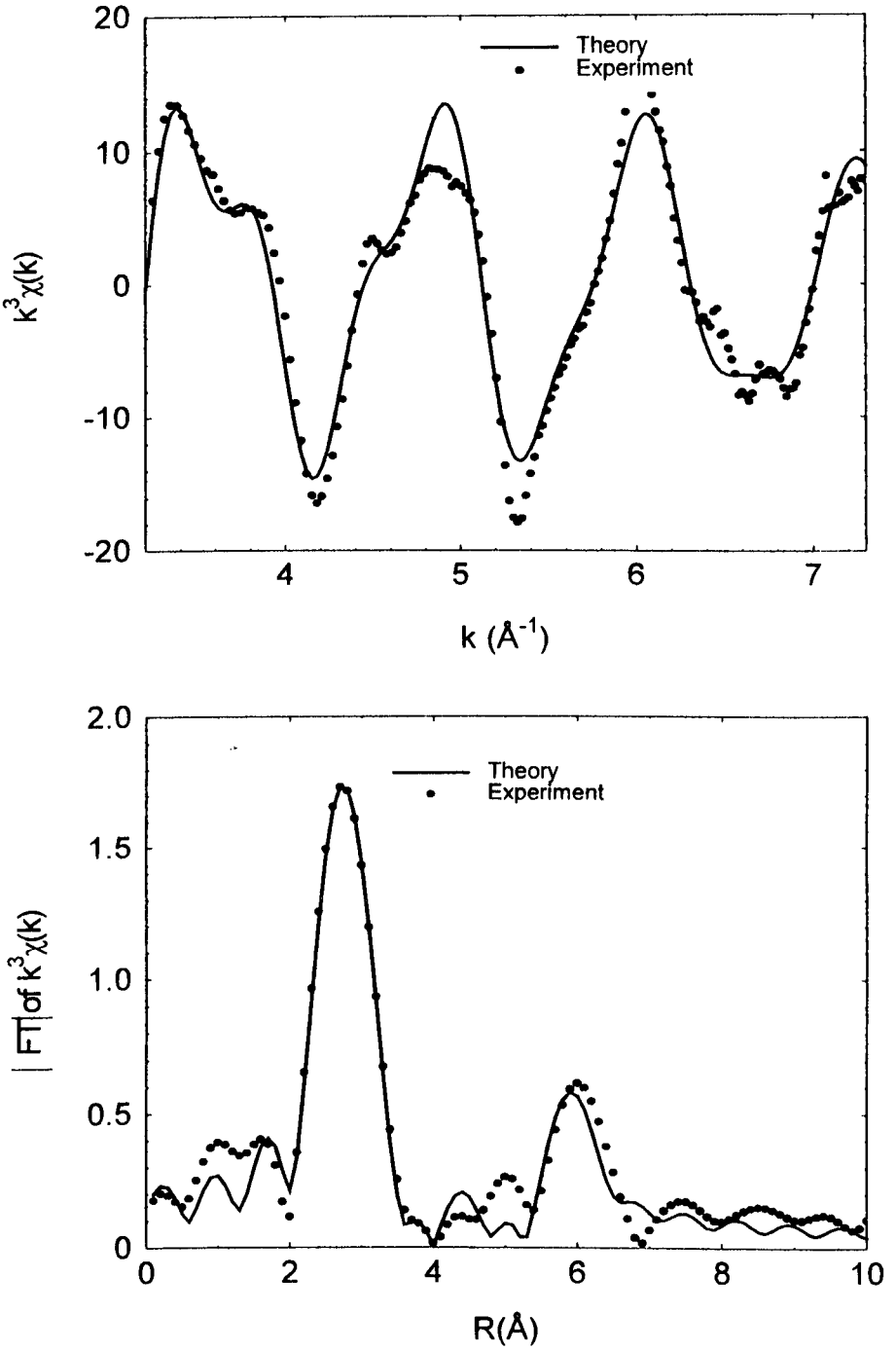

Figure 6.3, presents the experimental and the best fit of the EXAFS function of aluminium foil weighted by k^3 as well as their Fourier transform. EXAFS function above the Al K-edge.

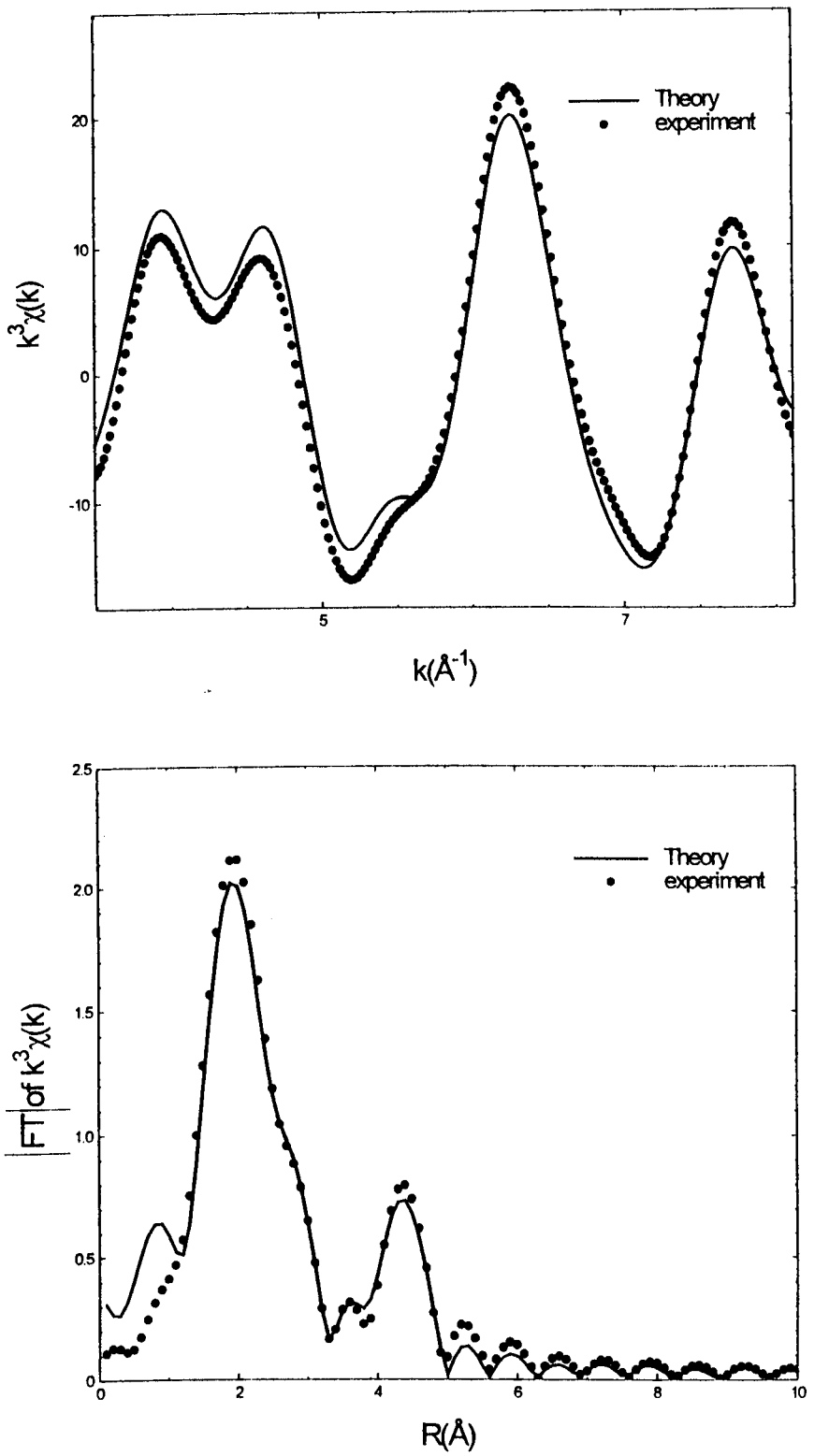

Figure 6.4 k^3 weighted EXAFS function of alpha alumina, a theoretical fit for the first 5 shells, and their fourier transform. Al-K edge

Shell No.	Type of Atom	Experimental Co-ordination Number	Crystallographic Co-ordination No.	Experimental Bondlength/ Å	Crystallographic Bond-length/ Å	Debye Waller Factor $2\sigma^2/Å^2$
1	O	2.8 ± 0.20	3	1.89 ± 0.01	1.855	.005 ± 0.001
2	O	2.6± 0.20	3	1.90 ± 0.015	1.97	.0044 ± 0002
3	Al	3.90 ± 025	4	2.75 ± 0.02	2.79	.002 ± 0.001
4	O	4.2 ± 0.60	3	3.22 ± 0.02	3.22	.006 ± 0.002
5	O	6.90 ± 0.95	4.2 ± 0.18	4.44 ± 0.02	4.52	.003 ± 0.001

Table 6.2 contains structural parameters obtained from the best fit of four summed α - alumina EXAFS spectra. The bond length and the co-ordination number values are compared with the crystallographic (4) values.

It is concluded that the phase shifts calculated in EXCURV92 through the procedure outlined in this section are acceptable and can be used to yield good theoretical fitting for the experimental EXAFS data. Based on the phase transferability property where for the same pair of absorber-backscatterer, the phase shift is transferable and can be used to fit the experimental EXAFS of the oxide film on aluminium with unknown structure.

6.3 EXAFS Results for Passivating Thin Oxide Films on Aluminium

In this section, the EXAFS, XANES, and ReflEXAFS results of the oxide films anodically grown on aluminium in different conditions are presented along with the structural parameters of each oxide.

6.3.1 EXAFS Results of Oxide Films on Aluminium in Aqueous Solution at pH 7

Total electron yield EXAFS spectra were collected for aluminium treated in aqueous solutions at pH 7. The phase shifts calculated in EXCURV92 and used to fit the model compounds are used to fit the EXAFS spectra collected for each oxide film.

6.3.1.1 Polarisation to + 2.5 V

The local structural parameters of the backscattering shells in the oxide film formed on aluminium polarised to + 2.5 V in aqueous solution are given in Table 6.3.

Shell No.	Type of Atom	Co-ordination No.	Bondlength/Å	Debye-Waller Factor, 2 σ^2/Å^2
1	O	4.2 ± 0.18	1.880 ± 0.002	0.01 ± 0.001
2	Al	4.0 ± 0.7	2.880 ± 0.006	0.03 ± 0.006

Table 6.3 Structural parameters of the oxide film formed by polarisation of aluminium in aqueous solution at pH 7 to + 2.5 V.

It is seen from table 6.3, that beside the oxygen backscattering shell, there is a contribution from a metallic aluminium shell as well. The aluminium metallic signal arises as a result of the fact that the oxide films formed here are thin and that the sampling depth is more than the thickness of the oxide film.

The presence of the metallic aluminium signal in the EXAFS spectrum complicates the analysis of these oxide. To obtain a good fit for the oxide contribution, it is necessary to include a metallic aluminium shell in the fitting of the EXAFS spectra. A fitting parameter, XE2 was used to a correction for different E_0 for phase shift due to the presence of aluminium signal beside that of the oxide.

Fig. 6.5, shows the experimental and theoretical EXAFS function, $k^3 \chi(k)$ as well as its Fourier transform for the oxide on aluminium polarised to +2.5 V in aqueous solution at pH 7.

6.3.1.2 Polarisation to +2.5 V and left connected for 4 hours

It was intended to check the effect of leaving aluminium electrode connected to the potentiostat for four hours on the oxide film which form in such conditions.

Shell No.	Type of Atom	Co-ordination No.	Bondlength/Å	Debye-Waller Factor, $2\sigma^2$/Å^2
1	O	4.75 ± 0.12	1.87 ± 0.001	0.01 ± 0.001
2	Al	1.84 ± 0.46	2.93 ± 0.01	0.024 ± 0.01

Table 6.4 Parameters of the local structure around aluminium absorbing atom in the oxide film formed by polarisation to + 2.5 V and then the sample was left connected to the voltage source for four hours.

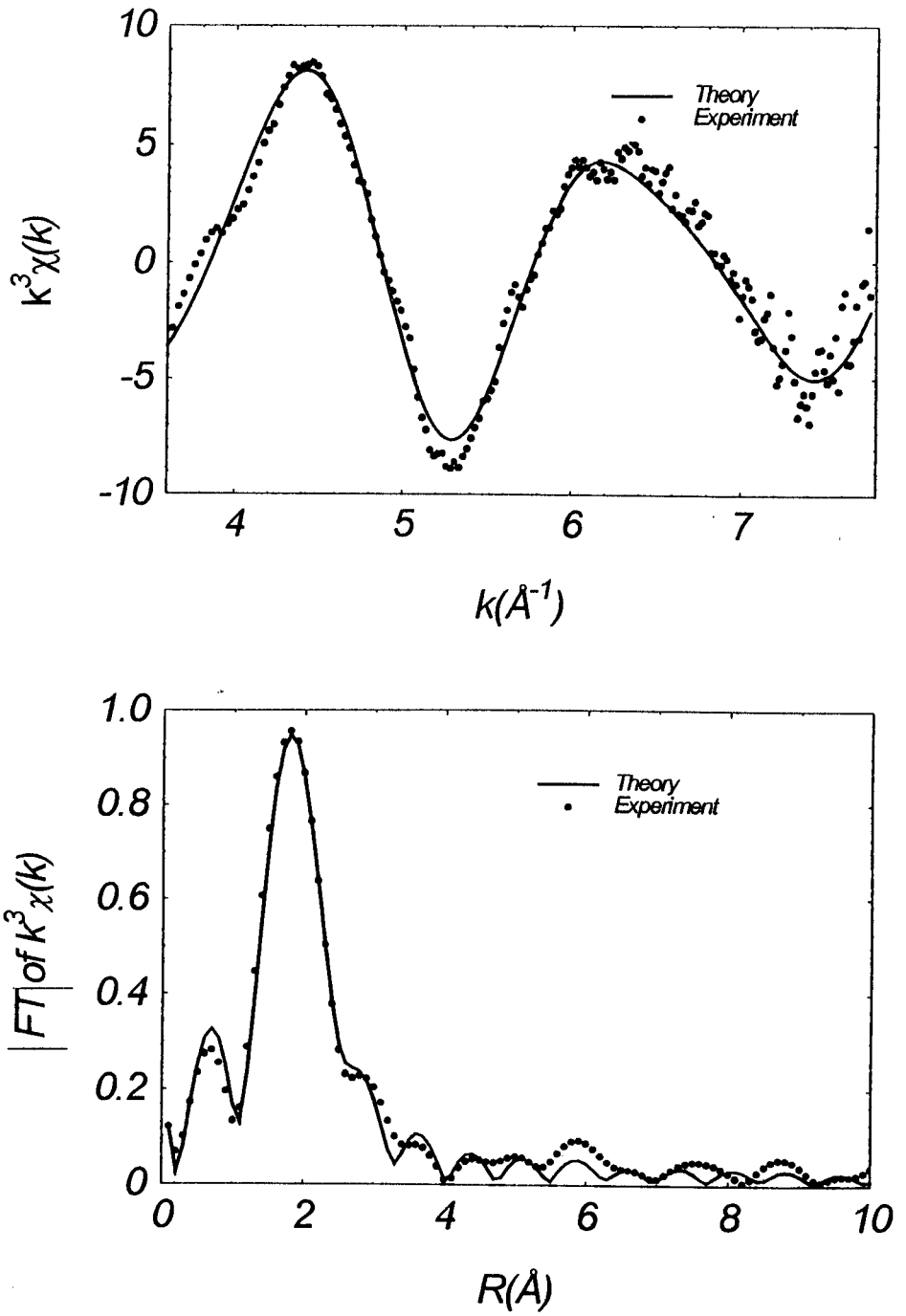

Figure 6.5, Experimental and theoretically fitted EXAFS function, $k^3\chi(k)$, for the oxide film formed by polarising aluminium to + 2.5 V in pH 7, also the Fourier transform is shown which indicate the shell distance in Å. Al K-edge

From the co-ordination number reported for the oxide formed on aluminium and left connected for four hours, it can be said that there is an increase in thickness. There is no change in the Al-O bond length between the oxide formed at +2.5 v and the one formed at the same potential and left connected for four hours. There has been no structural changes in this case. From the Al in the second shell, there is a noticeable drop in the co-ordination of Al-Al.

The theoretical best fit for the EXAFS k^3 weighted function and the Fourier transform of the oxide formed on aluminium polarised in pH 7 to +2.5 V and left connected for four hours is presented in fig. 6.6.

6.3.2 EXAFS of Films on Aluminium in Aqueous Media at pH 2

In this section, EXAFS results of aluminium cathodically polarised to -2.17 V and anodically polarised to + 2.5 V are presented. The structural parameters are presented in a tabulated form.

6.3.2.1 Polarisation to -2.17 V

The structure of oxide film that forms on aluminium cathodically polarised in aqueous media at pH 2 to -2.17 V was investigated by measuring the its EXAFS spectra. After EXAFS theoretical fitting, the parameters of the local structure of this oxide film are given in table 6.5.

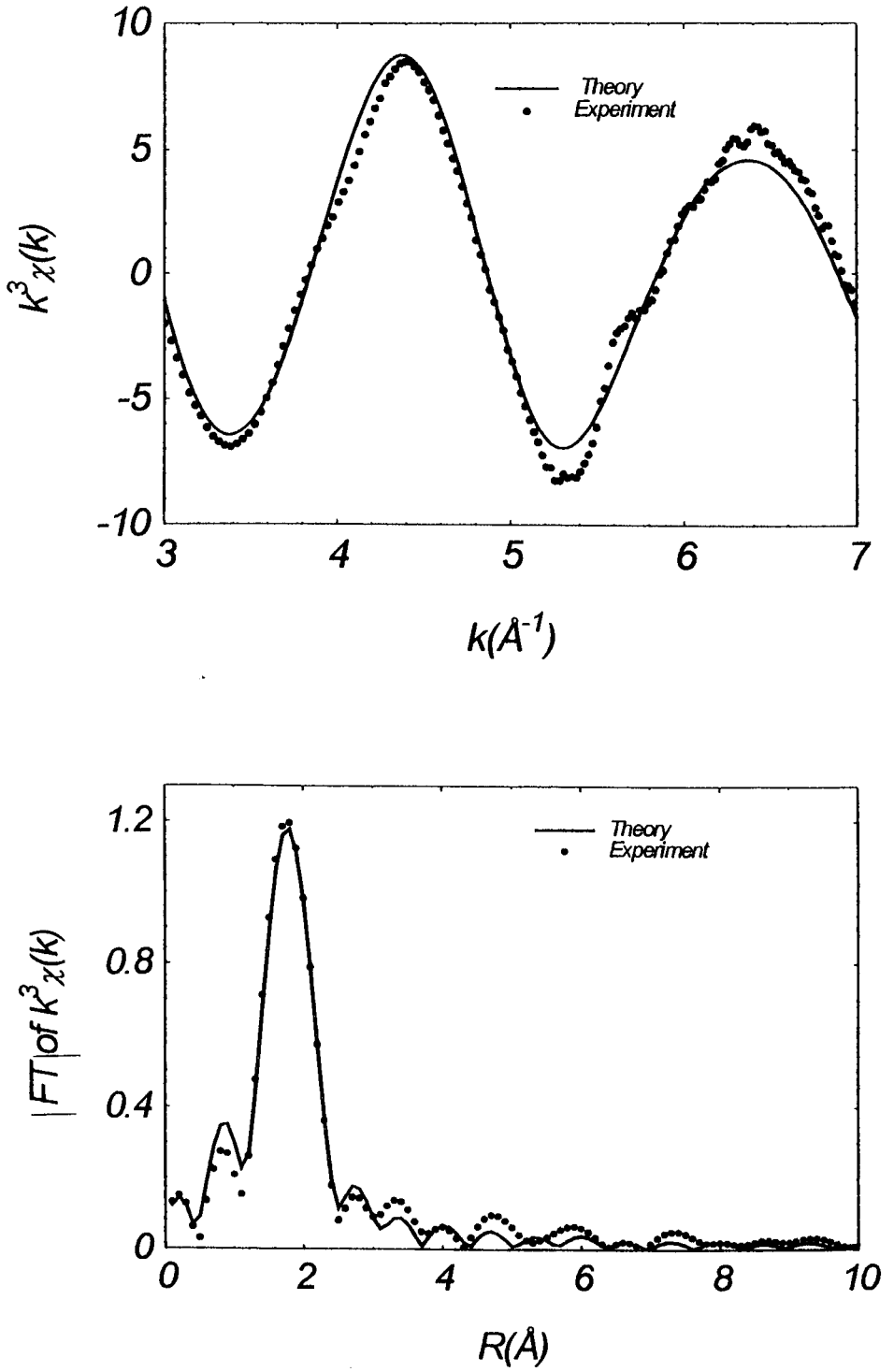

Fig. 6.6 Experimental and theoretically fitted $k^3\chi(k)$ are presented for the EXAFS of the oxide film formed by polarisation at +2..5V, pH7 and left connected for four hours, Fourier transform is given as well where the shell distance is indicated. Al K-edge EXAFS

Shell No.	Type of Atom	Co-ordination No.	Bondlength/Å	Debye-Waller Factor, $2\sigma^2/Å^2$
1	O	3.87 ± 0.142	1.87 ± 0.002	0.006 ± 0.001
2	Al	4.32 ± 0.68	2.88 ± 0.01	0.031 ± 0.005

Table 6.5 Bond length, co-ordination number for the two backscattering shells, where the first is due to the oxygen in the oxide film and the second shell is metallic aluminium.

Cathodic polarisation of aluminium in water at pH 2 to -2.17 V, leads to the formation of an oxide film which is thick but still not thick enough for the metallic aluminium signal to disappear. Figure 6.7 presents in a graphical way, the theoretically fitted and experimentally obtained EXAFS function, k^3 weighted and its` Fourier transform for the film formed on aluminium cathodically driven to -2.17 V in pH 2.

6.3.2.2 Polarisation to + 2.5 V

The oxide film in this case was formed by polarisation of aluminium to + 2.5 V in aqueous media at pH 2. Bond length between the absorbing aluminium atom and the aluminium and oxygen backscattering shells, their co-ordination number, and the Debye-Waller factor for these shells are presented in table 6.6.

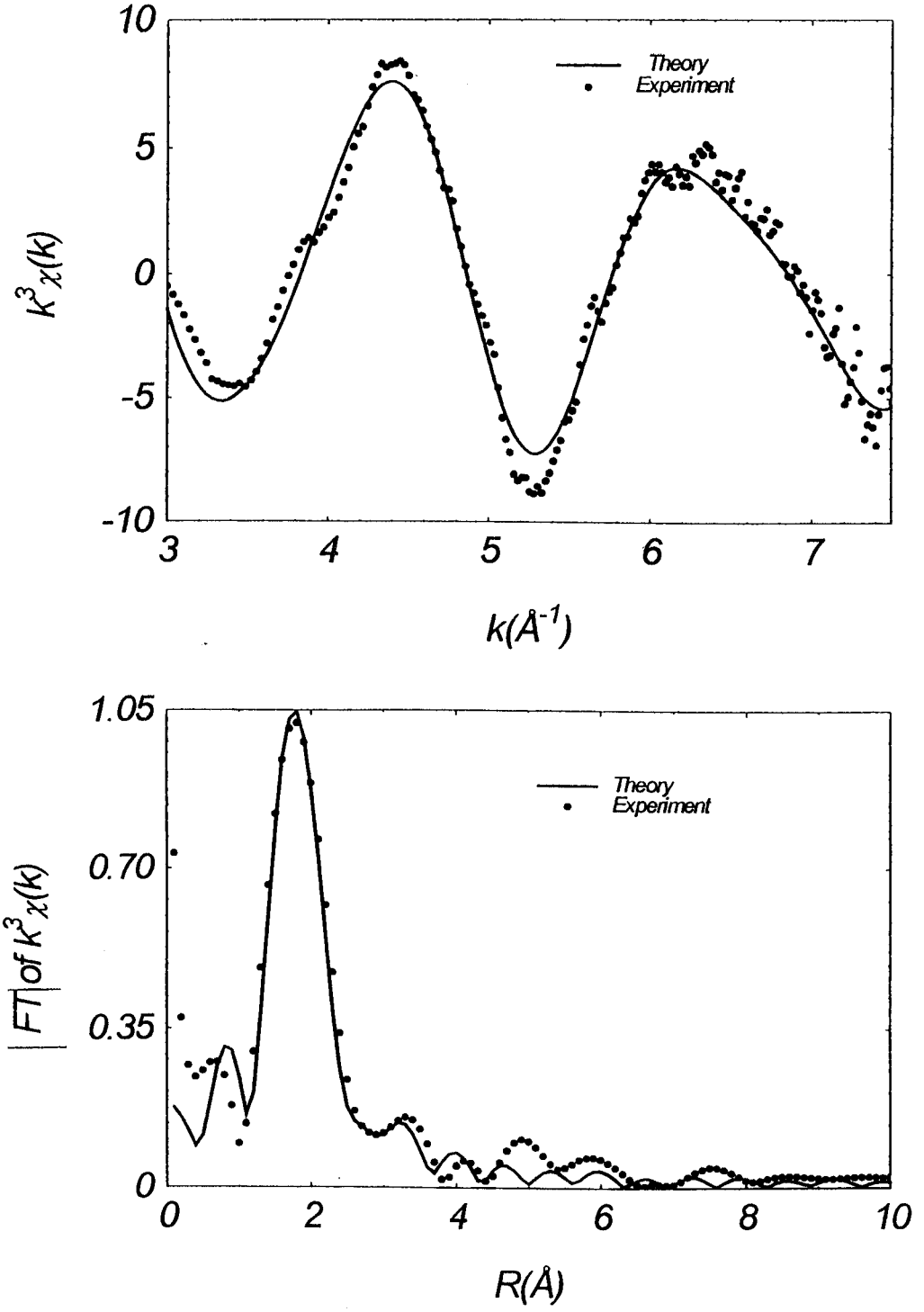

Figure 6.7 Experimental and theoretically fitted $k^3\chi(k)$ are presented for the EXAFS of the oxide film formed by polarisation to -2.17 V in pH 2, Fourier transform is given as well where the shell distance is indicated. Al K-edge

Shell No.	Type of Atom	Co-ordination No.	Bondlength/Å	Debye-Waller Factor, $2\sigma^2/Å^2$
1	O	3.8 ± 0.33	1.84 ± 0.002	0.015 ± 0.003
2	Al	3.0 ± 0.67	2.87 ± 0.006	0.018 ± 0.006

Table 6.6 Parameters of the local structure around aluminium absorbing atom in the oxide film formed by polarisation to + 2.5 V in aqueous solution at pH 2.

Based on the co-ordination number given for the oxygen shell in table 6.6, an oxide film grows under these conditions but it is not thick enough since there is a metallic aluminium contribution. A much thinner oxide film forms on aluminium anodically polarised in aqueous solution at pH at + 2.5 V, than the one which forms on aluminium cathodically polarised to - 2.17 V in the same environment.

The experimental and theoretical fit of the k^3 weighted EXAFS function of the film formed on aluminium in pH 2 at +2.5 V as well as its Fourier transform are given in fig. 6.8.

6.3.3 EXAFS of Films on Aluminium in Aqueous Solution at pH 10

6.3.3.1 At corrosion potential for an hour (immersion)

The oxide which structure was investigated was formed by immersing an aluminium sample in water at pH 10 for almost an hour. Total electron yield EXAFS

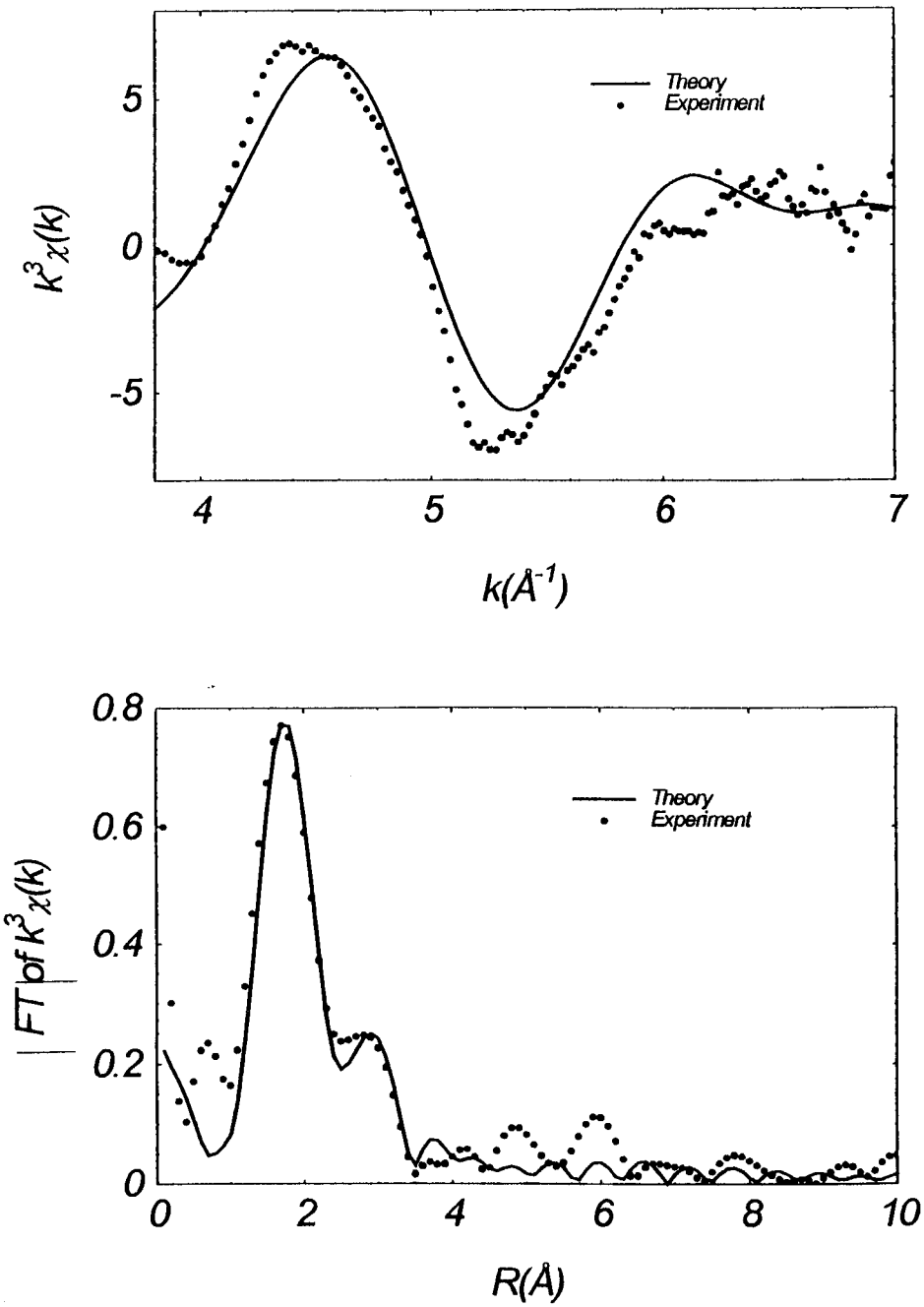

Figure 6.8 Experimental and theoretically fitted EXAFS function, $k^3\chi(k)$, for the oxide film formed by polarising aluminium to + 2.5 V in aqueous solution at pH 2, also the Fourier transform is shown which indicate the shell distance in Å. Al K-edge EXAFS

measurements were conducted to resolve this oxide local structure. The structural data of oxygen and aluminium shells are presented in a tabulated form.

Shell No.	Type of Atom	Co-ordination No.	Bondlength/Å	Debye-Waller Factor, $2\sigma^2/Å^2$
1	O	1.8 ± 0.7	1.9 ± 0.01	0.005 ± 0.014
2	Al	9.6 ± 2.37	2.85 ± 0.005	0.025 ± 0.008

Table 6.7 Parameters of the local structure around aluminium absorbing atom in the oxide film formed by immersion of aluminium in pH 10 aqueous solution for an hour.

From the co-ordination number presented for the metallic and the oxide shells in table 6.7, the EXAFS signal is totally dominated by that of the aluminium and this indicates that the oxide film formed under these conditions is thin.

6.3.3.2 Polarisation to -1.8 V

A total electron yield EXAFS spectrum was collected for aluminium cathodically driven to -1.8 V in aqueous media at pH 10. EXAFS data analysis was carried out and the parameters which describe the local structure of the surface oxide are presented in the table 6.8.

Shell No.	Type of Atom	Co-ordination No.	Bondlength/Å	Debye-Waller Factor, $2\sigma^2/Å^2$
1	O	1.8 ± 0.7	1.9 ± 0.01	0.005 ± 0.014
2	Al	9.6 ± 2.37	2.85 ± 0.005	0.025 ± 0.008

Table 6.8 Parameters of the local structure around aluminium absorbing atom in the oxide film formed by polarisation to - 1.8 V in aqueous solution at pH 10.

Again, no significant oxide film material has been formed under this set of conditions as indicated by the co-ordination number for metallic and the oxygen co-ordinating species.

6.3.3.3 Polarisation to + 0.9 V

A piece of pure aluminium was immersed in aqueous solution at pH 10 for an hour, then polarisation was performed to + 0.9 V. Using EXAFS technique by measuring the total electron yield, it was possible to resolve the local structure of this oxide after analysing the EXAFS data. The structural parameters are listed in table 6.9.

Shell No.	Type of Atom	Co-ordination No.	Bondlength/Å	Debye-Waller Factor, $2\sigma^2/Å^2$
1	O	3.8 ± 0.1	1.87 ± 0.01	0.003 ± 0.001
2	Al	2.7 ± .24	2.92 ± 0.01	0.018 ± 0.002

Table 6.9 Structural parameters of the oxide formed by polarisation of aluminium in aqueous solution at pH 10 to + 0.9 V.

From the co-ordination number of the oxide shell given in table 6.9, it is seen that polarising aluminium in pH 10 to +0.9V results in the formation of a thick anodic film but again it is not thick enough to cause metallic aluminium not to be seen in the EXAFS. Experimental EXAFS spectrum and its fit for the aluminium and oxide shells and the Fourier transform are presented in figure 6.9.

6.3.3.4 Polarisation to + 0.9 V and then left connected for 4 hours

In this case, aluminium which was polarised in pH 10 aqueous solution to + 0.9 V, was left in the solution and connected to the voltage source for four hours. To check the effect of this treatment on this film's thickness and structure, total electron yield EXAFS for this oxide was measured. The local structure of this oxide was obtained from the fitting of the experimental EXAFS spectrum and given in table 6.10.

Shell No.	Type of Atom	Co-ordination No.	Bondlength/Å	Debye-Waller Factor, $2\sigma^2/Å^2$
1	O	4.2 ± 0.3	1.89 ± 0.003	0.017 ± 0.001
2	Al	6.3 ± 0.4	2.88 ± 0.01	0.033 ± 0.006

Table 6.10 Structural parameters for the oxide film that forms on aluminium by anodic polarisation to +0.9V and then left for four hours connected to the potential source in alkaline (pH 10) aqueous media.

On the basis of oxygen co-ordination number reported in table 6.10, leaving the aluminium sample connected to the potential source after polarisation for four hours in pH 10, leads to further thickening of the oxide film. It can be seen from table 6.11 that

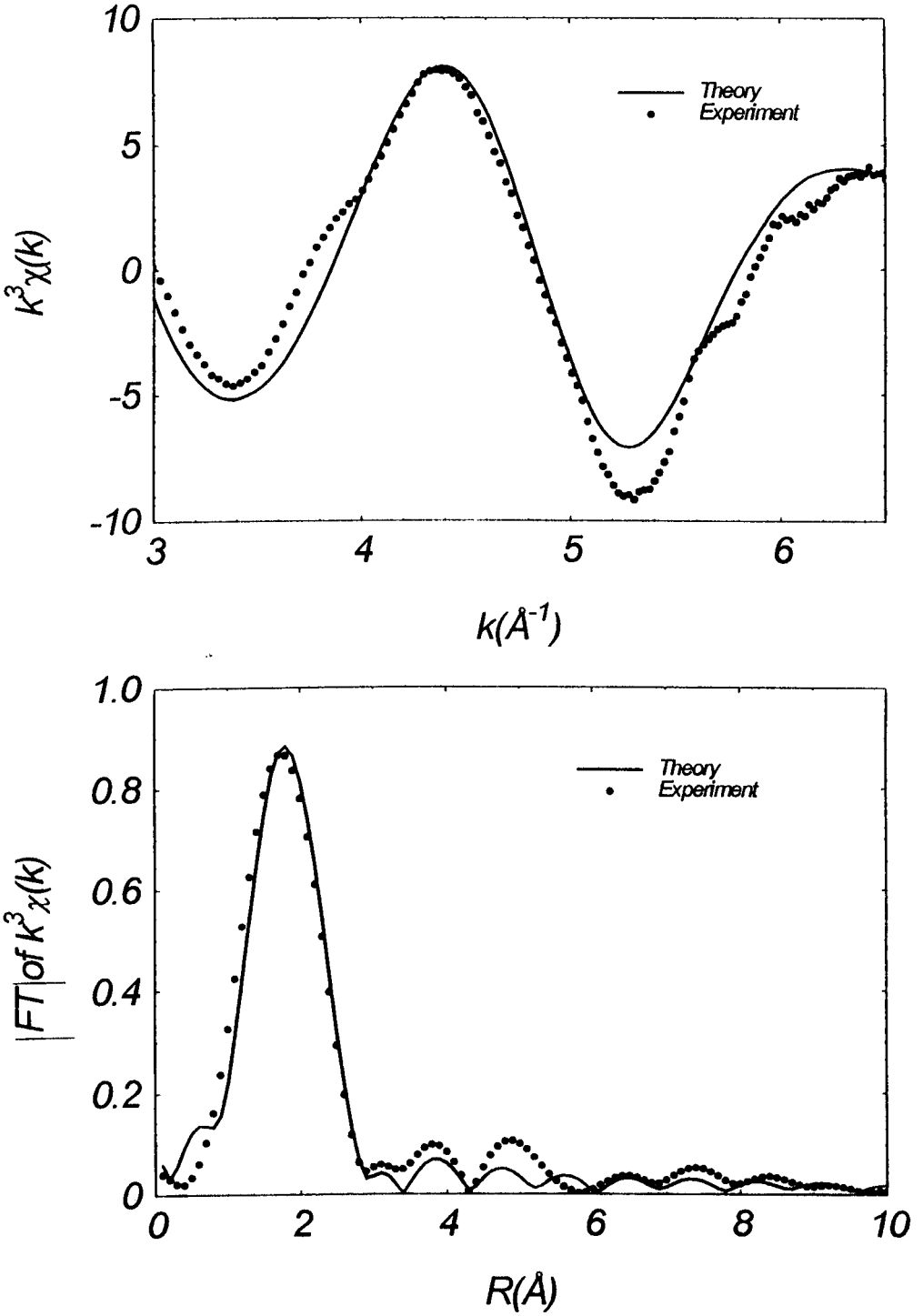

Figure 6.9 Experimental and theoretically fitted EXAFS function, $k^3\chi(k)$, for the oxide film formed by polarising aluminium to + 0.9 V in aqueous solution at pH 10, Al K-edge EXAFS

the metallic aluminium co-ordination has increased as well as the Debye-Waller factor, which mean that there is there is no change in the aluminium ratio in the total signal.

6.4 XANES Results

In this section, XANES spectra for different model compounds with known structures as well as those for the oxide films formed as described, are presented with their derivative. Fingerprinting is used to identify different structural features on the XANES of the oxide films formed on aluminium as described, and their derivatives.

6.4.1 XANES of Model Compounds

The XANES of different reference compounds with known structure, was measured to establish co-ordination number by matching the XANES of an unknown with that of a model compound where the co-ordination is well known.

Figure 6.10a, displays normalised absorption in arbitrary units as a function of relative energy (E= 0 is taken as the half peak position for the alpha alumina), for alpha alumina, gamma alumina, boehmite, gibbsite, andalusite, and yttrium aluminium garnet. It has been observed (5,6) that the first peak position in alpha alumina was at ~8 eV higher than that of aluminium metal(1560.0 eV). In the case of yttrium aluminium garnet, aluminium is tetrahedrally co-ordinated by oxygen. Boehmite (AlOOH), gibbsite [$Al(OH)_3$], alpha alumina, and aluminium is co-ordinated by six oxygen atoms. The peak at +0.8 eV indicates that aluminium is 6 co-ordinated. In gamma alumina, aluminium species are tetrahedrally co-ordinated as well as octahedrally, the first peak is at -1.0 eV. Andalusite has an equal amount of aluminium in 5 and 6 co-ordination and the first peak is at 0 eV. Robinson and Thompson (5)

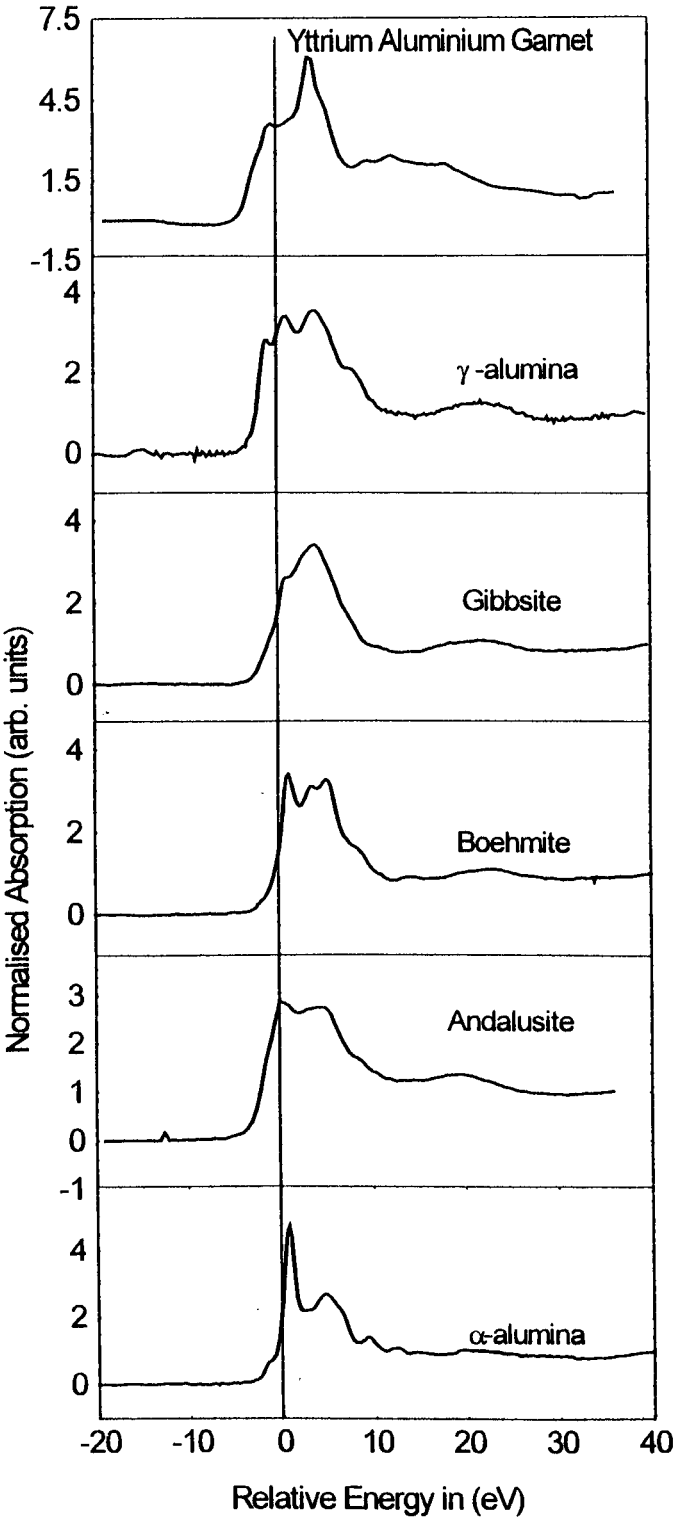

Fig. 6.10 (a) Normalised XAMES spectra of model compounds, alpha, gibbisite, andalusite, boehmite, gamma, and yttrium aluminium garnet. All have their energy adjusted to the edge energy of the alpha alumina taken as zero. Al K-edge

have observed that there is a constant energy between the first and the second peaks equal to 4.0 eV in the XANES of all the model compounds. They have suggested that the transitions contributing to the fine structure in the XANES are the same for all of these model compounds, but the energy of the 1s level which is the level from which the electrons excited is different. They explained the difference in the energy of the 1s level as a direct result of the change in the effective charge on the aluminium cation. This argument is supported by a reported study (7) where electron energy loss spectroscopy (EELS) technique was used to probe the electronic structure of alpha alumina and it was found that the same range of energy difference (4.1 eV) separates the two lowest levels in the conduction band. As a result, having a peak at ~ -7, -1.0, 0, or +0.8 eV is an indicator of the presence of aluminium in either the metallic state, or 4, 5, and 6 co-ordinated by oxygen respectively. Since the effective charge on the aluminium cation is +3 when it is octahedrally co-ordinated, so it is +2.5, and +2 for the 5, and 4 co-ordinated aluminium. Figure 6.10 b, present the derivative of the XANES spectra of the model compounds.

6.4.2 XANES of Aluminium at Different Preparation Stages

Fig 6.11a and b, displays the relative absorption and its derivative for alpha alumina measured in this investigation where it has a 6 co-ordination of oxygen, and the XANES of aluminium metal during different stages of the treatment prior to the polarisation process. It can be seen from this figure, that there is always an oxide film on the surface of aluminium. The 4 and 6 and 6 co-ordination is seen in the derivative of these oxide films, and even stronger feature for the six co-ordination is obvious in the case of metallic aluminium. It is not easy to determine if these oxide films form in the solution or after their removal. It should noted that the XANES of aluminium

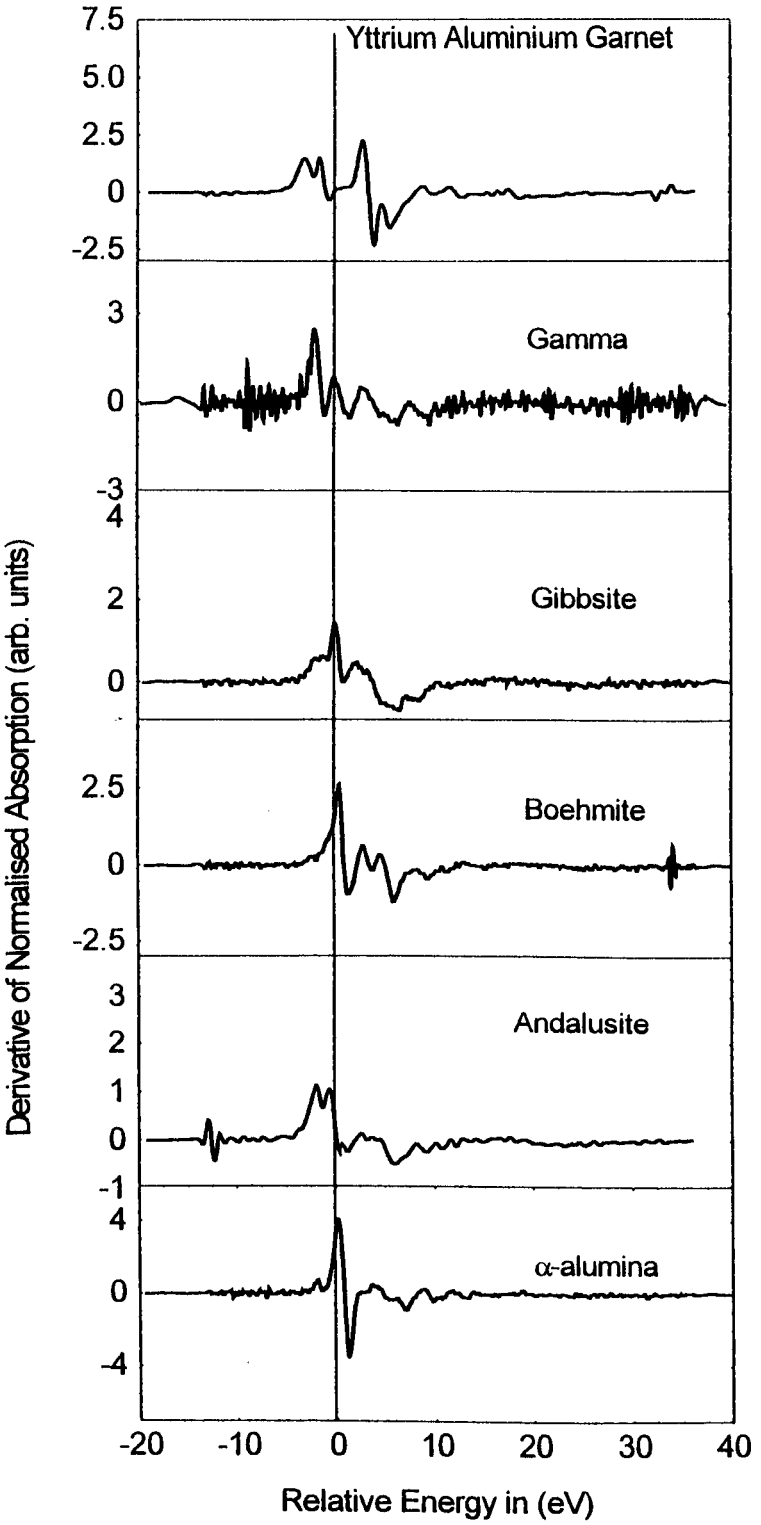

Fig. 6.10 (b) The derivative of Normalised XANES spectra of model compounds, alpha alumina, gibbisite, andalusite, boehmite, gamma alumina, and yttrium aluminium garnet. All have their energy adjusted to the edge energy of the alpha alumina taken as zero. Al K-edge

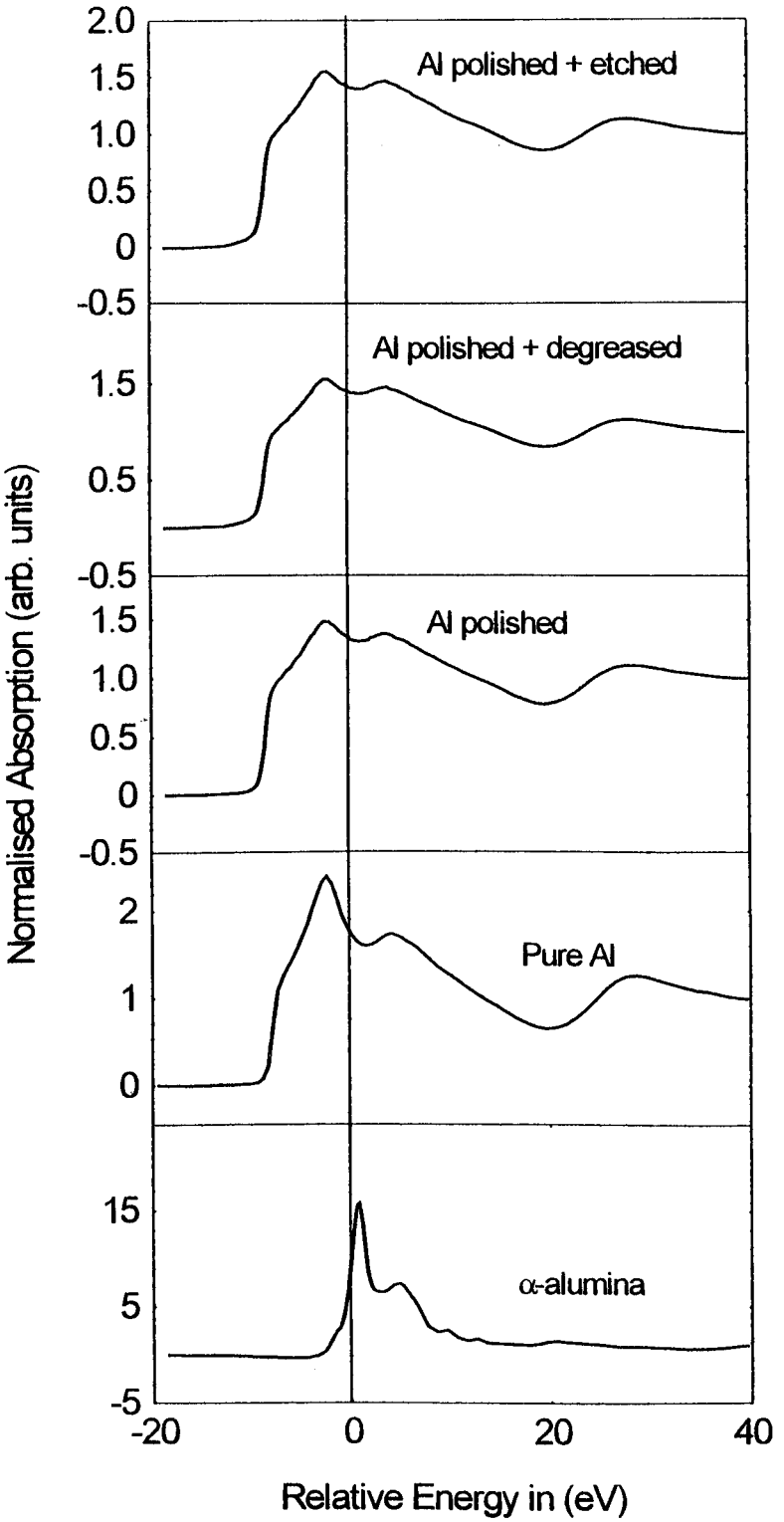

Fig. 6.11 (a) Normalised XANES spectra of aluminium metal at various stages of its surface preparation. Al K-edge

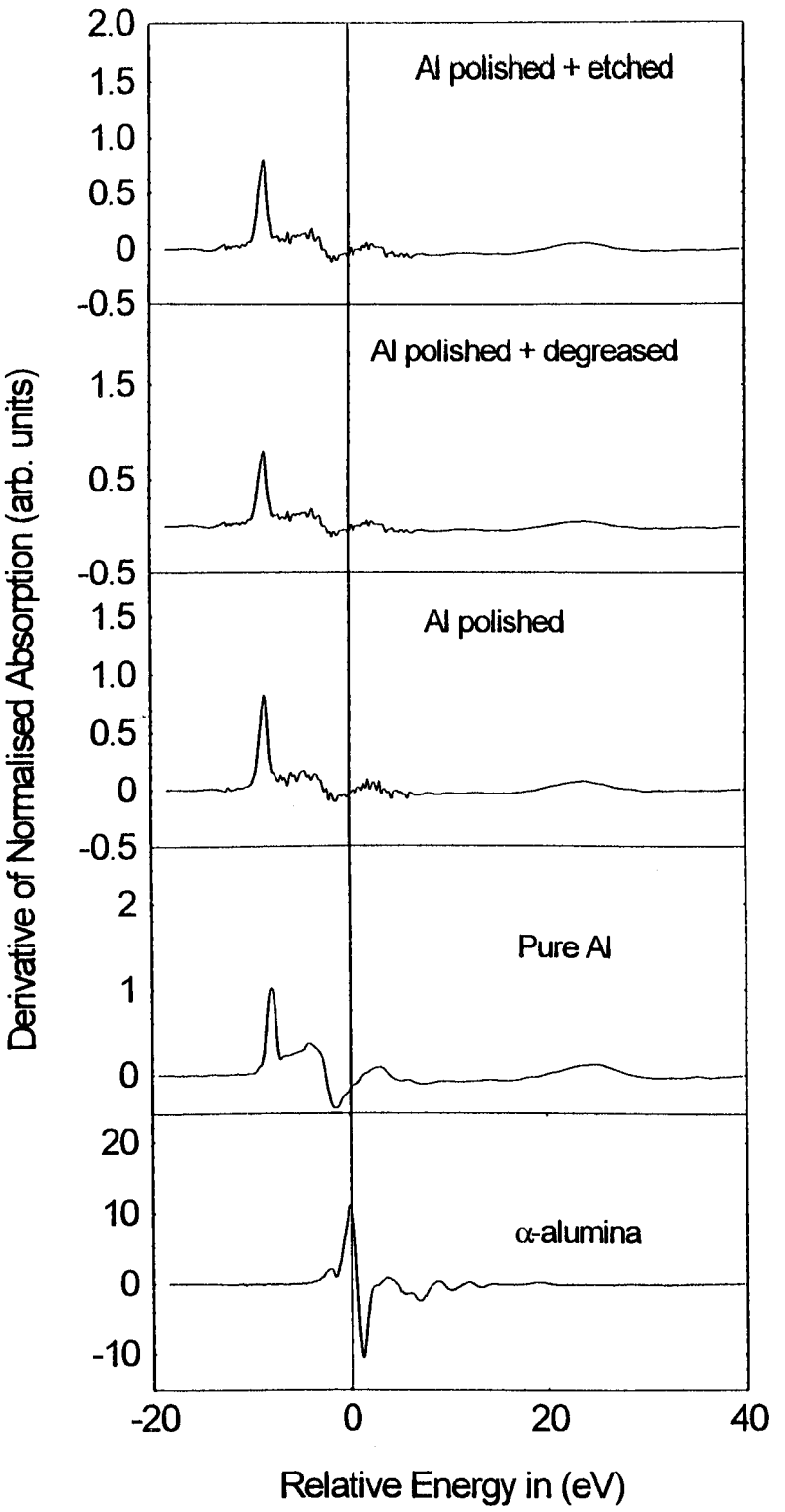

Fig. 6.11 (b) The derivative of Normalised XANES spectra of aluminium metal at various stages of its surface preparation. Al K-edge

metal foil was measured by transmission, whilst the XANES of oxide films on aluminium was collected by total electron yield. The choice of total electron yield was required, because the oxide films are superimposed on the aluminium surface.

6.4.3 XANES of Oxide Films on Al. Polarised at Various Potentials and Different pH's

The XANES results presented here are those of the oxide films formed as result of aluminium immersion and polarisation in aqueous solutions at pH 7, 2, and 10.

6.4.3.1 pH 7

Fig. 6.12 a shows the relative absorption of oxides formed on aluminium treated as indicated. From this figure, it can be seen that immersing aluminium in water at pH 7 for ~ 1 hour forms an oxide. Polarisation of aluminium to + 2.5 V results in the thickening of the oxide film on aluminium. This oxide is still not thick enough for the aluminium metal signal to disappear. From the derivative of the normalised XANES, it is obvious that the majority of aluminium is co-ordinated by 4 oxygen and some 6 co-ordination exists as well. Cathodic potentiodynamic sweep to -2.2 V does not result in oxide formation and it is only the air film which is present. From the derivative of the XANES at pH 7 given on fig 6.12 b, the peak position due to the metallic aluminium and of the oxide are clear.

6.4.3.2 pH 2

Figures 6.13 a and b, show the XANES and its derivative of the oxide films formed on aluminium surface as aluminium metal treated in different ways in aqueous media at pH 2 as mentioned on the figure. No oxide film grew when aluminium was held at

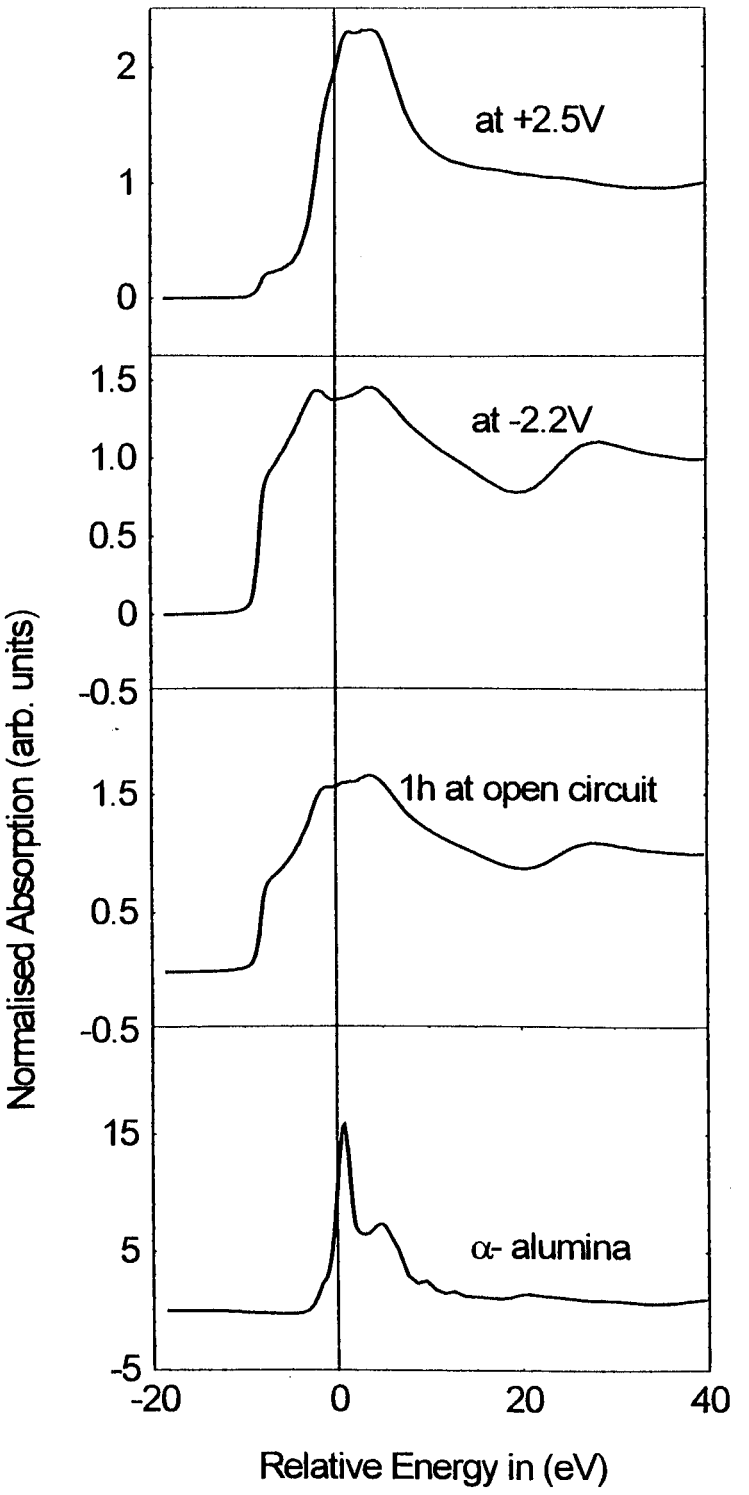

Fig. 6.12 (a) Normalised XANES spectra of aluminium metal in aqueous solution at pH 7 at open circuit, polarised to -2.2 V and + 2.5 V, also the derivative of these spectra is included Al K-edge

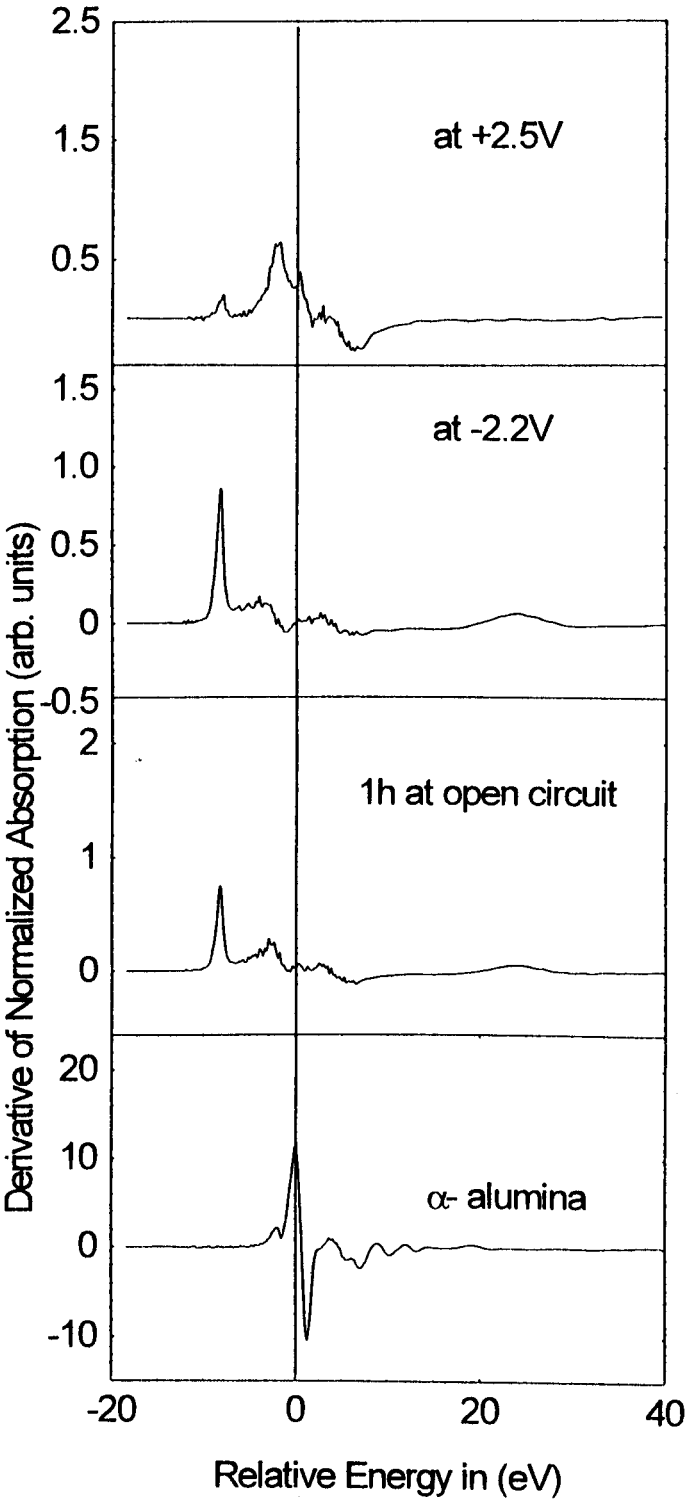

Fig. 6.12 (b) The derivative of Normalised XANES spectra of aluminium metal in aqueous solution at pH 7 at open circuit, polarised to -2.2 V and + 2.5 V, also the derivative of these spectra is included Al K-edge

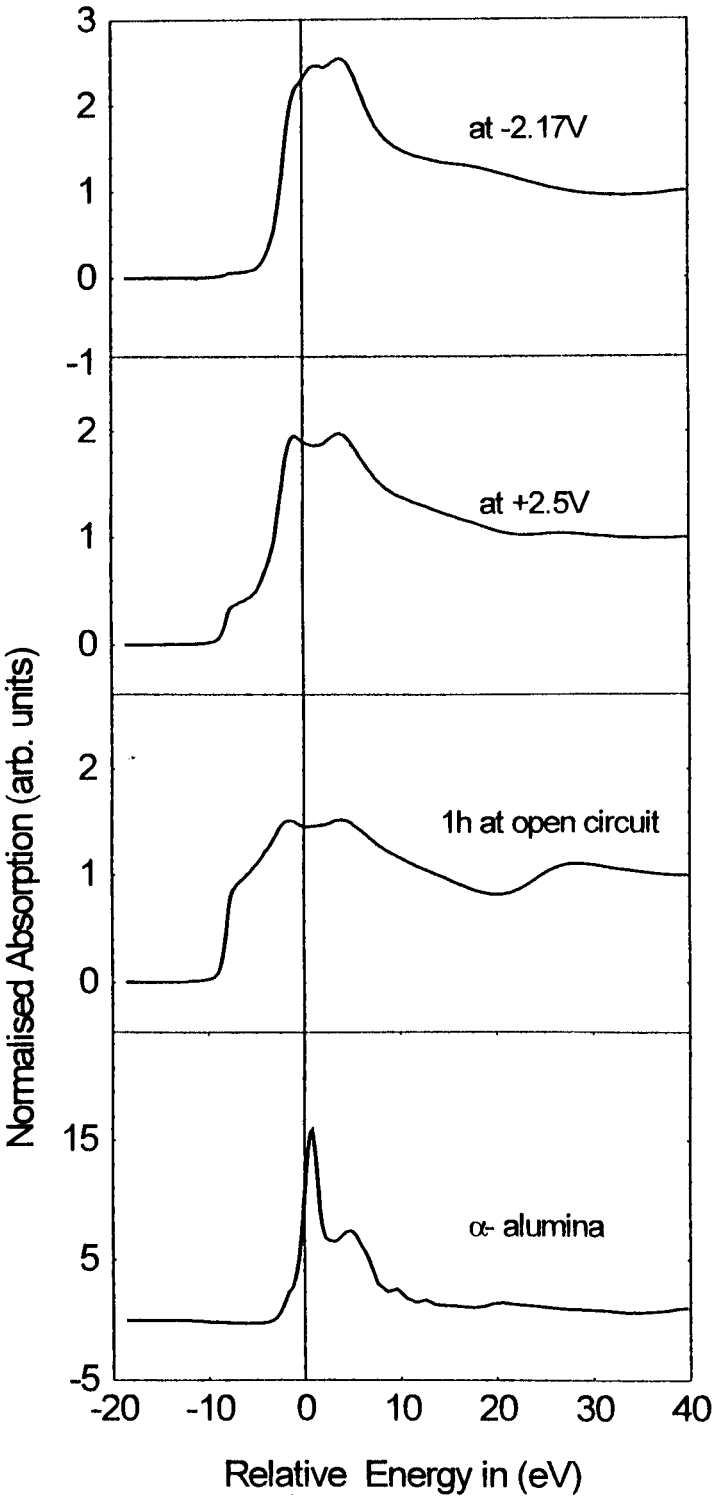

Fig. 6.13 (a) Normalised XANES spectra of aluminium metal in aqueous solution at pH 2 at open circuit for an hour, polarised to -2.17 V and + 2.5 V, also the derivative of these spectra is included Al K-edge

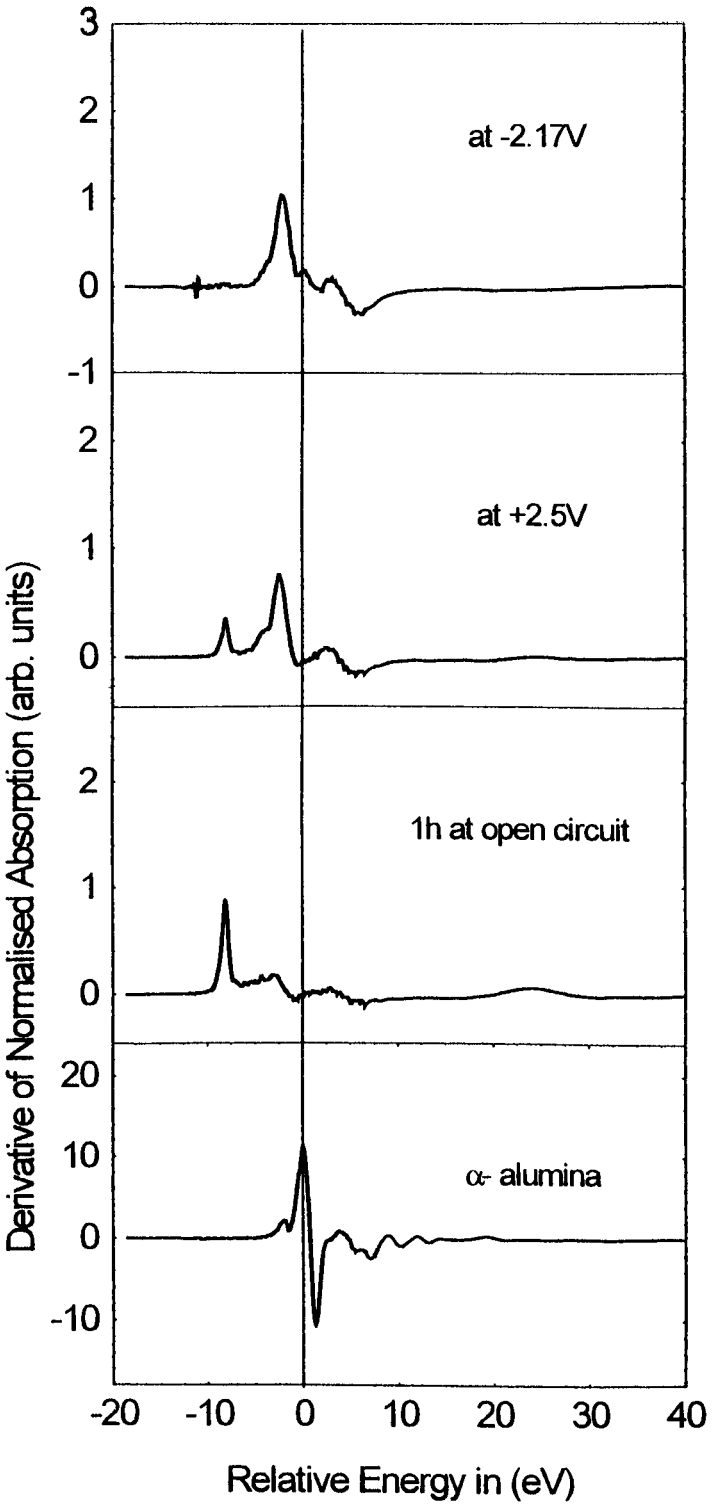

Fig. 6.13 (b) The derivative of Normalised XANES spectra of aluminium metal in aqueous solution at pH 2 at open circuit for an hour, polarised to -2.17 V and + 2.5 V, also the derivative of these spectra is included Al K-edge

open circuit in this solution. As seen from the figure, an oxide film grows on aluminium when anodised to + 2.5 V, whilst an even thicker oxide film forms when cathodically polarised to -2.17 V. It is clear from the derivative of the absorption that the peaks due to metallic aluminium and the oxide have different positions. It also can be concluded from the derivative of the XANES as seen in fig. 6.13 (b) that when cathodically polarised to -2.17 V, most of the aluminium species exists in the 4 co-ordination and some in 5 co-ordination, which disappears if polarised to + 2.5 V, no six co-ordination is seen. The effective charge on the cation is correlated to the co-ordination of the aluminium and this should be considered for all the structures.

6.4.3.3 pH 10

The XANES spectra for oxides formed by treating aluminium metal at different conditions in aqueous solution at pH 10 are displayed in Figure 6.14 a and its derivative is shown in fig. 6.14 b. In this figure, the normalised absorption signal is plotted as a function of the relative energy in the XANES range.

From fig. 6.14 a, it is clear that there is peak for the aluminium at open circuit, at -2.2 V, and +0.9 V. Aluminium in the oxides formed on aluminium formed at open circuit at pH 10, have a mixture of 4 and 6 co-ordination as seen from fig. 6.14 (b) which is the derivative of the XANES in this case. Also the 4 and 6 co-ordination in the case of aluminium cathodically and anodically polarised to - 2.2 V and + 0.9 are seen in fig. 6.14 (b). This indicates that there is no clear structural phase for the oxides that forms at these conditions. The aluminium metallic signal is present in all of the 3

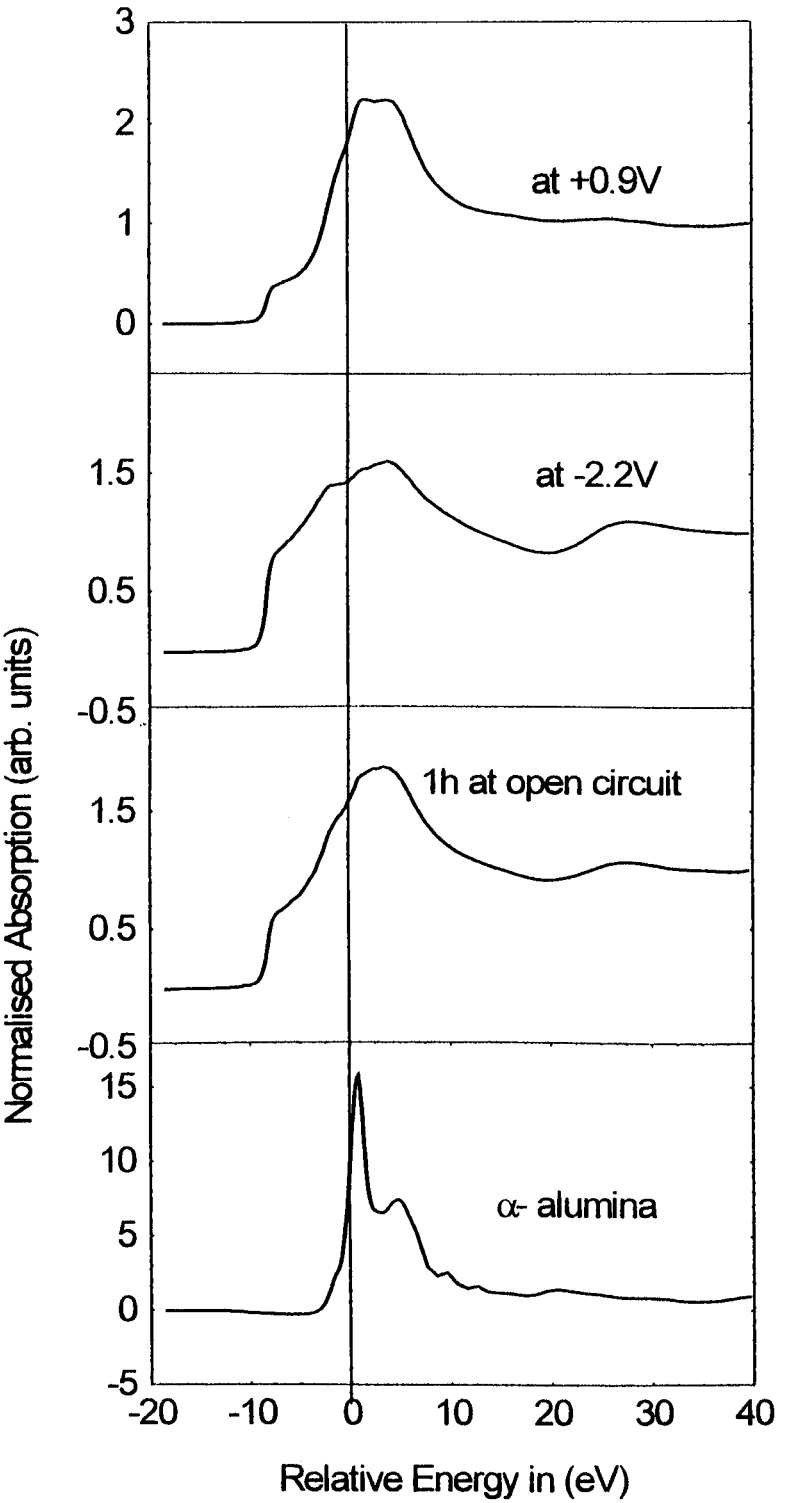

Fig. 6.14 (a) Normalised XANES spectra of aluminium metal in aqueous solution at pH 10 at open circuit for one hour, polarised to -2.2 V and + 0.9 V, also the derivative of these spectra is included, Al K-edge.

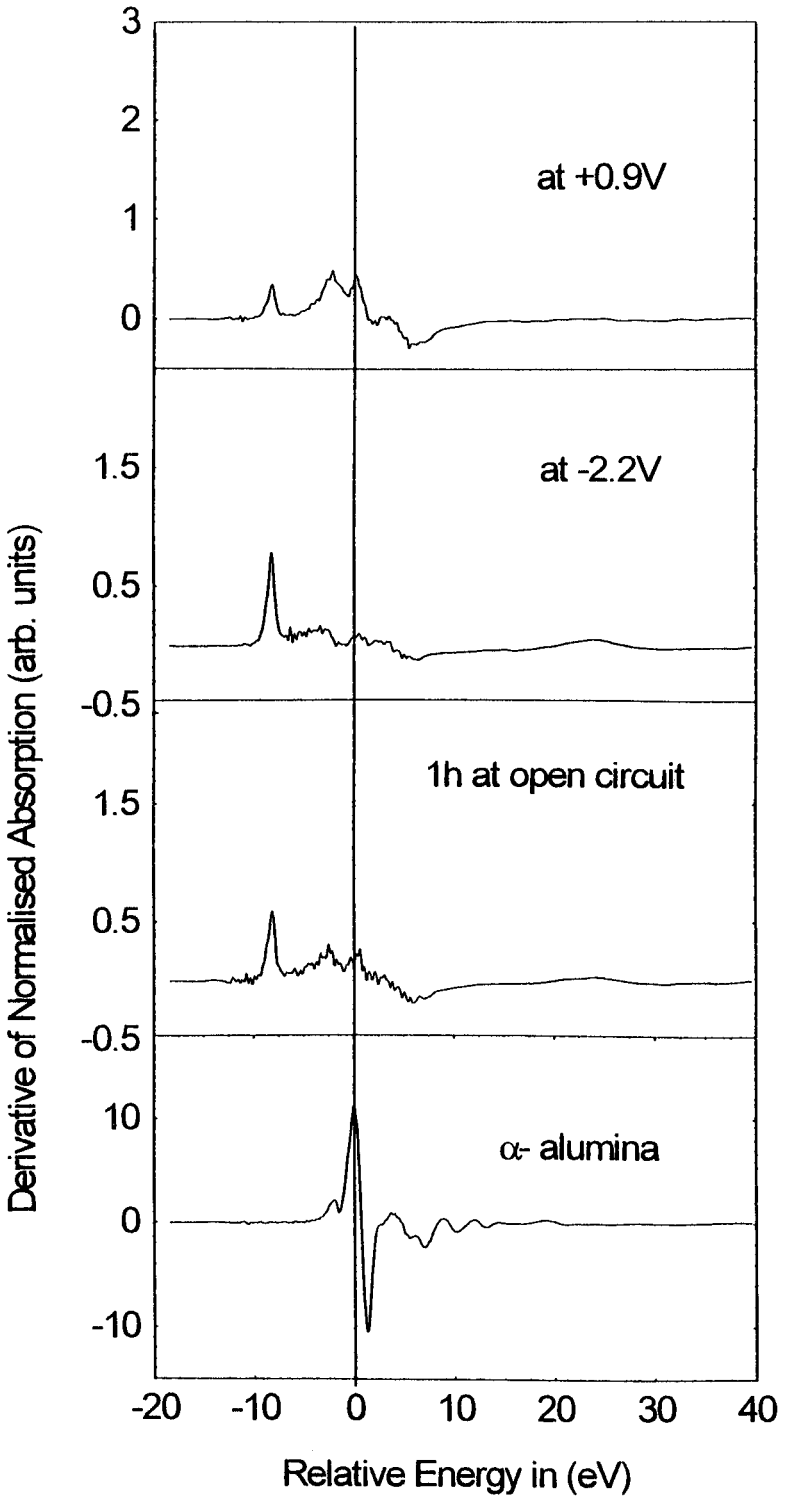

Fig. 6.14 (b) The derivative of Normalised XANES spectra of aluminium metal in aqueous solution at pH 10 at open circuit for one hour, polarised to -2.2 V and + 0.9 V, also the derivative of these spectra is included Al K-edge

spectra, but with different ratios. The oxide that forms at +0.9 V is much thicker than those that forms by immersion at corrosion potential, or cathodically polarised to -2.2 V. This oxide film as has been argued on the basis of the O 1s energy in chapter 5, is more of having an oxyhydroxide phase as seen in its XANES derivative.

6.5 ReflEXAFS Results

A wide range of aluminium film samples were prepared and chemically and electrochemically treated, but due to bad reflection quality and the cracks in the surface of the aluminium film, only the following spectrum for an aluminium film with the specified treatment was worth analysing in EXCURV92.

6.5.1 Reflectivity Curves

The reflectivity was measured as a function of the angle of beam incidence, so as to determine the critical angle. It can be seen that the critical angle was around 1 degree. Fig 6.15 shows the reflectivity as a function of angle for oxide film formed by immersing an aluminium sample in pH 10 aqueous solution for ~ 27 hours.

6.5.2 ReflEXAFS of oxide film on Aluminium at pH 10 for 27 hours

Table 6.11, presents the structural parameters for an oxide film on aluminium in pH 10 for ~27h, including bond lengths, co-ordination numbers, and the Debye-Waller factors along with the type of atoms in each shell.

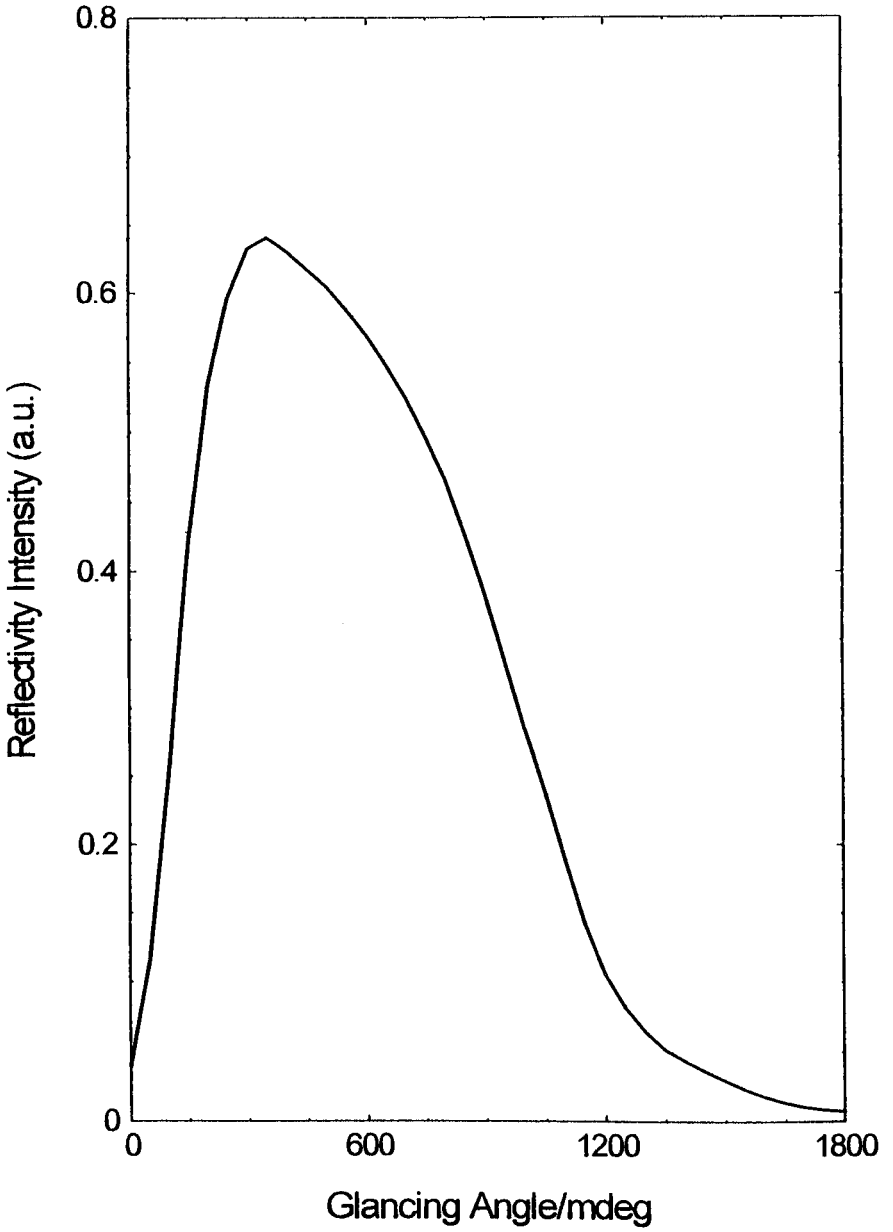

Fig. 6.15 Reflectivity profile of aluminium film immersed in aqueous solution at pH 10 for 27 hours, ReflEXAFS measured around the aluminium K-edge.

Shell No.	Type of Atom	Co-ordination No.	Bondlength/Å	Debye-Waller Factor, $2\sigma^2/Å^2$
1	O	2.6 ± 0.35	1.83 ± 0.01	0.006 ± 0.001
2	Al	14.3 ± 2	2.84 ± 0.01	0.017 ± 0.002

Table 6.11 Type of atoms in the backscattering shell, bond length and co-ordination number of each shell, and the Debye-Waller term for the respective shells of the oxide film formed on aluminium film immersed in aqueous solution at pH 10 for 27 hours. ReflEXAFS was measured at 750 mdeg.

From the value of the co-ordination number presented in table 6.11 for the aluminium shell, it is clear that the oxide film is thin also the first shell distance from the absorbing aluminium is 1.83 ± 0.01, which indicates that it is in tetrahedral co-ordination. There is strong metallic aluminium signal from the substrate. Figure 6.16, is the experimentally and theoretically fitted EXAFS function k^3 weighted of aluminium at open circuit for 27 hours in pH 10.

6.6 Discussion of Results

Some aspects of the EXAFS, XANES, and ReflEXAFS results of thin oxide films on aluminium surfaces from which their structure was resolved in this work, are compared with the XPS results presented for the same range of oxide films.

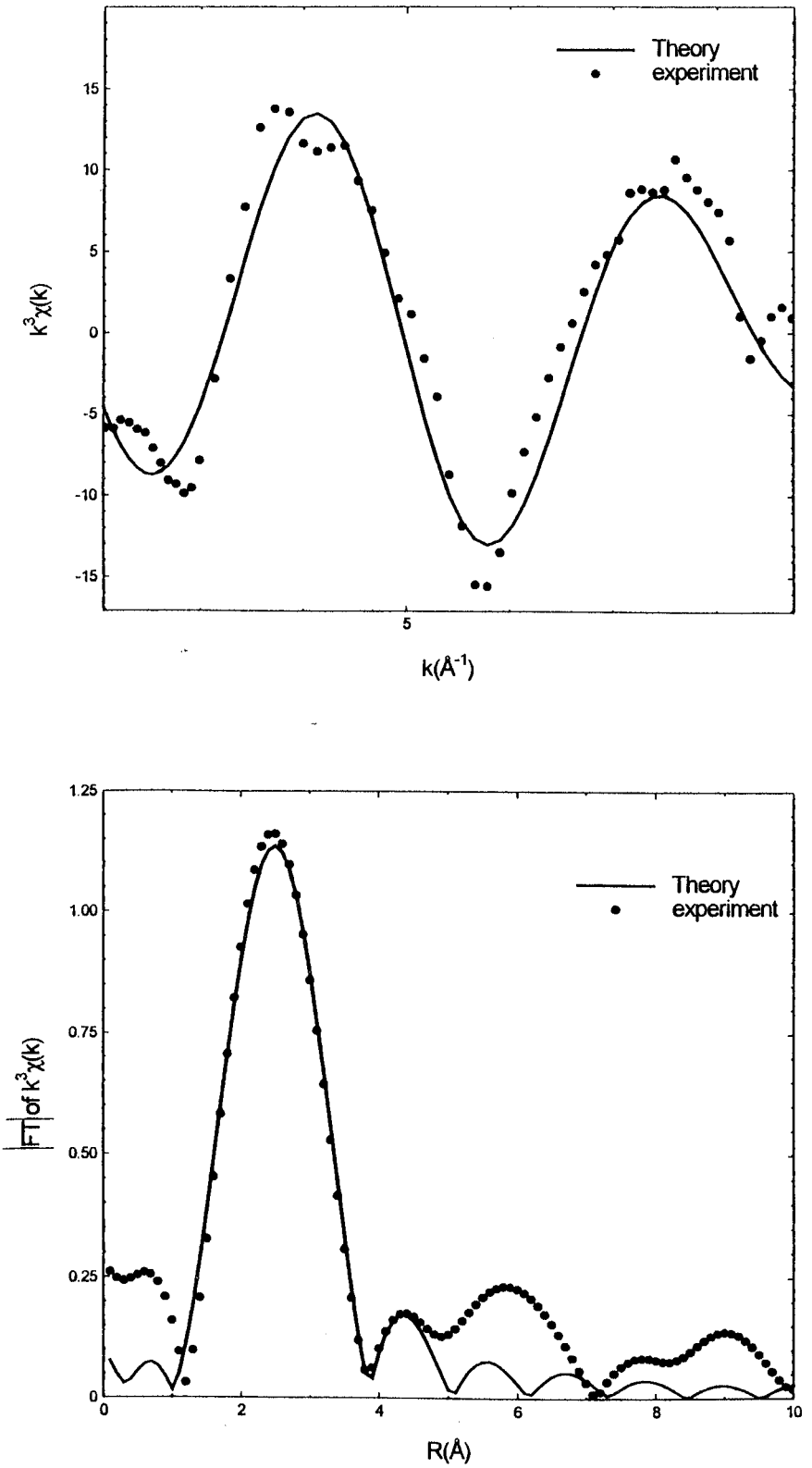

Figure 6.16, k^3 weighted reflection EXAFS of oxide film on aluminium immersed for 27 hours in aqueous solution at pH 10, theoretical best fit and their Fourier transform. Al K-edge.

6.6.1 EXAFS

From the EXAFS structural results for the passivating oxide layers anodically formed on aluminium at pH 2, 7, and 10 as described in this work and presented in tabulated form, an oxide film is always present on the aluminium surface. This does not mean that each aluminium surface treatment results in oxide film thickening.

From the co-ordination numbers given in the tables, it is clear that because the absorption is made up of a ratio of metallic aluminium and oxide which results in a co-ordination which sometimes is lower than 4. It is noticeable that for "thick oxides, co-ordination number was $\sim$ 4 whilst films which are close to air-formed ones, the co-ordination number becomes 2 or even less in some cases. Bond length is the most accurate of the structural parameters extracted from the EXAFS spectra. Based on the work undertaken by Norman et al. (8), a relationship between the bond length established from EXAFS experiments and the co-ordination number was worked out and reported by El-Mashri (9,10). In their approach, the crystal potential of solids which have ionic bonding can be expressed in such a way that a relationship between the measured bond length and the co-ordination number is established (11). A mixture of tetra- and octahedrally co-ordinated aluminium was found to correspond to different bond length values. The reported bond length for thin passivating layers on aluminium in this work indicate that their local structure is a mixture of 4 and 6 co-ordination.

From the EXAFS and XANES results of thin films on aluminium, it is clear that there is agreement with the XPS results of the same oxide films about their composition and structure where they do not show any crystalline phase.. Also, there is

an agreement about the formation and the thickness of this class of films in the work of Moshier et al. (12), but no agreement about their structure.

In almost all preparation conditions as described in this work, aluminium metal contribution was noticeable in the EXAFS spectra which indicates that the oxide film formed on aluminium is relatively thin. The fact that there is always a film on the surface of aluminium has been observed. In some cases only an air formed film is present. Based on the exact theoretical treatment of the EXAFS function and by the use of total electron yield, it has been possible to determine the local structure of alumina films.

6.6.2 XANES

From the XANES figures presented for aluminium surface during preparation and after immersion and polarisation in aqueous media at various pH's and polarised to various potentials, the structural features can be compared to those on the model compounds. In the case of XANES spectra of oxides formed, at -2.17 V in pH 2, +0.9 V in pH 10 and open circuit, and + 2.5 V in pH 7, they have a mixture of Al in 4 and 6 co-ordination.

6.6.3 ReflEXAFS

An aluminium ReflEXAFS spectrum is presented for an aluminium film immersed for ~ 27 hours in an aqueous solution at pH 10. EXAFS measurement in the total reflection mode is suitable for structural investigations of surfaces with a good reflectivity. ReflEXAFS can resolve the structure of a mono-layer systems.

References

(1) Hedin, L., and Lundqvist, Solid State Physics, **23**(1969)1
(2) Barth, U. Von., and Hedin, L., J. Physics, C, **5**(1972)1629
(3) Hirschfelder, J. O., Curtis, C. F., and Bird, R. B., "Molecular Theory of Gases and Liquids", Willey, USA, (1966)1037
(4) Sawada, H., Materials Research Bulletin, MERBUA, **29**(1994)127
(5) Robinson, J.., and Thompson, G. C., unpublished work
(6) McKeown, D. A., Waychunas, G. A., and Brown, G. E., J. Non- Cryst. Solids, **74**(1985)349
(7) Olivier, J., and Poirier, R., Surface Sci., **105**(1981)347
(8) Norman, D., Brennen, S., Jaeger, R., and Stohr, J., Surface Science, **L297**(1981)105
(9) EL-Mashri, Ph.D. Thesis, University of Warwick, 1983
(10) EL-Mashri, S. M., Jones, R. G., and Forty, A. J., Phil. Mag., **A48**(1983)665
(11) Pauling, L., "The Nature of The Chemical Bond". (Iahtacha: Cornell University Press), USA, 1960
(12) Moshier, W. C., Davis, G. D., and Ahearn, J. S., Corros. Sci., No-8, **27**(1987)785

7. Chapter Seven Conclusions and Further Work

The different aspects of anodic oxide films on aluminium, whether they are thin passivating layers or the much thicker ones, are interesting to investigate. The determination of structural parameters was made by the use of x-ray absorption spectroscopy based techniques, where the structure of two classes of anodic films on aluminium was investigated.

Firstly, the local structure about tungsten species incorporated into the anodically formed alumina oxide films during anodisation of aluminium in tungstate aqueous solution at 100 V was determined. Even though other techniques, such as XPS and electron microscopy aided by ultramicrotomy are capable of confirming the presence of incorporated electrolyte species in anodic films on aluminium it has not been possible to use these techniques to resolve the structure of the incorporated species. The potential of the EXAFS technique in solving structures of electrolyte incorporated species which have short range order was demonstrated for the first time in this work. The local structure of tungsten incorporated species was determined from the bond length of the W-O pair from the single shell analysed EXAFS spectrum. It was found that the bond length was 1.79 ± 0.01 Å and tungsten was co-ordination by 4 oxygen atoms. It is evident that even though the structural parameters presented for tungsten in alumina oxides indicate that it is in the tungstate (WO_4^{2-}) form, these can not be the species which are outwardly mobile under the influence of the field. The species that are outwardly mobile may be metallic tungsten linked in some way to Al^{3+} in the

aluminium oxide and resulting in the tungsten being dragged outward along with the aluminium cation which is outwardly mobile. As far as the structure of tungsten species in the alumina oxide films is concerned, based on the bond length and the co-ordination number, it has a short range order co-ordinated with 4 oxygen atoms, the other possibility is that tungsten incorporates into the alumina oxide itself and becomes a part of its structure.

It can be concluded that during anodisation, tungsten species when incorporated into the oxide film, are transformed under the influence of the high field and are outwardly mobile. The previous statement implies that tungstate species are transformed by some mechanism into a positively charged species which move outward with the egress of Al^{3+} species. As the tungstate species are initially adsorbed at the oxide/ solution interface, tungstate becomes positive through the loss of its oxygen. This stripping process eventually leads to the production of W metal cation which is positively charged and outwardly mobile under the field.

Secondly, the main theme of this work, was to resolve the local structure of passivating thin films anodically grown on aluminium in water under different experimental conditions. The structure of these films as in the case of tungsten in thick alumina films, was characterised by the use of EXAFS in terms of bond lengths and co-ordination numbers. Supporting evidence of the conclusions drawn from comparative XANES and XPS results about the structure of thin films on aluminium are cited.

Comparison of the XPS results of the air-formed film with those of the surface film on aluminium formed by immersion in aqueous solutions at pH 2, 7, and 10, shows that they are as thin as an air formed film. This evidently indicates that aluminium

undergoes corrosion in these conditions and that the air formed film has been formed once aluminium has been removed from the solution. As far as the formation and thickness of oxide films on aluminium is concerned, the XPS results reported in this thesis agree with those of Moshier et al. (1). The charge corrected binding energy of the Al 2p transition of the oxide formed when aluminium is immersed in boiling water for more than 10 minutes was found to be 78 eV. The structure of the oxide that forms under these condition is known to be pseudoboehmite. The charge corrected E_b of Al 2p due to the oxide films on aluminium polarised to different potentials in water at various pH's reported in this work is ~ 74 eV. There is a difference of 4 eV between the binding energies of the crystalline boehmite and that of the thin layers on aluminium. This leads to the suggestion that the structure of the films formed on aluminium polarised in aqueous media within the voltage range of -2.2 to + 2.5 V, is not of a crystalline nature and it is surely not of a boehmite form as was indicated by Moshier. The E_b values for the Al 2p in each oxide were ascertained by checking that the E_b of the O 1s has the correct value for oxygen in aluminium oxide as was reported by Fuggle (2) to be 532.4 eV if no charging exist.

In almost all preparation conditions as described in this work, aluminium metal contribution was noticeable in the EXAFS spectra which indicates that the oxide film formed on aluminium is relatively thin. The fact that there is always a film on the surface of aluminium has been observed. In some cases only an air formed film is present. Based on the exact theoretical treatment of the EXAFS function and by the use of total electron yield, it has been possible to determine the local structure of alumina films.

EXAFS and XANES studies of the structure of passivating layers on aluminium polarised under the same conditions as mentioned in the thesis, relied on the bond length and co-ordination number determination. The precision of the structural parameters determined for these films and reported in chapter six was due to the precision in calculating the phase shifts of oxygen and aluminium. From the EXAFS and XANES results of thin films on aluminium, there is an agreement with the XPS results of the same system reported in this thesis as well as with the work reported by Moshier et al (1) about the formation and the thickness of these films. The E_b value of the Al 2p at various depths of the passivating films on aluminium, does not change as a function of depth and this can lead to the conclusion that the composition is homogeneous. This shows that bombarding the oxide film surface with argon ions does not cause structural rearrangements. XPS data did not show incorporation of any electrolyte species, such as, S, Na, or Cr from the etching agent, into the film material during polarisation, even though it has been reported (3) that some incorporation, especially of sulphur into the film happens. Based on the low amount of electrolyte and also the low range of potential to which aluminium was polarised, it is debatable whether any of these species incorporate at all.

The average value for bond length reported in chapter six for the Al-O single shell in these films was ~ 1.88 Å and in some cases even less. Based on the relationship reported by EL-Mashri (3) where by measuring the bond length, the co-ordination number can be determined, the value reported here does not indicate an octahedrally co-ordinated aluminium. For aluminium to be 6 co-ordinated, the bond length has to have a value of at least 1.92 Å. This leads to the conclusion that the structure of the passivating

films on aluminium formed under the stated conditions comprise a mixture of tetrahedral and octahedral co-ordination. Even though in some cases, there is a higher percentage of aluminium co-ordinated by six oxygen atoms than four, it has never been seen in this study that a pure 6 co-ordination of the boehmite or the gibbsite exists.

XANES structural features of model compounds of known crystallographic structure was used in a "fingerprinting" way and compared with the XANES of the oxide films formed on aluminium as described in this study. XANES of the films of unknown structures have confirmed the XPS results about these oxide films and under what set of conditions a film forms, and its thickness. The XANES of the passivating films on aluminium formed in the potential range -2.17 - + 2.5 V and on immersion in pH 2, 7, and 10 solutions have showed that none of these films have a structure which relates to those of boehmite, gibbsite or any other crystalline form of aluminium oxides. The XANES results indicate that these films have a mixture of co-ordination of 6 and 4 around the aluminium atom. The EXAFS findings that the structure of passivating layers on aluminium is not crystalline and that it has a mixture of co-ordination are confirmed by the XANES study. Even in the case of thicker oxide films the six oxygen co-ordination feature does not show.

A wide range of oxides were formed on aluminium thin films, but because of their poor reflectivity and in some cases the film has been washed away completely, it was not possible to obtain good quality ReflEXAFS data. No conclusions about any features of the films formed on aluminium films are drawn here and it is recommended that care and attention should be considered when preparing aluminium films. Making thicker aluminium films, treating the aluminium films as desired as soon as these films are

formed, and limiting their exposure to the solution especially the aggressive ones, are recommended measures to produce specimens with good reflectivity.

7.1 Suggested further work

1. It is interesting to investigate the structure of passivating films formed as described in this work on aluminium alloyed with copper, zinc, nickel, and others at different percentages.

2. Theoretical simulation of the XANES spectra and comparison with experimental results and relating the results to the EXAFS results.

3. It will be interesting to check the influence of chloride addition to the aqueous electrolyte and the effect it will have on the structure, thickness, and composition of these films after aluminium immersion for different duration's.

It is clear from this investigation that the EXAFS, XANES, and ReflEXAFS techniques can play an important role in solving the structure of electrolyte incorporated species into anodic films. Structural analysis of thin passivating oxide films on aluminium are the subject of investigation by the use of EXAFS, and the technique has shown its capabilities in this aspect. X-ray absorption spectroscopy has an important role to play in resolving the structure of this system on other metals. This can shed light on passivity and the passivation mechanism and other phenomenon occurs on metallic electrodes, such as the corrosion process, which is related to it. The XANES region is rich in structural and electronic information because multiple scattering becomes the dominant process and it samples most of the atomic and electronic environment around it.

References

(1) Moshier W. C., Davis, G. D., and Ahearn, J. S., Corro. Sci., **27**(1987)785
(2) Fuggle, J. C., Warson, L. M., Fabian, D. J., and Affossman, S., Surface Science, **41**(1975)61
(3) EL-Mashri, S. M., Ph.D. Thesis, University of Warwick, 1985